UNIVERSITÉ DE STRASBOURG

ÉCOLE DOCTORALE MSII

Laboratoire ICube, Strasbourg, France

THÈSE présentée par :

Ivan HERNANDEZ GALINDO

soutenue le **19 décembre 2023**

pour obtenir le grade de : **Docteur de l'université de Strasbourg**
Discipline : Sciences de l'imagerie
Spécialité : Télédétection

A multiscale/multi-temporal study of Lake Surface Water Temperature (LSWT) using thermal satellite sensors: application to lakes of Grand-Est region, France, and Kyrgyzstan

THÈSE dirigée par :
Mme NERRY Françoise — Directrice de recherche, CNRS
Co-encadrant:
M YESOU Hervé — Ingénieur de Recherche, ICube

RAPPORTEURS :
M SOBRINO José Antonio — Professeur, Universitat de Valencia
M KOURAEV Alexei — Maitre de conférences, LEGOS

AUTRES MEMBRES DU JURY :
M LI Zhao-Liang — Directeur de Recherches, CNRS
M LE-SOLLEUZ Antoine — Maitre de conférences, École de Mines Nancy
M CRÉTAUX Jean François — Ingénieur CNES, LEGOS

Acknowledgments

I want to express my heartfelt gratitude to the following individuals and organizations who have played a significant role in the completion of this doctoral thesis:

I am deeply thankful to my primary supervisor, Françoise NERRY, for her guidance, mentorship, and unwavering support throughout the research process. Their insightful feedback and expertise have been invaluable in shaping the direction of this work. I am also grateful to my co-supervisor Hervé YESOU for his contributions and valuable insights, I am indebted for his mentorship, encouragement, and wisdom. Their guidance has been a source of inspiration throughout my academic journey.

I extend my appreciation to the members of my doctoral committee for their constructive feedback and valuable suggestions for this thesis. Their expertise has enriched the quality of my research.

I want to acknowledge my colleagues and peers who have provided a stimulating academic environment. The exchange of ideas and collaborative efforts have been instrumental in broadening my perspective and enhancing the overall quality of this research.

I am deeply grateful to my family and friends, who have been a constant source of encouragement, understanding, and support. Your patience and belief in my abilities have sustained me through the challenges of doctoral research.

I acknowledge the financial support from the National Council of Science and Technology of Mexico (CONACYT), which made this PhD possible. Additionally, I extend my gratitude to the ICube Laboratory of the University of Strasbourg for providing a conducive research environment and resources essential for completing this thesis.

I sincerely thank the participants and collaborators who generously contributed their time, expertise, and insights to this research. Your willingness to engage in this study has been invaluable.

I also acknowledge the support from the CEOP-AEGIS organization, directed by Massimo Menenti, in which the acquisition of instrumentation and trips were possible to conduct the validation campaign in Issyk-Kul Lake in 2021. I also thank Jean Francois CRETAUX from the LEGOS team for accepting me in the research team he led for the Cal/Val campaign in the same Lake in 2021.

In conclusion, I am grateful to everyone who has played a part, direct or indirect, in realizing this doctoral thesis. Their support has been instrumental, and I am genuinely thankful.

Ivan HERNANDEZ-GALINDO
December 2023
Strasbourg, France

Content

Acknowledgments i

List of Figures iv

List of Tables vi

List of Acronyms vii

Résumé I

Chapter 1. Introduction ***1***

1.1 Context 1

1.2 State of the art 9

1.2.1 LSWT retrieval from moderate spatial resolution satellites 11

1.2.2 LSWT retrieval from high spatial resolution satellites 16

1.3 Objectives 21

1.4 Structure of the thesis 22

Chapter 2. Methodology ***24***

2.1 Algorithms to retrieve LSWT from Landsat 8-9 27

2.1.1 Mono Window Algorithm (MWA) 27

2.1.2 Single Channel Algorithm (SCA) 29

2.1.3 Practical Single-Channel Algorithm ($PSCwvc$) 30

2.1.4 Split Window Algorithm (SWA) 31

2.2 LSWT from Sentinel-3 (SLSTR) 32

2.3 LSWT from MODIS (Terra) 33

2.4 LSWT from ECOSTRESS 34

2.5 Split Window Algorithm (SWA) for ECOSTRESS 36

Chapter 3. Study area and data ***38***

3.1 Location and Characteristics of the Lakes 38

3.1.1 Issyk-Kul Lake 38

3.1.2 Gerardmer and Longemer Lakes 41

3.1.3 Plobsheim Lake 43

3.2 Imagery data 44

3.2.1 Landsat 8-9 (TIRS) 45

3.2.2 MODIS (Terra) 47

3.2.3 Sentinel-3 (SLSTR) 48

3.2.4 ECOSTRESS 48

3.2.5 Datasets from CCI Lakes 49

3.2.6 Atmospheric water vapor content (wvc) and near-surface air temperature (T_0). 50

3.3 Ground data 51

3.3.1 Datasets from Meteorological Stations 51
3.3.2 In-situ datasets from buoys 52
3.3.3 Torrent Board 54
3.3.4 Radiometer CIMEL 312-2 57
3.3.5 Infrared Camera FLIR T-560 58

Chapter 4. LSWT Retrieval Results and Discussion 59

4.1 Sensors Intercomparison 60

4.2 LSWT Retrieval Analysis from Sensors 63
4.2.1 Landsat 8 63
4.2.2 LSWT for Sentinel-3 (SLSTR) 66
4.2.3 LSWT for MODIS (Terra) 70
4.2.4 LSWT for ECOSTRESS 73
4.2.5 SWA for ECOSTRESS 76

4.3 Ground Validation 77
4.3.1 Validation campaign in Issyk-Kul in October 2021 77
4.3.2 Validation campaign in Issyk-Kul in May 2023 83
4.3.3. Ground validation in Gerardmer and Longemer Lakes 85
4.3.4 Validation campaign in Plobsheim Lake in April 2023 88
4.3.5 Validation campaign in Plobsheim Lake in June 2023 92

4.4 Discussions 95
4.4.1 Sensors Intercomparison 95
4.4.2 LSWT Retrieval 97
4.4.3 Ground validation 100

Chapter 5. Conclusions and Perspectives 104

5.1 Conclusions 105

5.2 Perspectives 109

References 113

List of Conferences 127

List of Figures

Figure 1. *The hydrological cycle in a natural ecosystem (Water Cycle | National Oceanic and Atmospheric Administration, n.d.)* 2
Figure 2. *Spectral irradiation for a 300 K blackbody with an example of atmospheric transmittance (Zhao et al., 2019)* 5
Figure 3. *Illustration of stratification in a lake and the LSWT acquisition using satellites (Perrone et al., 2021)* 7
Figure 4. *The empirical relationship between $\mathcal{E}_{min}$ and MMD (spectral contrast), based on 86 laboratory reflectance spectra of rocks, soils, vegetation, snow, and water (Gillespie et al., 1998). 95% of the samples fall within ±0.02 emissivity units of the regression line, corresponding to an error in T of about ±1.5 K at 300 K. The $\mathcal{E}$min-MMD relationship follows a simple power law: $\mathcal{E}_{min}$=0.994-0.687*MMD0.737* 26
Figure 5. *LSWT retrieval process for Sentinel 3 at Level 2.* 32
Figure 6. *LSWT retrieval process for MODIS at Level 3.* 34
Figure 7. *LSWT retrieval process for ECOSTRESS at Level 2.* 35
Figure 8. *Location of Issyk-Kul Lake, Kyrgyzstan, Central Asia (Alifujiang et al., 2020)* 38
Figure 9. *Bathymetry of the Issyk-Kul Lake, Kyrgyzstan (LEGOS Laboratory)* 39
Figure 10*. Average annual air and water temperature variations of Issyk-Kul Lake at MS Cholpon-Ata (1972-2009) (Alifujiang et al., 2020).* 40
Figure 11. *Location of the Gerardmer and Longemer Lakes.* 41
Figure 12. *Lake of Gérardmer (ICube, 2021).* 42
Figure 13. *Lake of Longemer (ICube, 2021).* 43
Figure 14. *Lake of Plobsheim (Plans d'eau - Fédération de Pêche Du Bas-Rhin, n.d.).* 44
Figure 15. *Bandwidth of the exploited data and new future sensors for TIR imagery.* 45
Figure 16. *Spectral Response Functions (SRFs) of Landsat-8 and Landsat-9 bands (Ye et al., 2022b).* 47
Figure 17. *CCI Lakes v.2.0.2 sample for 07 August 2019.* 49
Figure 18. *GRID values for water vapor content from ECMWF.* 50
Figure 19. *GRID values for air temperature from ECMWF.* 51
Figure 20. *Dataset example of the Cholpon-Ata Meteorological Station in 2020.* 52
Figure 21. *Buoy in Gérardmerd Lake is used to measure the temperature at various levels of the lake (Suivi Climatique National & Fonctionnement Des Lacs: Une Bouée Installée Sur Le Lac de Gérardmer - Gerardmer Info, n.d.).* 53
Figure 22. *On the left, a buoy in Lake of Plobsheim used to measure the temperature at various levels of the lake (Plans d'eau - Fédération de Pêche Du Bas-Rhin, n.d.); on the right, a map of the location of the seven buoys in the Plobsheim lake.* 54
Figure 23. *Torrent Board* 56
Figure 24. *On the left are the Spectral responses of the CIMEL 312-2 at the central wavelength of each band (Payan et al., 2004); on the right, the CIMEL-312-2 is in operation in the field.* 57
Figure 25. *FLIR Camera T-560.* 58
Figure 26. *Samples of LSWT in the Issyk-Kul Lake in 2019 derived from the Landsat 8 mono-channel algorithms and multi-sensors in °C* 61
Figure 27. *Sensors intercomparison (Landsat 8 mono-channel algorithms, Sentinel-3, MODIS, Meteorological Station, and CCI Lakes) in the Issyk-Kul Lake in 2019* 62
Figure 28. *A sample from the Issyk-Kul Lake in 2019 of the SWA method showing the Banding/stripping effect.* 64
Figure 29. *Samples of LSWT in the Issyk-Kul Lake in 2019 derived from the Landsat 8 mono-channel algorithms* 64
Figure 30. *LSWT estimates in the Issyk-Kul Lake in 2019 derived from Landsat 8 mono-channel algorithms, compared to in-situ data and CCI Lakes product.* 65
Figure 31. *LSWT estimates in the Issyk-Kul Lake in 2019 from Sentinel-3, CCI Lakes, and in-situ data.* 67

Figure 32. *LSWT time series estimates in the Issyk-Kul Lake in 2020 derived from Sentinel-3, in-situ data, and CCI Lakes* *69*
Figure 33. *LSWT estimates in the Issyk-Kul Lake in 2019 derived from MODIS, in-situ data, and CCI Lakes* *70*
Figure 34. *LSWT time series estimates in the Issyk-Kul Lake in 2020 derived from MODIS, in-situ data, and CCI Lakes* *72*
Figure 35. *LSWT time series estimates in the Issyk-Kul Lake in 2019 derived from ECOSTRESS, in-situ data, and CCI Lakes* *73*
Figure 36. *LSWT time series estimates in the Issyk-Kul Lake in 2020 derived from ECOSTRESS, in-situ data, and CCI Lakes* *75*
Figure 37. *LSWT time series estimates in the Issyk-Kul Lake in 2019 derived from ECOSTRESS (SWA), in-situ data, and CCI Lakes* *76*
Figure 38. *Spatial distribution of the collection of the data in the field campaign in Issyk-Kul October 2021* *78*
Figure 39. *LSWT and air temperature measurements in the Issyk-Kul Lake by sensors on the Torrent Board on 05/Oct/2021 from 10:34 a.m. to 10:40 a.m. (local time)* *79*
Figure 40. *LSWT and air temperature measurements in the Issyk-Kul Lake by sensors on the Torrent Board on 05/Oct/2021 from 12:03 a.m. to 12:12 p.m. (local time)* *80*
Figure 41. *LSWT and air temperature measurements in the Issyk-Kul Lake by sensors on the Torrent Board on 05/Oct/2021 from 4:45 p.m. to 5:40 p.m. (local time)* *80*
Figure 42. *LSWT and air temperature measurements in the Issyk-Kul Lake by sensors on the Torrent Board on 07/Oct/2021 from 11:30 a.m. to 11:38 a.m. (local time)* *81*
Figure 43. *LSWT and air temperatures were measured in the Issyk-Kul Lake by sensors on the Torrent Board on 08/Oct/2021 from 3:20 p.m. to 4:23 p.m.* *82*
Figure 44. *LSWT derived from Sentinel-3 (left) and MODIS (right) in the Issyk-Kul Lake on 08/Oct/2021* *82*
Figure 45. *Spatial distribution of the data collection in the field campaign in the Issyk-Kul Lake on May 2023* *83*
Figure 46. *Temporal distribution of the data collection in the field campaign in the Issyk-Kul Lake on May 2023* *84*
Figure 47. *LSWT estimates in the Gerardmer Lake from 2021 to 2022 derived from in-situ data, ECOSTRESS, and Landsat 8-9 (SWA)* *85*
Figure 48*. LSWT estimates in the Longemer Lake from 2021 to 2022 derived from in-situ data, ECOSTRESS, and Landsat 8-9 (SWA)* *87*
Figure 49. *Spatial distribution of the data collection in the field campaign in Plobsheim Lake on April 2023* *88*
Figure 50. *LSWT estimates in the Plobsheim Lake in 2022 from in-situ data (buoys 2 and 4), MODIS, ECOSTRESS (SWA), and Landsat 8-9 (SWA)* *89*
Figure 51. *Multi-sensors validation in the Plobsheim Lake on 21/04/2023* *90*
Figure 52. *Spatial variability from multi-sensors in the Plobsheim Lake on 21/04/2023* *91*
Figure 53. *Spatial distribution of the data collection in the field campaign in the Plobsheim Lake on June 2023* *92*
Figure 54. *Multisensors validation in the Plobsheim Lake on 16/06/2023* *93*
Figure 55. *Spatial variability from multi-sensors in the Plobsheim Lake on 16/06/2023* *94*

List of Tables

Table 1. *Standard Thermal Infrared Instruments and Future Missions* 24
Table 2. *Coefficients* $a10$ *and* $b10$ *for the Landsat 8 TIRS Band 10 and associate Root Mean Square* 28
Table 3. *Values of* wvc *for Standard atmospheres* 28
Table 4. *Coefficients* a_k *in* $B(Ts)wvc$ *Model for Landsat 8 TIRS1 Data for Different* wvc *subranges* 31
Table 5. *The acquisition time for the sources to compare.* 60
Table 6. *Differences in temperatures in the Issyk-Kul Lake in 2019 between the meteorological station and all the sensors with their respective MAE and RMSE* 63
Table 7. *Differences of temperatures in the Issyk-Kul Lake in 2019 between the meteorological station and the Landsat 8 mono-channel algorithms and CCI Lakes with their respective MAE and RMSE* 66
Table 8. *Differences in temperatures in the Issyk-Kul Lake in 2019 between the in-situ data, CCI Lakes, and Sentinel-3 with their respective MAE and RMSE* 68
Table 9. *MAE and RMSE derived from the differences in temperatures in the Issyk-Kul Lake in 2020 between the in-situ data, CCI Lakes, and Sentinel-3* 69
Table 10. *Differences in temperatures in the Issyk-Kul Lake in 2019 between in-situ data, CCI Lakes, and MODIS with their respective MAE and RMSE* 71
Table 11. *MAE and RMSE derived from the differences in temperatures in the Issyk-Kul Lake in 2020 between the in-situ data, CCI Lakes, and MODIS* 72
Table 12. *MAE and RMSE derived from the differences in temperatures in the Issyk-Kul Lake in 2019 between the in-situ data, CCI Lakes, and ECOSTRESS* 74
Table 13. *MAE and RMSE derived from the differences in temperatures in the Issyk-Kul Lake in 2020 between the in-situ data, CCI Lakes, and ECOSTRESS* 75
Table 14. *MAE and RMSE derived from the differences in temperatures in the Issyk-Kul Lake in 2019 between in-situ data, CCI Lakes, ECOSTRESS, and ECOSTRESS (SWA)* 77
Table 15. *Measurements obtained in the Issyk-Kul Lake on the* 10^{th} *and* 11^{th} *of May 2023 with the Sentinel-3 and MODIS satellites and comparison at the same time with the CIMEL 312-2* 84
Table 16. *MAE and RMSE derived from the differences in temperatures in the Gerardmer Lake from 2021 to 2022 between in-situ data, ECOSTRESS, and Landsat 8-9 (SWA)* 86
Table 17. *MAE and RMSE derived from the differences in temperatures in the Longemer Lake from 2021 to 2022 between in-situ data, ECOSTRESS, and Landsat 8-9 (SWA)* 88
Table 18. *MAE and RMSE derived from the differences in temperatures in the Issyk-Kul Lake in 2022 between in-situ data, ECOSTRESS (SWA), and Landsat 8-9 (SWA)* 89
Table 19. *Measurements validation in the Plobsheim Lake on 23 April 2023 with the Torrent Board, CIMEL 312-2, ECOSTRESS, Landsat 8, Sentinel-3 and MODIS* 91
Table 20. *MAE and RMSE derived from the differences in temperatures in the Plobsheim Lake in 2022 between in-situ data (Torrent Board) and the Camera FLIR-T560.* 94

List of Acronyms

AATSR	Advanced Along-Track Scanning Raiometers
ASTER	Advanced Spaceborn Thermal Emission and Reflection Radiometer
AVHRR	Advanced Spaceborn Thermal Emission and Reflection Radiometeranced Very High Resolution Radiometer
BT	Brightness Temperature
CCI Lakes	Climate Change Initiative for Lakes
CEOP-AEGIS	Coordinated Asia-European long-term Observing system of Qinghai-Tibet Plateau hydro-meteorological processes and the Asian-monsoon systEm with Ground satellite Image data and numerical Simulations
CNES	The French National Centre for Space Studies
ECMWF	European Centre for Medium-Range Weather Forecast
ECOSTRESS	ECOsystem Spaceborne Thermal Radiometer Experiment on Space Station
EOS	Earth Observing System
ERA	ECMWF Interim Re-analysis
ESA	European Space Agency
ETM+	Enhanced Thematic Mapper Plus
EVC	Essential Climate Variable
FY-4	Feng-Yun 4 series
ISRO	Indian Space Research Organisation
ISS	International Space Station
LST	Land Surface Temperature
LSTE	Land Surface Temperature and Emissivity
LSTM	Land Surface Temperature Monitoring
LSWT	Lake Surface Water Temperature
MAE	Mean Absolute Error
MODIS	Moderate Resolution Imaging Spectroradiometer
MODTRAN	Moderate resolution atmospheric TRAsmittance and radiance
NASA	The National Aeronautics and Space Administration
RMSE	Root Mean Square Error
SBG	Surface Biology and Geology
SLSTR	Sea and Land Surface Temperature Radiometer
SRF	Spectral Response Function
T_0	Air temperature
TIR	Thermal InfraRed
TOA	Top of the Atmosphere
TRISHNA	Thermal infraRed Imaging Satellite for High-resolution Natural resource Assessment
wvc	Water vapor content

Résumé

Les lacs jouent un rôle essentiel dans l'écosystème hydrologique et donc sur la régulation de cette ressource cruciale que constitue l'eau douce. En raison de leur sensibilité au climat et leur capacité à s'adapter rapidement aux changements, ils sont considérés comme des sentinelles du changement climatique. En complément du suivi des surfaces/hauteurs, de la fréquence de formation de glace sur les lacs, et des évolutions de la qualité des eaux, la température de surface de l'eau du lac (LSWT – Lake surface Water Température) est une mesure physique cruciale pour l'étude des phénomènes hydrologiques et météorologiques liés au changement climatique.

La LSWT mesure la température d'une fine couche de surface du lac. Cependant, elle a un impact significatif sur l'environnement aquatique et la chimie de l'eau, ce qui en fait une indication cruciale de l'état de santé des lacs. En outre, les conditions météorologiques et l'atmosphère qui entourent les grands lacs sont influencés par la température de l'eau de surface du lac. De nombreuses applications nécessitent des données sur la température de l'eau avec des résolutions spatiales et temporelles accrues, comme par exemple l'étude du cycle hydrologique et du changement climatique, de l'habitat de l'ecosystème aquatique, la pêche et l'aquaculture ainsi que la gestion de la qualité de l'eau.

La recherche presentée dans cette thèse vise à acquérir et à analyser la LSWT à l'aide de capteurs satellitaires TIR tels que Landsat 8-9, ECOSTRESS, Sentinel-3 et MODIS. Ces capteurs fournissent des informations précieuses en prévision de nouvelles missions TIR telles que TRISHNA en 2025 (CNES-ISRO) et de missions à plus long terme telles que LSTM (ESA Copernicus) et SBG (NASA), toutes deux en 2028. Cette thèse estime la LSWT de plusieurs lacs, tels que le lac Issyk-Kul au Kirghizstan et les lacs Gerardmer, Longemer et Plobsheim en France. Pour évaluer la LSWT, des résolutions temporelles et spatiales modérées et élevées sont envisagées afin d'obtenir des mesures spatiales et temporelles plus denses. Ces densités de résolutions sont nécessaires pour comprendre les processus et la dynamique dans le domaine thermique et ses changements dans le temps et l'espace. En outre, plusieurs validations de la

LSWT par comparaison avec des mesures in situ et de données issues de campagnes de validation ont été menées sur les lacs considérés dans cette étude sur différentes années.

L'organisation de cette thèse est la suivante :

Le chapitre 1 présente le contexte de l'extraction de la LSWT avec une approche multirésolution multi-capteurs. La littérature existante dans le domaine de l'infrarouge thermique provenant de différentes études et applications a été étudiée. Les objectifs de cette thèse sont également présentés dans ce premier chapitre.

Le chapitre 2 décrit les différents algorithmes permettant d'obtenir les données LSWT au niveau 1 de l'imagerie Landsat 8, 9 et ECOSTRESS, ainsi que l'analyse des produits LSWT utilisés dans cette recherche et leurs étapes de géotraitement, telles que l'application de masques de nuages pour certains des produits.

Le chapitre 3 décrit les caractéristiques physiques et climatologiques des régions considérées comme zones d'étude. Il présente également la liste et la description des ensembles de données utilisés pour cette recherche, tels que les produits LST (Land Surface Temperature), utilisés pour extraire le LSWT et les images de niveau 1 utilisées pour exécuter les algorithmes d'extraction avec ses paramètres atmosphériques d'entrée.

Le chapitre 4 présente les résultats de la comparaison des algorithmes pour Landsat 8-9 et ECOSTRESS, la performance des produits LST et de leurs masques de nuages, ainsi que validation croisée entre tous les capteurs TIR et les ensembles de données in situ. En outre, ce chapitre explique les résultats obtenus, leurs implications ou conséquences, en décrivant les limites de cette recherche par rapport aux contributions à la littérature antérieure.

Le chapitre 5 présente la somme des principaux résultats, conclusions et perspectives, où certains de ces résultats donnent lieu à des suggestions pour l'avenir.

Le **chapitre 1** présente l'importance de l'eau douce en tant que ressource naturelle, le rôle des lacs dans l'écosystème hydrologique. Il décrit également les méthodes de détermination de la température de surface de l'eau (LSWT) à l'aide de techniques multi-capteurs et multi-résolution, ainsi que l'ensemble de la littérature actuelle dans le domaine de l'infrarouge

thermique classé par type de résolution spatiale et temporelle : moyenne et haute résolution. Ce chapitre énonce aussi les objectifs de cette thèse, qui peuvent se résumer ainsi :

- Obtenir et analyser la LSWT à partir de plusieurs capteurs avec des résolutions spatiales, temporelles, et spectrales différentes. Cette synergie permettrait d'obtenir des mesures spatiales et temporelles de la LSWT plus denses nécessaires à la compréhension des processus et de la dynamique dans le domaine thermique et de ses changements dans le temps et l'espace. Les capteurs TIR utilisés dans cette étude sont classés en fonction de leurs résolutions spatiales et temporelles. Pour la basse résolution spatiale, nous avons utilisé MODIS (Terra) et SLSTR (Sentinel-3), tous deux avec une résolution de 1 km et un temps de revisite quotidien. Comme haute résolution spatiale nous avons utilisé (i) ECOSTRESS, qui est un capteur à bord de l'ISS (International Space Station) ayant une résolution de 70 m et un temps de revisite de 3 à 5 jours, et (ii) TIRS, embarqué sur les satellites Landsat 8 et Landsat 9, avec une résolution de 100 m et un temps de revisite de 16 jours.
- Valider la LSWT en la comparant avec des mesures in situ. Des campagnes de validation ont été menées sur le lac Issyk-Kul (Kirghizstan), ainsi que sur trois lacs de la région française du Grand-Est (lacs de Gerardmer, Longemer, et Plobsheim).

Le **chapitre 2** décrit les différents algorithmes permettant de récupérer les données LSWT et les produits LSWT utilisés par satellite :

<u>Landsat 8/9</u>

Les algorithmes d'obtention de la LSWT à partir de Landsat 8/9 ont été obtenus à partir de la littérature afin d'effectuer des comparaisons et de déterminer la méthode la plus fiable dans le cadre de cette recherche. Les méthodes utilisées sont les suivantes :

- Algorithme mono-canal (MWA – Mono Window Algoritm)
- Algorithme à canal unique (SCA – Single Channel Algorithm)
- Canal unique basé sur le contenu en vapeur d'eau (PSCwvc – Practical Single Channel)
- Algorithme à deux canaux (SWA – Split Window Algorithm)

Ces méthodes utilisent une approche à un seul canal (TIR1 - Bande 10), laissant de côté le TIR2 - Bande 11, en raison des effets de lumière parasite qui affectent ce canal. Cependant, la NASA a récemment mis à jour et mis à disposition la Collection 2 pour Landsat 8 et 9, où les performances des instruments radiométriques ont été améliorées, rendant possible l'utilisation de la méthode SWA. L'information obtenue de cette manière devrait être plus précise que les méthodes utilisant un seul canal.

Sentinel-3, MODIS, ECOSTRESS

En outre, l'analyse LSWT utilisant les produits dérivés LST des capteurs TIR à moyenne et haute résolution a été réalisée :

- LSWT de Sentinel-3 (SLSTR)
- LSWT de MODIS (Terra)
- LSWT de ECOSTRESS (Algorithme à deux canaux (SWA) pour ECOSTRESS : Cet algorithme a été développé car les résultats fournis avec le produit original (ECO-LSTE) obtenus avec l'algorithme TES ont montré être surestimés.

Les températures obtenues à partir des données multi-résolutions et multi-capteurs provenant des satellites à haute résolution (Landsat 8-9, ECOSTRESS) et des satellites à résolution modérée avec un temps de revisite quotidien (Sentinel-3 et MODIS) sont comparées avec les données de la station météorologique, des bouées, des instruments installés sur la planche Torrent, du radiomètre CIMEL 312-2 et de la caméra FLIR. L'utilisation de plusieurs capteurs et la synergie de leurs données permettent de surmonter les inconvénients de capteurs individuels et d'améliorer la précision et la couverture globales des mesures de LSWT.

Des zones d'intérêt ont été définies pour les quatre lacs afin d'évaluer les températures représentatives de ces zones et de réduire l'incertitude de l'utilisation de pixels qui pourraient ne pas être associés à l'eau.

Le **chapitre 3** présente les caractéristiques physiques et climatologiques des régions d'étude. Pour cette thèse, nous avons considéré le lac Issyk-Kul (Kirghizstan, Asie centrale) comme

premier cas d'étude. Le lac Issyk-Kul est le septième lac le plus profond du monde avec une profondeur maximale de 668 m, une altitude de 1 607 m et une surface d'eau de 6 230 km^2.

Les autres lacs étudiés dans le cadre de cette recherche sont des lacs de la région Grand-Est (France) : Le lac de Gérardmer, d'une superficie de 1,16 km^2, d'une profondeur de 36,2 m et d'une altitude de 660 m ; le lac de Longemer, d'une superficie de 0,76 km^2, d'une profondeur de 29,5 m et d'une altitude de 668 m. Ce sont des lacs glaciaires situés dans le massif des Vosges en France. Enfin le lac de Plobsheim, avec une superficie de 6,6 km2, est le plus grand plan d'eau du département du Bas-Rhin et est une retenue artificielle aux eaux claires et peu profondes de 3 m en moyenne.

Ce troisième chapitre présente également la liste et la description des ensembles de données utilisés pour cette recherche, tels que les produits LST, l'imagerie de niveau 1 pour exécuter les algorithmes de détermination de la LSWT et les paramètres atmosphériques d'entrée :

Données d'imagerie

Un ensemble d'images de 2019 à 2023 a été sélectionné à partir des satellites avec leurs capteurs et produits correspondants

- Landsat 8-9 (TIRS)
- MODIS (Terra)
- Sentinel-3 (SLSTR)
- ECOSTRESS
- CCI Lakes (produit LSWT)
- Colonne de vapeur d'eau atmosphérique (wvc) et température de l'air près de la surface (T_0)

Données sol et atmosphériques

Fichiers des données des stations fixes météorologiques

- Données in situ provenant de bouées
- Planche Torrent : contient des capteurs pour mesurer la température de l'eau, la température de l'air et l'humidité.

- Radiomètre CIMEL 312-2
- Caméra infrarouge FLIR T-560

La station météorologique située sur le site dans la zone nord de la région du lac Issyk-Kul fournit deux valeurs journalières de température de l'eau. Pour les lacs de Gerardmer et Longemer, des données in situ ont été fournies par des bouées qui ont mesuré les températures de profil depuis 50 cm jusqu'à la profondeur maximale (34 m pour Gérardmer et 29 pour Longemer), enregistrant une température chaque heure. Les mesures des bouées du lac de Plobsheim sont effectuées à l'aide d'enregistreurs multi-paramètres fixés sur 7 bouées situées à environ 1 m sous la surface de l'eau, réparties du nord au sud du lac, avec une fréquence d'acquisition de 30 minutes.

D'autre part, les ensembles de données CCI Lakes v. 2.0.2 qui sont une combinaison de produits ATSR-2, AATSR et AVHRR-3, avec une résolution spatiale de près de 1 km (1/120 degrés), avec une résolution temporelle journalière ont été utilisés.

Le **chapitre 4** présente les résultats obtenus et leurs analyses et la comparaison des estimations de LSWT avec les études précédentes. Lors de l'étude du lac Issyk-Kul, les LSWT obtenues avec les algorithmes PSCwvc et le SCA pour Landsat 8 ont montré une meilleure fiabilité dans l'approximation des LSWT avec d'autres sources (MWA, SWA), autour de 1 à 2 °C. Des études précédentes utilisant ces algorithmes ont conclu que le SWA et SCA sont fiables par rapport aux mesures in situ, et les erreurs d'estimation ont été attribuées à la qualité des données de la vapeur d'eau atmosphérique.

En termes d'intercomparaison des capteurs, Sentinel-3 et les données de la station météorologique ont montré des valeurs LSWT cohérentes entre elles (1 °C), tout comme ECOSTRESS et MODIS, bien qu'avec une plus grande variation (1-2 °C). Des études antérieures comparant ces capteurs avec des mesures in situ ont montré qu'ECOSTRESS sous-estimait la température de surface au printemps et en été, comme observé dans la présente étude.

La validation au sol a été effectuée en octobre 2021 sur le lac Issyk-Kul. L'instrumentation utilisée pour cette campagne comprenait des capteurs pour mesurer l'humidité, la température de l'eau et de l'air, installés sur une plateforme flottante appelée planche Torrent, un

instrument assemblé dans le cadre de cette thèse au laboratoire ICube (équipe TRIO). Une seconde mission Issyk-Kul s'est déroulée en avril 2023, permettant de receuillir des mesures de températures de surface cette fois à l'aide d'un radiometre CIMEL 312-2.

Aux dates d'acquisition terrain, certains capteurs satellitaires (ECOSTRESS et Landsat 8) n'étaient pas disponibles. Cependant, il y a eu un passage de Sentinel-3 et un de MODIS . Malgré la couverture nuageuse, les mesures de terrain effectuées par la planche Torrent ont pu être comparées avec ces deux capteurs. Les mesures à 5 cm et à 10 cm de profondeur affichaient des valeurs légèrement inférieures aux températures plus profondes (15 et 35 cm), la différence entre ces deux plages étant inférieure à 0,2 °C environ. La température de l'air n'a pas montré de forte corrélation avec les températures de l'eau, avec des températures de l'air entre 14,5 et 16,5 °C. Les LSWT de Sentinel-3 sont les valeurs les plus proches des LSWT de la planche Torrent (0,3 °C), et les LSWT de MODIS montrent une différence de 1,3 °C par rapport à la planche Torrent ce qui tend à montrer que Sentinel-3 fournit des valeurs plus fiables.

Pour les zones d'étude situées en France, plus précisément pour les lacs de Gerardmer et de Longemer, des séries temporelles d'images Landsat 8-9 et ECOSTRESS couvrant la période de janvier 2021 à mai 2022 ont été traitées. Une analyse spatio-temporelle a été réalisée afin d'observer les différentes variations de températures et de comparer ces résultats avec les mesures in-situ. Les températures de la collection 2 de Landsat 8-9 ont été obtenues à l'aide de l'algorithme SWA. Les ensembles de données fournis par Landsat 8-9 sur Gérardmer et Longemer sont plus proches des mesures in situ (écart de 2-3 °C) que ceux d'ECOSTRESS (écart de 5 °C), où les températures ont chuté à des niveaux très bas, ce qui pourrait être associé à la présence de nuages au-dessus de la région. En outre, les valeurs de l'écart-type sont plus élevées pour ECOSTRESS dans la plupart des dates représentées.

Sur le lac de Plobsheim, les températures des bouées dans le lac sont plus proches des températures de ECOSTRESS (1-2 °C) que de celles de MODIS ou de Landsat 8-9 (3-4 °C). Pour la validation sur le terrain, la différence entre le radiomètre CIMEL 312-2 et la planche Torrent est inférieure à 1 °C, alors que les différences sont inférieures à 2 °C par rapport aux autres capteurs (ECOSTRESS, Landsat 8-9, MODIS et Sentinel 3). D'autre part, les valeurs dérivées de la

caméra FLIR-T560 présentent des différences supérieures à 2 °C par rapport au reste des capteurs, mais inférieures à 2 °C par rapport aux valeurs de la planche Torrent.

Le **chapitre 5** présente la somme des principaux résultats, conclusions et perspectives. Différentes approches d'extraction des LSWT à partir de satellites à haute et moyenne résolution ont été testées et comparées. Les satellites et leurs capteurs correspondants utilisés pour cette recherche sont Landsat 8-9 (TIRS), MODIS (Terra), Sentinel-3 (SLSTR) et ECOSTRESS. Une première série d'images a été sélectionnée, sur la base de critères tels que la date d'acquisition, un temps clair et une couverture aussi large que possible, avec au moins une image par mois ; cependant la disponibilité d'ECOSTRESS était réduite à Issyk-Kul.

Les premiers résultats de cette analyse ont été l'application du processus de détermination de la LSWT sur le lac Issyk-Kul avec MWA, PSCwvc et SCA, après avoir exclu SWA en raison de la lumière parasite dans Landsat 8 collection 1, provoquant un effet de bande ou de stripping, fortement visible dans la bande 11 (TIRS-2). D'autre part, pour les algorithmes à canal unique appliqués à la collection 1 de Landsat 8, la MWA n'est pas aussi cohérente que la PSCwvc ou la SCA à la méthode de validation croisée, ce qui explique que ces deux dernières méthodes aient montré une meilleure fiabilité pour l'approximation de la LSWT entre les différents ensembles de données et produits.

Pour effectuer la validation dans le lac Issyk-Kul la planche Torrent transportant les capteurs pour mesurer l'humidité, les températures de l'air et de l'eau (jusqu'à 35 cm de profondeur) a été développée. Elle a permis de montrer que les LSWT pour Sentinel 3 sont les valeurs les plus proches des LSWT de la planche Torrent, avec une différence de 0,3 °C et une difference d'heure d'acquisition de 4 heures. Pour les LSWT par MODIS, comparées aux valeurs de la planche Torrent, les températures ont des différences de 1,3 °C et une difference d'heure d'acquisition de 3 heures. Cela peut être expliqué par un couvert nuageux à l'heure du passage du MODIS.

D'autre part, l'analyse sur les lacs de Gérardmer et de Longemer a montré que les données d'ECOSTRESS ont des valeurs sous-estimées de 5 °C et les données Landsat 8-9 de 2 °C. Pour l'analyse à la même date entre ces deux sources, les jeux de données sont généralement

cohérents entre eux. Cependant, les températures obtenues avec l'algorithme de SWA pour Landsat 8-9 sont plus proches des données in situ. L'analyse de ECOSTRESS a été limitée au masque de nuages pour présenter une image plus propre, mais ce masque n'a pas réduit l'écart-type des résultats.

Dans le cas du plan d'eau de Plobsheim, les mesures de température issues de Landsat 8-9 ont présenté des différences plus élevées que ECOSTRESS et MODIS (ce qui pourrait être lié à une limitation de la détection du masque nuageux pour Landsat 8-9), bien qu'elles soient cohérentes entre elles. Les valeurs de ECOSTRESS et MODIS sont plus fiables par rapport aux mesures in-situ. D'autre part, pour la validation sur le terrain, les valeurs de LSWT issues d'ECOSTRESS et de Landsat 8-9 sont plus proches des mesures in-situ dérivées de la planche Torrent et du radiomètre CIMEL. Il faut noter que les mesures dérivées de la caméra FLIR-T560 ont montré le plus grand écart par rapport à celles obtenues par l'ensemble des capteurs déployés sur le terrain, mais moins de différence avec les valeurs de la planche Torrent. Cela peut être dû à des difficultés de manipulation de la caméra ou à des problèmes de calibration de cet instrument.

De façon générale, en ce qui concerne la performance des produits LSWT utilisés, on peut dire que ceux qui utilisent la méthode SWA pour leur génération, contrairement à ceux qui utilisent l'algorithme TES (ECOSTRESS), ont démontré une meilleure proximité par rapport aux valeurs in-situ. Nous pouvons conclure que SWA ne demande pas de corrections atmosphériques préalable au contraire de l'algorithme TES, où la précision peut être affectée par des perturbations dans les conditions atmosphériques.

Sentinel-3 est une nouveauté dans cette étude car, jusqu'à cette recherche, il n'y a pas eu d'études antérieures où les températures des lacs ont été estimées avec ce capteur. La nouveauté réside également dans la comparaison de Sentinel-3 avec des satellites à haute résolution tels que ECOSTRESS et Landsat 8-9, où l'approche sectorielle pour ECOSTRESS est testée pour comparer la même méthode d'extraction en utilisant des méthodes d'approche sectorielle.

Les estimations LSWT du radiomètre CIMEL CE 312-2 montrent une bonne fiabilité par rapport aux capteurs de la carte Torrent, avec moins de 1 °C de différence de température, contrairement à la caméra FLIR-T560, qui montre une plus grande différence de température entre tous les capteurs et moins de 2 °C de différence avec les capteurs des valeurs de la carte Torrent. Cela pourrait être dû à des problèmes d'étalonnage de l'instrument.

En termes de perspectives, pour obtenir une validation et un suivi optimaux des températures des lacs, des mesures expérimentales et par satellite doivent être mises en œuvre. Certaines recommandations pourraient être envisagées à cette fin Collecte de données au sol (in situ) et des satellites :

- Déployer des capteurs de température compris à la surface, au milieu et au fond du lac.
- Mettre en place un système de contrôle et de mise à jour continus afin de garantir l'exactitude de l'ensemble des données relatives à la température des lacs. En outre, des radiomètres et des caméras FLIR pourraient être utiles pour compléter la surveillance.
- Combiner des mesures multipoints au sol avec des données LSWT à haute résolution spatiale acquises à partir de plates-formes de véhicules aériens sans pilote (UAV) - des drones ou des avions équipés de capteurs thermiques.
- Acquérir des données de télédétection par satellite avec des capteurs les plus fiables comme Sentinel-3, voire de MODIS pour les grands lacs d'extension principalement, et celles de Landsat 8-9 et d'ECOSTRESS (SWA) pour les lacs plus petits.
- En ce qui concerne la mesure de la température à différentes profondeurs, l'imagerie satellitaire et aérienne peut être utilisée pour estimer la profondeur des lacs. En effet, le LiDAR (Light Detection and Ranging) et l'altimétrie satellitaire peuvent fournir des informations sur l'élévation de la surface de l'eau, qui peuvent ensuite être utilisées pour déduire la profondeur.

Dans le futur, une analyse plus approfondie des images pourrait être envisagée à partir de capteurs à faible résolution tels que Fengyun-4 (FY-4A), équipé de l'instrument AGRI (Advanced Geosynchronous Radiation Imager) pour le produit LST, avec une résolution spatiale de 4 km, une résolution radiométrique IR de 10,3 à 13,8 µm et une résolution temporelle de 15 minutes. AGRI constitue donc l'outil optimal pour couvrir la résolution temporelle limitée offerte par les capteurs TIR à résolution modérée et élevée.

Analyser les possibilités de synergie entre le domaine optique thermique et les micro-ondes passives (ensembles de données en bande C et en bande L) pour éviter le problème de la couverture nuageuse, en appliquant un processus de réduction d'échelle, reste une voie à explorer.

Chapter 1. Introduction

This chapter introduces the context of freshwater as an essential resource, the role of lakes in the hydrological ecosystem, and Land Surface Water Temperature (LSWT) retrieval using a multi-sensor, multi-resolution technique. The aims of this thesis are also stated in this chapter, along with the body of current literature on the thermal infrared domain used in various investigations and applications.

1.1 Context

Between 1992 and 2020, 53% of the most extensive worldwide lakes had substantial storage decreases. Around one-quarter of the world's population resides in a basin of a draining lake, where a combination of climate warming, increasing evaporative demand, human water consumption, and sedimentation contribute to the decrease in natural lake volume (Yao et al., 2023). Within the freshwater resource context, as a fundamental need for our society, lakes are essential for social and economic processes and for the sustainable development of the regions. These processes and development include food production and water provision for agricultural, domestic, and industrial use. Lakes are also significant as a hydrological ecosystem related to the quality of the environmental status of a region. They are considered sentinels of climate change due to their ability to respond to changes in various climate factors rapidly and convey multiple signals of climate change (Alsdorf et al., 2007; Dokulil, 2014; Williamson et al., 2009; K. Yang et al., 2019). The lakes are part of the water cycle, where the evaporation, condensation and precipitation may take place, interacting with the atmosphere, surface water, and groundwater throughout the hydrological cycle (Figure 1). The exchange between lakes and the atmosphere affects the heat budget, which regulates lake water temperatures. Water temperature determines ecological conditions, influencing lakes' water chemistry and biological processes and affecting their living organisms (Peng et al., 2021). Rising water temperatures can lead to the extinction or altered distribution of cold-water species, as warm-water species may

outcompete or replace them (Solheim et al., 2010). For instance, in aquatic ecosystems, the increase in temperature affects primary production and algal community composition, leading to changes in community structure, especially in environments with tempertures between 25 to 30 °C (Dallas, 2008). Yang et al. (2022) state that the rise in lake surface water temperature (LSWT) has several consequences on the growth and reproduction of aquatic creatures and plants in the lake. Higher water temperatures impact the metabolic rate of organisms in the environment, resulting in changes in the species of aquatic plants and a decrease in phytoplankton numbers. Changes in LSWT can also affect the algae composition in the lake. The warming of LSWT can affect temperate fish's reproductive and life cycles. Furthermore, warming LSWT can impact the biochemical activities of many species in the lake, such as nutrient release and the creation of distinct development conditions for some algae groups (Yang et al., 2022).

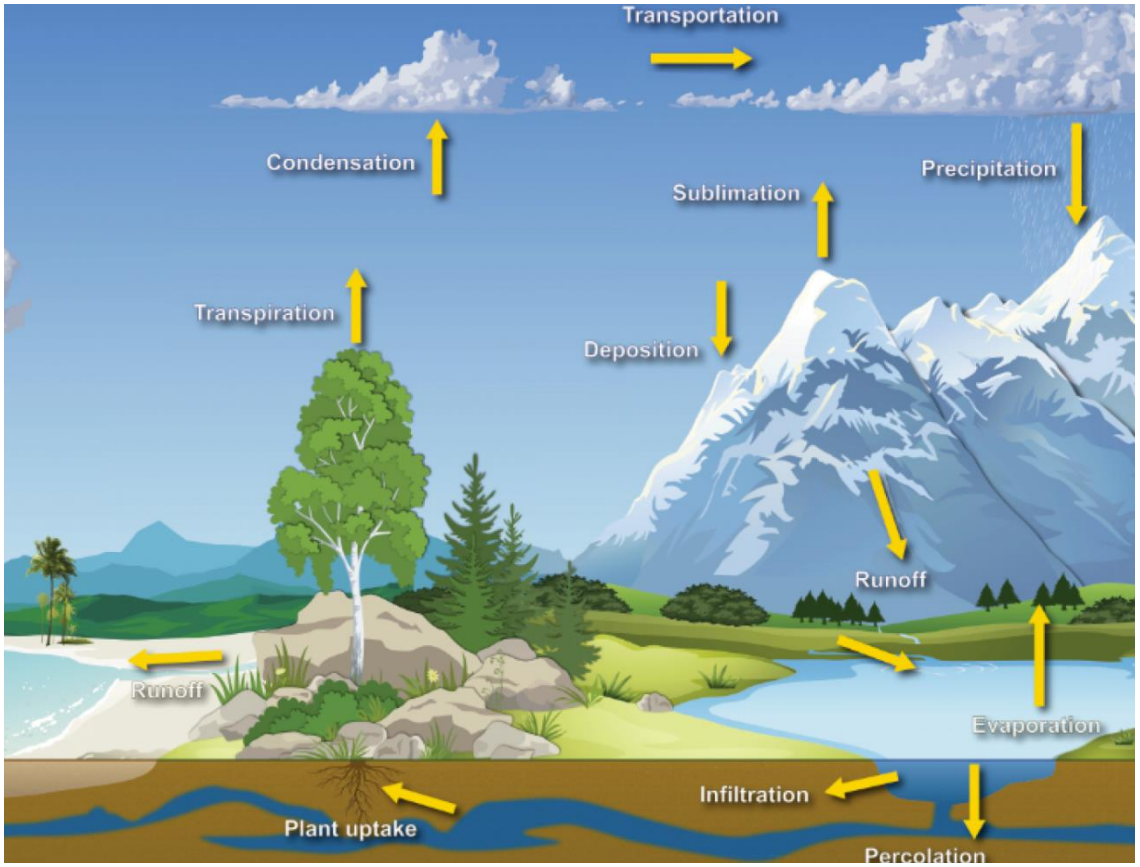

Figure 1. *The hydrological cycle in a natural ecosystem (Water Cycle | National Oceanic and Atmospheric Administration, n.d.)*

The study of surface energy and water balance and other applications, including evapotranspiration, climate change, and vegetation monitoring, rely heavily on land surface temperature (LST) (Dash, 2005). LST provides valuable information about surface energy and water balance processes at regional and global scales (Zheng et al., 2019). Due to surface features and atmospheric factors, estimating LST with high accuracy using satellite thermal infrared (TIR) data is complex. Uncertainties aspects like atmospheric transmittance/radiance coding, understanding of land surface emissivity, atmospheric profiles, and topographic influences all affect how well LST is estimated, resulting in errors in LST estimation from satellite data, making it challenging to find representative and thermally homogeneous areas for ground LST validation (Li et al., 2017). The same authors highlighted the challenges in current LST products, such as spatial discontinuity and short periods. They suggested effective methods to overcome them, discussing the significant applications of LST products in various fields, including agricultural drought monitoring, thermal environment monitoring, and climate change studies. It also suggested the necessity of spatiotemporal seamless LST data. It offered perspectives to optimize retrieval methods and promote their applications, concluding that satellite observation provides the only way to measure LST worldwide, allowing for large-area coverage and regular temporal revisiting. Regarding TIR imagery, the study acknowledges the continuous development of LST retrieval algorithms, newly launched TIR instruments, and new releases of LST products (Li et al., 2023).

LSWT is an essential physical parameter in studying meteorological and hydrological phenomena (Yang et al., 2019). Climatic factors such as air temperature, solar radiation, and cloud cover, additionally to geographical factors including depth, lake altitude, surface, and continentality, could influence the variation of the LSWT (Layden et al., 2015; Sharma et al., 2015). Like the oceans, the water temperature of lakes is controlled by the exchange between the atmosphere, showing a strong correlation with the air temperature and producing variations in the heat fluxes composing the high heat budget (Peng et al., 2021; Schneider et al., 2019). Maps representing the LSWT, revealing patterns or variations that hint at the underlying structure and behavior of water, can help to provide information on the vertical thermal

structure of the lake, determined by the turbulence, particularly in the upper mixed layer, influencing the local weather helpful in monitoring the quality of the water and as a good indicator of climate change (Fiedler et al., 2014; Woolway, 2014).

Validation is the process of assessing, by independent means, the quality of the data products derived from the system outputs (Justice et al., 2000). The validation for LST products derived from satellite-borne observations determines LST product uncertainties, which is vital for various applications and provides feedback to the developers of LST retrieval algorithms for improvements (Coll et al., 2009; Li et al., 2014). The temperature-based (T-based), the radiance-based (R-based), and the intercomparison methods are three methods for validating LST products (Guillevic et al., 2014; Li et al., 2013). They provide different levels of information about the quality of LST (Guillevic et al., 2018; Guillevic et al., 2014) and can be operated complementary to gain a more comprehensive assessment of the uncertainty of LST products (Gomis-Cebolla et al., 2018; Liu et al., 2015). The following sections present these three methods' principles, advantages, and disadvantages.

In terms of ground validation sources for LSWT, one of the methods to measure water temperature is using in-situ sensors, either automatic or manual thermometers, such as buoys distributed at different lake locations and at different intervals and depths. Thus, datasets are produced more heterogeneously; however, for studying the lakes' dynamics, datasets must have spatial coverage (Lieberherr et al., 2018). Besides, these methods have logistics limitations, are costly and time-consuming, and the instrumentation sometimes could be exposed to outdoor damage (Dyba et al., 2022). Another excellent method for identifying the dynamic of the temperature, having localized spatial coverage and homogeneous datasets for evaluating how these temperatures could affect a lake's ecosystem, is the use of airborne sensors. However, a disadvantage of employing these instruments is that only specialists can execute this technology, which adds substantial time and extra effort to their deployment (Glen George, 2012; Rahaghi et al., 2018).

Besides the in-situ measurements, satellite-based observations are another method to study the variation of the LSWT by using instruments measuring in the thermal infrared range

(Battarbee et al., 2008; Guo et al., 2022). This technique offers the advantage of obtaining information in challenging or inaccessible areas on Earth. Thermal Infrared Radiation (TIR), within the electromagnetic spectrum, is the wavelength range from 8 to 14 μm (Schneider et al., 2019). The amount of electromagnetic radiation (light) emitted, reflected, or transmitted by a surface or object at a specific wavelength or frequency is referred to as spectral radiance, a key term in remote sensing (Shaw et al., 2013).

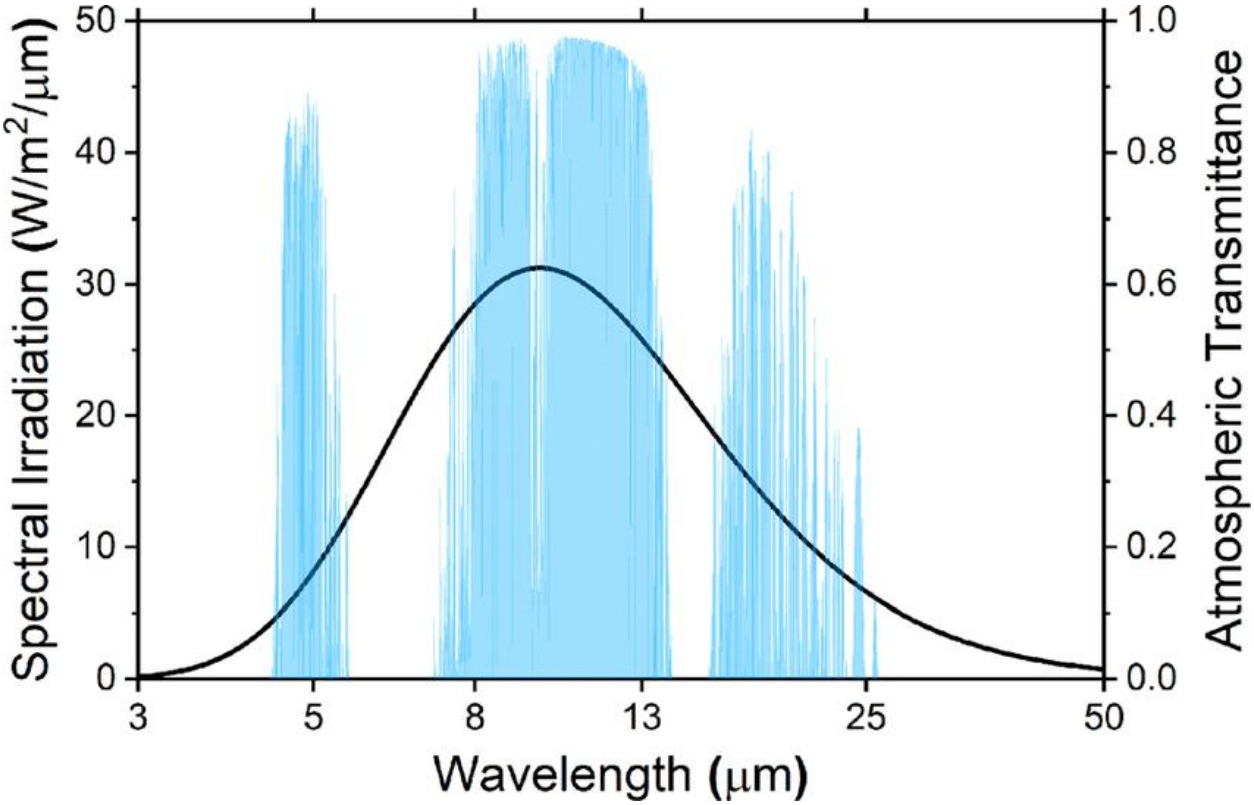

Figure 2. *Spectral irradiation for a 300 K blackbody with an example of atmospheric transmittance (Zhao et al., 2019)*

According to Wien's Displacement Law, all materials with a temperature over 0 K produce radiation. This Law is a fundamental principle in thermal radiation that describes the relationship between the wavelength of the maximum intensity of radiation emitted by a blackbody and its temperature. It states that the wavelength of maximum intensity (λ_{max}) is inversely proportional to the temperature (T) of the blackbody (Becker & Li, 1990). Wien's displacement law states that the spectral radiance of black-body radiation per unit wavelength

peaks at the wavelength λ_{max}, it is given by $\lambda_{max} = \frac{2898}{T}$ (in µm/K) (*Radiant Flux - Wikipedia*, n.d.). For instance, the temperature of a blackbody at 300 K (Figure 2), which is the earth's average temperature, has its peak of the radiated energy emitted at the longer wavelength of 9.7 µm. The wavelength range between 8 and 13 µm, which is also the spectral region used by the sensors considered in this research, is usually termed the atmospheric window due to the high atmospheric transmittance (highlighted in blue), which refers to the measure of how much electromagnetic radiation can pass through the Earth's atmosphere without being absorbed or scattered (Zhao et al., 2019).

Measurements from sensors of satellite missions facilitate temporal and spatial temperature variations at different scales from different surface temperatures in the TIR domain, helping to understand the physical processes in the water cycle (Michel et al., 2021). The remote sensing observations and in-situ measurements agreed with the warming trend of global and regional lakes (Peng et al., 2021).

Unfortunately, instrument noise and drift, sun glare, residual cloud contamination, misspecification of air attenuation, and surface emissivity effects are the principal sources of inaccuracy in satellite-derived LSWTs. Additionally, other innacuray can be derived from the possible differences in measurement at different levels of a lake (Figure 3), known as stratification, which is a common occurrence in many lakes and reservoirs when comparing temperatures from the skin surface (satellites) and in-situ temperatures at different levels. The stratification describes the vertical layering of water in a lake that results from the equilibrium of buoyancy and turbulence forces. During stratification, the lake consists of different layers, including the epilimnion, or mixed layer, it is the part of the water column immediately below the water surface; the thermocline, which it is layer in a thermally stratified lake where there is a rapid change in temperature with depth; and hypolimnion, which is the most dense and coolest layer in contact with the lake's bottom and it is separated by the thermocline. The specific depths of these layers can vary from lake to lake, and factors such as lake size, wind speed, water clarity, and geographical location influence the depths of each stratification layer (Woolway, 2014).

These sources of inaccuracy can cause discrepancies between radiometric skin surface temperatures associated with satellite retrievals and bulk water temperatures recorded by surface buoys. The cold skin (the very thin layer of water at the very surface of a lake that is slightly cooler than the underlying water), and warm layer (below the cold skin layer, there is often a layer of warmer water) influence the temperature variations between the skin and bulk water temperature, which it refers to the average temperature of the entire water mass within the lake (Crosman et al., 2009). Besides the limitations, such as cloud cover or sensor failure, there are TIRS sensors that provide frequent revisit times (once per day). However, they offer a spatial resolution of 1 km or, in the case of the geostationary meteorological satellites, 15-minute measurements with a 4 km spatial resolution. In contrast, there are sensors with lower temporal resolution (16 days) but presenting a better spatial resolution (70-100 m) (Silvestri et al., 2020). Considering this, the use of missions with TIRS channels restricts the number of sensors exploited to retrieve temperatures, where the lack of studies by combining multi-sensors at different resolutions exists. Hence, using and analyzing multi-spatial and temporal resolution sensors should be able to extract the LSWT more accurately for a better interpretation of the dynamics in the regions of interest (Tavares et al., 2019).

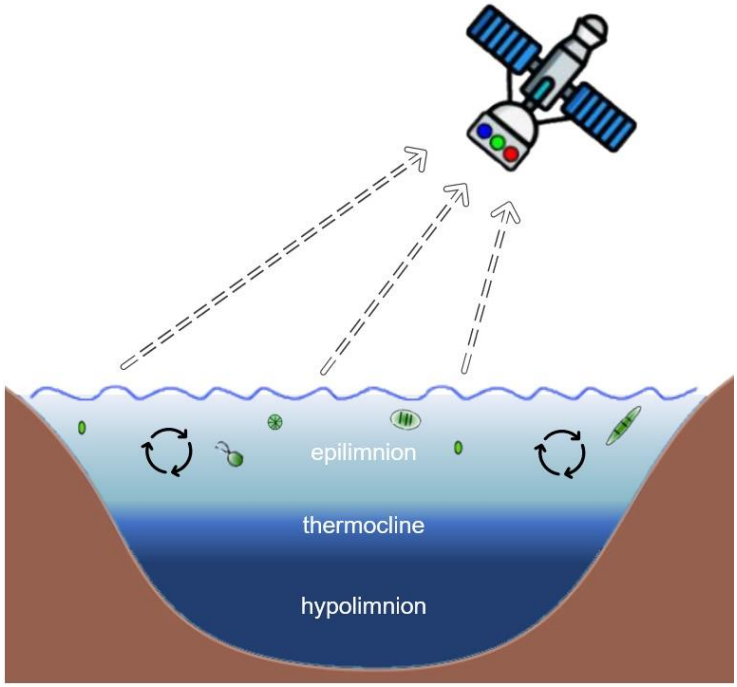

Figure 3. *Illustration of stratification in a lake and the LSWT acquisition using satellites (Perrone et al., 2021)*

Moreover, the current satellites will serve as precursors of new missions, carrying onboard multispectral bands with high spatial resolutions in the TIR domain below 100 m. Missions such as the Thermal Infrared Imaging Satellite for High-resolution Natural Resource Assessment (TRISHNA) is a collaboration between The French (CNES) and Indian (ISRO) space organizations. This satellite, planned for 2025, contains five bands to measure the visible and the near-infrared and four bands to measure the thermal infrared signal of the surface atmospheric system worldwide. Moreover, the TRISHNA mission will have daytime and nighttime overpasses with a 1- to 3-day repeat cycle and a 60-m spatial resolution, contributing to the water temperature study (Lagouarde et al., 2018; Michel et al., 2021). Besides, the European Space Agency (ESA) is launching the LSTM (High Spatio-Temporal Resolution Land Surface Temperature Monitoring) mission, equipped with two satellites, which will complement the existing Copernicus Sentinel system in 2028. Thermal infrared (TIR) surveillance capabilities across land and coastal areas in support of agriculture management services are part of this objective, providing enhanced measurements of LST. Although it may offer various other services, this mission will also contribute to water temperature study (Koetz et al., 2018). Another future mission planned for 2028 called SBG (Surface Biology and Geology) from NASA will aim to gather spectroscopic and multispectral data on the whole planet to understand better the nature, functioning, and health of Earth's ecosystems, including those found in the aquatic environment to study the water quality (Cawse-Nicholson et al., 2021). Overall, the new thermal infrared missions are essential for expanding our understanding of the Earth's surface and meeting societal requirements. These missions offer good spectral and thermal imagery, enabling a variety of uses and improving our knowledge of the Earth's ecosystems and processes.

1.2 State of the art

Various studies have extensively used TIR sensors to study water surface temperature. These studies are essential for understanding the thermal behavior of oceans, lakes, rivers, and other water bodies and their interactions with the environment. Previous studies utilized TIR sensors to analyze the vertical profiles of lakes and reservoirs to help the monitoring of the water temperature and their stratification, thermal pollution, and changes in aquatic ecosystems. Derived from this, and as the LSWT is a recognized Essential Climate Variable (ECV) that complements water quality data in environmental monitoring of several lakes throughout the world, the Copernicus Global Land Service (CGLS) includes applications derived from satellite observations such as the The LSWT product Version 1. It consists of two components: a historical dataset of Collection of 1 km LSWT from 2002 until 2012 generated from the AATSR instrument on Envisat and a Near Real Time (NRT) dataset of 1 km LSWT from the SLSTR instrument on Sentinel-3A from April 2018 until the present (Lake Surface Water Temperature | Copernicus Global Land Service, n.d.; VITO Earth Observation - Lake Surface Water Temperature Product Catalogue, n.d.).

The LSWT observations and reconstructions are valuable for numerical weather prediction, lake model validation, and expanding our understanding of the climatology of lakes globally (Globolakes: Data, n.d.). An example of the use of remote sensing to inland water is the generation of datasets derived from global data on open and permanent water bodies obtained from the Land Cover Climate Change Initiative (LC CCI) project. The purpose of these datasets was to provide auxiliary information for measuring LSWT, where the main findings were the generation of a global map of open permanent water bodies at a resolution of about 300 meters created using satellite imagery and other sources; the derived datasets, including distance-to-land, distance-to-water, water-body identifiers, and lake-center coordinates, were made available for use by the scientific community in various applications related to climate change, water resources, and regional environments; overall they provided valuable information for studying inland water and its relation to climate and water cycles (Carrea et al., 2015a, 2015b; Dataset Record: GloboLakes: High-Resolution Global Limnology Dataset V1, n.d.;

Dataset Record: GloboLakes: Lake Surface Water Temperature (LSWT) v4.0 (1995-2016), n.d.). Another study by MacCallum et al. (2012) developed a method to obtain estimates of LSWT using satellite imagery from the along-track scanning radiometers (ATSRs) for large lakes worldwide. This method is called optimal estimation (OE) and probabilistic cloud screening, which is a Bayesian approach that utilizes look-up tables (LUTs) to quantify the joint distribution for cloud observations. These LUTs define the expected distribution for cloud conditions based on observations of brightness temperatures in all channels, 1.6 mm reflectance, and the local standard deviation (LSD) of 11 mm brightness temperatures. Additionally, there is a separate LUT that defines the LSD distribution for clear sky. However, it's mentioned that these LUTs were generated empirically for observations over the ocean and may not be entirely suitable for lakes. The method considers various physical properties such as elevation, salinity, and atmospheric conditions through forward modeling of observed radiances. The authors obtained LSWTs for 258 of Earth's largest lakes from 1995 to 2009 and compared them to in situ observations, finding satellite in-situ differences of around 0.1 to 0.7 K. The method improves coverage and consistency between channel-view combinations (MacCallum et al., 2012). Additionally, the authors applied empirical orthogonal function (EOF) techniques to reconstruct the complete time series of LSWT from observations with gaps due to cloud cover.

A study of global lake responses to climate change combining the satellite-derived and in-situ data, in terms of LSWT, observed the rapid and widespread warming of lakes globally from 1985 to 2009, influenced by the lake surface energy budget and associated atmospheric and in-lake drivers (Woolway et al., 2020). In another study in terms of global lake response, Ades et al. (2019) analyzed the LSWT of 923 lakes in 2018 and found temperature anomalies averaged +0.17 °C compared to the 1996-2016 average, where the satellite data showed a continuing warming trend. According to regional analysis, lakes in Europe and East Asia had the most positive anomalies, strongly in European lakes, but lakes in North America, notably in the area around Canada, presented a cooling trend. These results show a consistent rise in LSWT, with East Asia and Europe warming the most (Lake Surface Temperatures | Copernicus, n.d.)

LSWT can be effectively measured from space using satellite remote sensing techniques, allowing for large-scale and continuous monitoring of LSWT globally. It helps study climate

change effects, assess water quality, and manage water resources, providing information such as lake water temperature's spatial and temporal variability. Integrating multiple satellite sensors and ground-based measurements can help improve the accuracy of satellite-derived lake water temperature estimates. In the future, developing increasingly sophisticated satellite sensors and data processing methods would enhance the precision and dependability of satellite-derived lake water temperature observations (Measuring Lake Water Temperature from Space | Weather and Climate @ Reading, n.d.)

Some studies analyzed and retrieved surface water temperature data derived from the TIR sensors classified by the different types of spatial resolution: moderate spatial resolution such as AVHRR, ATSR, MODIS, and Sentinel-3; and High spatial resolution such as ASTER, Landsat ETM+, Landsat 8, Landsat 9 and ECOSTRESS; however, all these studies have focused mainly on each satellite individually or compared with few other sensors with similar type of spatial resolution generally. Some of the characteristics of the medium and high spatial resolution satellites are listed inTable 1.

1.2.1 LSWT retrieval from moderate spatial resolution satellites

Previous studies analyzing the LSWT using moderate spatial resolution satellites such as AVHRR, ATSR, MODIS, and Sentinel-3 are covered. This type of sensor's resolution are well-suited for observing and monitoring a variety of Earth's surface features due to their intermediate level of detail. While these satellites allow the observation of various surface extensions, considering their spatial resolution of 1 km, they may not provide the level of detail required for very high-resolution applications.

A study evaluated the radiometric accuracy of MODIS TIR imagery by comparing it with in situ data collected during a calibration field campaign conducted in Lake Titicaca. It examined its sensitivity to changes in atmospheric temperature and water vapor profiles. The study results show good agreement between the MODIS TIR data and atmospheric radiative transfer code MODTRAN4.0 in bands 31 and 32 (11 to 12 μm), where the accuracy of MODIS TIR was evaluated with measurements in-situ from that Lake. The sensitivity analysis revealed that

changes in atmospheric temperature and water vapor profiles have negligible effects on the calculated radiances in certain bands. However, the error analysis indicated that accurate atmospheric temperature and water vapor profiles are necessary to estimate calibration accuracies in certain bands. The study also highlighted the use of Lake Titicaca as a vicarious calibration site due to its clear-sky conditions and accurate emissivity calculation. The results of the field campaign showed that the lake surface kinetic temperatures measured with well-calibrated TIR radiometers provide valuable data for evaluating the absolute calibration accuracy of the MODIS TIR data (Wan et al., 2002).

Schneider et al., 2009, analyzed the trend of LSWT using ATSR-1, ATSR-2 on board the ERS-1 and the ERS-2 missions, and MODIS data for six lakes in California and Nevada. The LSWT data derived from these satellites showed high accuracy, with an RMSE of less than 0.3 K. Schneider & Hook (2010) analyzed nighttime LSWT of 167 large inland lakes worldwide using AVHRR data, finding an average temperature increase rate of 0.045 ± 0.011°C/yr−1 from 1985 to 2009, with an RMSE of 0.013 °C yr^{-1}, the satellite-derived trends from 1985 to 2009 were in good agreement with the trends from in situ data.

Politi et al., 2012, used the NOAA AVHRR thermal data to monitor LSWT in European lakes, highlighting the lack of studies focusing on lake response to environmental changes in Europe and the importance of monitoring the condition of European lakes towards sustainable systems with good ecological status as required by policies such as the EU Water Framework Directive (WFD). The main findings of the study were that the NOAA AVHRR thermal data has been demonstrated as a reliable tool for estimating LSWT in lakes with different characteristics and across multiple sites in Europe, showing that both the multichannel SST estimation (MCSST) and non-linear SST estimation (NLSST) split window algorithms have a solid potential to estimate LSWT in European lakes. The MCSST algorithm's accuracy was slightly higher than the NLSST algorithm, with a bias of 1.22 °C and an accuracy (measured with RMSE) of 2.29 °C. The NLSST algorithm had a bias of -0.89 °C and an accuracy of 2.22 °C. The proposed remote sensing approach methodology shows promising results toward replacing resource-intensive field-based lake monitoring programs. Sharma et al. (2015) constructed a dataset of lake surface

water temperature (LSWT) using AVHRR and ATSR data for 291 lakes worldwide. They found high accuracy between the remotely sensed LSWT data and in-situ measurements, with a root mean square error (RMSE) ranging from 0.03°C to 1.15°C. Another study using AVHRR focused on the impact of climate change on surface water temperatures in the Great Lakes. It aims to predict future water temperatures in Lakes Superior, Huron, Erie, and Ontario under different CO2 emission scenarios. The study utilized empirical models based on the relationships between surface water and local air temperatures. It analyzed the annual cycles of surface water temperatures in the lakes using remotely sensed data and historical temperature records. LSWT in the Great Lakes exhibit linear warming in spring, plateau in mid-summer, and linear cooling in fall. The warming and cooling rates remain relatively constant yearly, while plateau values vary substantially across years. Substantial increases in surface water temperatures and increases in summer stratification were expected (Trumpickas et al., 2009)

Some previous studies using MODIS imagery found that using one of the products (MOD11) to analyze the LSWT provided by this satellite, retrieved by using the generalized split-window algorithm, has provided good RMSE values and small biases compared to other sources such as Landsat 7 ETM+, MODIS-Aqua, and in-situ measurements (Crosman et al., 2009; Liu et al., 2015; Reinart et al., 2008a; Tavares et al., 2019; Wan et al., 2010; Xiao et al., 2013). Wan et al. (2017) used MODIS data to create comprehensive datasets of LSWT for 374 lakes on the Qinghai-Tibet Plateau. These datasets included LSWT measurements during both daytime and nighttime. The study was mainly based in the use of MODIS data for understanding the LSWT dynamics in this region.

Additionally, the studies mentioned that NOAA/AVHRR and MODIS satellite data have higher temporal resolution (capturing data at frequent time intervals) but lower spatial resolution (offering less detailed information) compared to Landsat and ATSR data. In another study, (Luo et al., 2019) analyzed the spatiotemporal changes of LSWT in Dianchi Lake in China from 2001 to 2017 using MODIS (MOD11A2) images, showing a rise of LSWT over the 17 years of study by 0.12°C/yr $^{-1}$ ($P < 0.002$) in daytime and 0.09°C/yr $^{-1}$ ($P < 0.05$) for nighttime. Besides, Crosman and Horel (2009) determined that the MODIS level 2 LST product (MOD11) effectively monitors

variations in LSWT of Utah's Great Salt Lake using thermal imagery from MODIS between 2000 and 2007. This study utilized 3345 images from MODIS to monitor variations in LSWT, where long-term in situ measurements are rarely available. The MODIS imagery provides a multi-year record of the LSWTs of the lake, allowing the observation of spatial, diurnal, seasonal, and annual variations, presenting a cold bias of around 1.5 °C compared to in situ temperature observations for the Great Salt Lake. Pour et al., 2014 investigated the impact of incorporating MODIS imagery onboard the Terra and Aqua satellites and the Advanced Along-Track Scanning Radiometer (AATSR) onboard the ENVISAT satellite-based observations of LSWT on the initial state of the HIRLAM numerical weather prediction model, by analyzing of these variables for two winter seasons in northern Europe. These experiments were compared to the results of pure prognostic parameterizations and assimilation of in-situ LSWT observations. The objective analyses of the lake surface state, based on the satellite observations, were found to improve the description of the state compared to the other methods. The findings of this study showed that the introduction of space-borne LSWT observations improved the description of the lake surface state compared to the results of pure prognostic parameterizations or assimilation of in-situ lake temperature observations. The validation of the objective analyses against independent observations demonstrated the benefit of utilizing remote-sensing observations for improving the operational weather forecast. This study concluded that introducing satellite-based LSWT observations into the analysis of lake surface state can enhance the description of these variables compared to existing parameterizations and limited in-situ observations.

Other moderate TIR resolution satellites are the Sentinel-3A and Sentinel-3B. Although there is a lack of studies using these satellites to estimate the LSWT, previous studies have used this sensor to estimate the land surface temperature, showing high-quality observations and providing reliable results. One study by (Pérez-Planells et al., 2021) suggested two dual-angle algorithms and two emissivity-dependent split-window methods with viewing angle dependency for obtaining Land Surface Temperature (LST) using Sentinel-3 SLSTR sensor data. The operational LST product of Sentinel-3 SLSTR and in-situ data from a rice paddy location validated these methods. The same authors stated that the operational Sentinel-3A SLSTR product has a systematic uncertainty of 1.3 K and a precision of 1.3 K. In comparison, the

Sentinel-3B SLSTR operational LST product revealed a systematic uncertainty of 1.5 K and a precision of 1.2 K. In terms of uncertainty and precision definitions, we have that the first one addresses how well we know the true value, taking into account various sources of errors. Precision, on the other hand, focuses on the consistency and reproducibility of measurements. Compared to the present iteration of the operational SLSTR product, the results show that the emissivity-dependent split-window methods suggested in the study, coupled with previously published algorithms without angular dependency, produce more exact and accurate LSTs.

Another study by Yang et al. (2020) investigates alternative algorithms for retrieving LST using the SLSTR onboard Sentinel-3A and 3B satellites. As potential algorithms, 17 split-window algorithms (SWAs) specifically focus on investigating and validating land surface temperature (LST) from Sentinel-3 SLSTR data. The SWAs were tested for sensitivity and accuracy using simulation data and in-situ LST measurements after being trained using a worldwide simulation dataset. Eleven SWAs had high training accuracy; nine showed minimal sensitivity to the LSE and the uncertainty of the column water vapor content. According to evaluation based on various simulated datasets and in-situ LST observations, these nine SWAs have similar accuracy with minor systematic errors and RMSEs lower than 1.0 K. The same accuracies of the SWAs were validated based on in-situ LST measurements at six locations, including water sites with RMSE ranges of 1.57-1.62 K and 0.49-0.61 K for Gobabeb Lake (Namibia) and Lake Constance (Switzerland), respectively (Yang et al., 2020).

Additionally, a study by Zarei et al. (2021) assessed the Sentinel-3 SLSTR LST product's correctness, and two validation methods—direct and indirect—were used. Indirect validation compared to the MODIS LST product and LST using the non-linear split-window (NSW) technique, whereas direct validation compared the product to field data. Sentinel-3 estimated the LST using two emissivity estimation techniques: the classification-based emissivity method (CBEM) and the NDVI thresholding method (NDVI-THM). When calculating LST, the NDVI-THM technique produced superior results. Sentinel-3 LST data, MODIS LST products, and LST approximated using NSW displayed comparable accuracy findings for LST fluctuations over the seasons. In the summer season, the lowest accuracy for Sentinel-3 LST products was estimated, as shown by the most significant bias, standard deviation, and root mean square error (RMSE)

values. The highest accuracy was during winter, with the lowest bias, standard deviation, and RMSE values.

As mentioned, the accuracy reduction in measurements obtained from TIR sensors is mainly caused by meteorological and climatological conditions such as cloud cover and water vapor. Some previous studies have found that using NOAA AVHRR used to be adequate as it provided an excellent spatial accuracy result in terms of the water temperature of a lake (1° K accuracy). However, due to the temporal resolution of 1 day, the possibility of studying the temperature's long-term variation during a day added higher uncertainty (Li et al., 2017). On the other hand, data from most modern satellite sensors have improved their spectral, radiometric, temporal, and spatial resolutions. Even though the LSWT provided by these sensors refers to the top layer temperatures or skin temperature (Figure 3), this can be associated to the temperature of the air-water interface and can differ from the bulk temperature by as much as a few degrees (Woolway, 2014). However, this information is still precious to study the variation of temperatures in lakes for different applications such as water-quality variables, heat budget, evaporation estimation, and climate change happening on the lakes (Tavares et al., 2019).

In conclusion, the choice of using moderate TIR resolution depends on the specific research objectives and the scale of the study. Moderate-resolution sensors are advantageous for broader coverage, temporal frequency, and statistical significance, while high-resolution sensors excel in capturing fine detail and small-scale phenomena. Researchers often choose the resolution that aligns with their study goals and the characteristics of the water bodies they are investigating.

1.2.2 LSWT retrieval from high spatial resolution satellites

This section references previous studies that analyze the LSWT using high spatial resolution satellites such as ASTER, Landsat ETM+, Landsat 8, Landsat 9, and ECOSTRESS. This spatial resolution data allows us to study smaller lakes when considering their decametric resolution. High spatial resolution data provides more accurate temperature measurements. In a coarse-resolution dataset, temperature values represent averages over larger areas, potentially

masking critical local variations. Thus, high spatial resolution data allows for a more precise characterization of temperature patterns.

Using imagery from the Landsat satellites makes it possible to study various aspects related to the variability of the LSWT. For example, in a study for the LSWT variation conducted on 35 lakes and reservoirs and 24 estuaries in America using Landsat 5 Thematic Mapper (TM) and Landsat 7 Enhanced Thematic Mapper Plus (ETM+) data, the temperature mean absolute error was 1.34 °C in lake pixels >180 m from land, 4.89 °C at the land-water boundary, and 1.11°C in estuaries based on comparison against discrete surface in situ measurements (Schaeffer et al., 2018). Giardino et al., 2001 used Landsat Thematic Mapper (TM) data to map LSWT distribution in a mountainous area of Italy, with a root mean square error of 0.3°C. Simon et al. (2014) extracted LSWT of freshwater lakes in France (Lakes Bimont and Bariousses) using single-band thermal infrared Landsat data, obtaining high accuracy with an r^2 value higher than 0.9 and an RMSE of 1 and 2°C. Another study using Landsat 8 was compared with field measurements of the vertical temperature gradient at different depths for 23 Arctic lakes in the summer of 2013, demonstrating high precision with an error range of 0.11°C ~ 0.46 °C, where the RMSE with the in-situ bulk temperatures were 0.41 °C (Huang et al., 2017). Also, a study investigated the variations in water temperature and their impacts on ecosystem processes in Poyang Lake, the largest freshwater lake in China, using remote sensing data to assess the temperature cycle of the lake. The study demonstrated the effectiveness of using Landsat 7 thermal imagery to assess the spatial heterogeneity of water temperature in Poyang Lake. It compared the spatial distribution of water temperature derived from a hydrodynamic model with the temperature derived from Landsat data and found good agreement between them. This comparison suggests that remote sensing data can be a valuable tool for monitoring and understanding the behavior of water temperature in large floodplain lake systems like Poyang Lake (Li et al., 2017). Also, a study showing the advantages and limitations of using satellite imagery to assess the physical, chemical, and biological characteristics of water bodies, precisely the surface water temperature, explored different atmospheric correction algorithms, such as the split-window algorithm, that can improve the accuracy of satellite temperature data; this study performed in three lakes, Bimont and Treignac in France, and Lake Geneva in

Switzerland. The perspectives for using satellite data in water ecosystem studies include optimizing models for French terrains, utilizing recent data from Landsat 8, and the necessity of synchronous data during satellite passes. The temperature variability in water bodies was significant, ranging from 2 to 5 °C. The authors concluded that combining satellite and in-situ data is crucial for a holistic assessment of water body conditions, adding the perspectives for future research to improve atmospheric correction algorithms, utilizing Landsat 8 imagery, and the importance of synchronous data during satellite passes (Danis et al., 2014). In addition to this study, Tormos et al. (2016) discussed in their report "Estimation of the surface temperature of water bodies using Landsat imagery: Algorithms and Results" the estimation of the surface temperature of water bodies using Landsat 4, 5, 7 and 8 satellites, developing algorithms to estimate surface temperature, considering calibration coefficients, and atmospheric water vapor content. This report highlighted the importance of surface temperature estimation as it is a significant characteristic of lacustrine ecosystems and plays a role in vertical mixing and stratification processes. The findings in this study indicate that the estimation of surface temperature using Landsat imagery is satisfactory, with an accuracy of approximately 1.5 to 2 °C. However, the errors in estimation referred to the quality of atmospheric water vapor data.

Being Landsat 9 the latest launch for a Landsat series satellite, there is already a study showing a split window algorithm designed for Landsat-8 based on Jimenez-Munoz et al. (2014) to estimate the LST, achieving accuracy after being validated over sites in the U.S.A., with four SWA methods. The accuracy and noise sensitivity of the results under various observation settings were calculated using the simulation dataset to choose the optimum algorithm. The findings reveal that the ground validation accuracy is around 1.574 K, better than the previous Landsat-9 LST product. Furthermore, the obtained LST pictures exhibit a geographical distribution comparable to the Landsat-9 LST products, with RMSEs ranging from 0.31 to 2.87 K in different places. (Ye et al., 2022a). Recently, there are no studies found using Landsat-9 to analyze the LSWT. Another study using Landsat 5 and Landsat 7 imagery from 1999 to 2016 created the LakeSST dataset, containing the LSWT data for 442 French inland water bodies. The quality of the temperature measurements was assessed by comparing them to in situ data, considering the cold skin and warm layer effects on the satellite temperature measurements,

which can impact the accuracy of the data. The overall RMSE was about 1.2 °C, concluding that the LakeSST dataset can be used for studies on the temporal evolution of the LSWT and geographical studies of temperature patterns (Prats et al., 2018). Another recent study in 2023 analyzed satellite data from Landsat 5 TM, Landsat 7 ETM+, and Landsat 8 for 535 lakes in the North Slave Region of the Northwest Territories in Canada from 1984 to 2021 to estimate their LSWT. This study showed good agreement with in-situ observations with the single channel algorithm as the method of LSWT retrieval used, resulting in a RMSE value of 1.7 °C, where spatial and temporal changing temperature trends over the past 38 years were found (Attiah et al., 2023).

Another of the latest high-resolution satellites is the mission ECOSTRESS, where previous studies compared the performance of this sensor, showing compatibility with existing TIR sensors with similar radiometric characteristics (ASTER and Landsat-8) and an improvement in terms of temporal availability for sampling LST (Li et al., 2021; Shi et al., 2021; Silvestri et al., 2020). (Li et al., 2021) evaluated (LST) products, including ECOSTRESS, GOES-R, Landsat Provisional, Sentinel-3, MODIS LST products (MOD11A1 and MYD11A1), MODIS/Aqua LST product (MYD21A1), and VIIRS/NPP LST product (VNP21A1), showed generally good agreement with in-situ measurements of LST in the U.S. Corn Belt. The biases of all LST products, both nighttime and daytime, were generally within ±2 °C and ±3 °C, respectively, indicating reasonable accuracy for agricultural applications. Among the LST products evaluated, ECOSTRESS achieved the highest agreement with ground observations for daytime LST, with an overall absolute bias of less than 0.9 °C and a root mean squared error (RMSE) of less than 2.3 °C. MODIS LST products (MOD11A1 and MYD11A1) slightly underestimated daytime LST but still had overall absolute biases of less than 0.9 °C and RMSEs of less than 2.9 °C. In another study by Shi et al. (2021), ECOSTRESS thermal data was evaluated for several South Florida estuaries, Chesapeake Bay, and Lake Okeechobee. It may not be possible to accurately determine the surface temperature of tiny bodies of water with operational coarse-resolution satellite thermal sensors built for the global seas. Sea Surface Temperature (SST) from ECOSTRESS substituted the ECOSTRESS (LST) product. A modest underestimating of SST using ECOSTRESS LST was discovered, with the underestimation being more pronounced at night (-1.13 °C) than during

the day (-0.64 °C). Compared to fall and winter (-0.57 0.98 °C), the underestimation of ECOSTRESS LST was considerably more apparent in spring and summer (-1.25 1.39 °C). The ECOSTRESS SST's root-mean-square uncertainties were typically 1-2 °C. One more study by Silvestri et al. (2020) established that heat-related events, including heat waves, volcanic eruptions, and fires, may be studied using ECOSTRESS. The Advanced Spaceborne Thermal Emission and Reflectance Radiometer (ASTER), the Landsat 8 TIRS sensors, and ECOSTRESS temperature data were compared in the study's analysis of thermal anomaly locations. The study revealed that the three sensors had a robust correlation and mean value agreement. According to this, using ECOSTRESS, coupled with ASTER and Landsat 8, may increase the accessibility of satellite high-resolution thermal data. Surface temperatures were extracted from ECOSTRESS and ASTER data using the Temperature and Emissivity Separation (TES) technique, while Landsat 8 data were estimated using the single-channel algorithm. The moderate-resolution atmospheric transmission (MODTRAN) radiative transfer model eliminated atmospheric impacts in the data.

As shown on some of the previous studies using moderate and high spatial resolution TIR sensors to retrieve and analyze the LSWT, in most of the lakes around the world, it was found that the LSWT is rapidly increasing at a rate of 0.3°C/decade (O'Reilly et al., 2015; Witze, 2015). In some lakes, the warming rate of LSWT is faster than the local air temperature. However, a study conducted in lakes on the Qing-Tibet Plateau found that the warming rate of LSWT was almost the same as that of the regional air temperature. In the USA, the LSWT in summer shows a significant warming trend, with a warming rate double that of the air temperature (Yang et al., 2022).

Although there are different studies to understand the LSWT, there is still a lack of global observations to monitor better the dynamics of the surface water, leaving some incertitude about the temporal and spatial variability of the surface water and the accuracy in the predictions for these variations (Alsdorf et al., 2007). Overall, these studies demonstrate the advancements in remote sensing technology for obtaining accurate LSWT data and provide valuable insights into understanding lake temperature dynamics across different regions.

1.3 Objectives

Some of the multi-resolution and multi-sensor satellite missions carrying onboard thermal infrared sensors are evaluated in this research, which will provide valuable resources and information as predecessors of the new TIR missions such as TRISHNA in 2025 (CNES-ISRO) and more long-term missions such as LSTM (ESA Copernicus) and SBG (NASA) both in 2028. This analysis has been developed by using temperature retrieval methods per sensor and observing the compatibility of measurements between them, where this will be helpful to improve their spatial, spectral, and temporal resolution, as typically, sensors in this domain have lower spatial resolution than those in the visible or near-infrared domain such as Spot 6 and 7 (1.5 m), Landsat-9 (30 m) and Pleiades (50 cm). Their revisit times are limited or might be affected by the cloud cover.

1) The first objective will be the retrieval and analysis of the LSWT from multiple sensors with different spatial, temporal, and spectral resolutions and thus make a comparison to obtain denser measurements, both spatially and temporally, of the LSWT to obtain accurate information for the understanding of the processes and dynamics in the thermal domain and its changes in time and space. Hence, the multi-resolution, multi-sensor approach can help overcome some of the shortcomings of individual TIR sensors and provide a more comprehensive and accurate observation of the thermal properties of the LSWT.

The TIR sensors considered in this research have at least two thermal channels to apply the split window algorithms, even though mono-channel algorithms were applied to Landsat 8, and are classified according to the type of resolution as follows:

- Moderate spatial resolution: MODIS (Terra) and SLSTR (Sentinel-3), with 1 km and daily revisit time.
- High spatial resolution: ECOSTRESS with 70 m and revisit time every 3-5 days, TIRS (Landsat 8 and Landsat 9) with 100 m and revisit time every 16 days.

By using multiple sensors and with the comparison of their data, drawbacks of individual sensors could be overcome and improve the overall accuracy and coverage of LSWT measurements.

2) As another critical point, the validation of the LSWT, defined as the assessment of the quality from measurements provided by the products, can be reached by applying the inter-comparison with the different surface temperature products, comparison against in situ observations, and by observing the time-series analysis (Schneider et al., 2019). Hence, validation was carried out with the available in situ data from the various measuring devices deployed on the lake Issyk-Kul, located in the eastern region of Kyrgyzstan in Central Asia, and over three lakes in the Grand East region of France (Gerardmer, Longemer, and Plobsheim Lakes). A significant part of the validation was made by a cross-validation method evaluated with other LSWT products, such as CCI Lakes and Meteorological Station datasets, where access to in situ data was provided through the LEGOS Institute.

1.4 Structure of the thesis

This thesis comprises five chapters: Introduction, methodology, study area and data, results of the LSWT and discussion, conclusions, and perspectives.

The first chapter introduces the context of the retrieval of LSWT with a multi-resolution multi-sensors approach. The existing literature on the thermal infrared domain from different studies and applications and the objectives for this thesis are also presented in this chapter.

The second chapter describes the different algorithms to retrieve LSWT at Level 1 imagery from Landsat 8, 9, and ECOSTRESS, as well as the analysis of the LSWT products used in this research and their geoprocessing steps, such as the cloud masks application for some of the products.

Chapter three describes the physical and climatological characteristics of the considered regions as the areas of study. It also presents the list and description of the datasets used for

this research, such as the LST products, Level 1 imagery to perform retrieval algorithms, and its atmospheric parameters inputs.

Chapter four, results for the intercomparison of the algorithms for Landsat 8-9 and ECOSTRESS. Performance of the LST products and their cloud masks. Cross-validation between all the TIR sensors and the in-situ datasets. Besides, an explanation of the obtained results and the comparison of the LSWT estimations to previous studies. Discuss its implications or consequences by describing this research's limitations and contributions to the previous literature.

This fifth and final chapter states the sum of the main findings, conclusions, and perspectives, where some of these findings give rise to suggestions for further study in this area.

Chapter 2. Methodology

There are various spatial and temporal resolutions of the most common sensors (Table 1), not limited to this list, aboard different satellite missions providing Thermal Infrared bands to estimate land and sea surface temperatures.

Satellite/Sensor	Spatial resolution	Revisit time	Years of coverage	Main purpose	Type of spatial resolution
Meteosat-7-11/MSG-MVIRI-SEVIRI	3 km	15 minutes	1997 - To date	High impact weather	Low
Himawari-8-9/MTSAT	5 km	10 minutes	2015 - To date	SST and Water vapor	Low
AGRI-GIIRS/Feng Yung (FY-4A/B)	4 km	15 minutes	2016 - To date	HSST and Water vapor	Low
AHVRR/POES	1 km	1 day	1989 - To date	Global sea surface temperature	Moderate
Terra & Aqua/MODIS	1 km	1-2 days	2000 - To date	Global dynamics in oceans/land	Moderate
AATSR/Envisat	1 km	35 days	2002 - 2012	Sea surface temperature	Moderate
Sentinel-3A/SLSTR	1 km	1-2 days	2016 - To date	Sea and land surface temperature	Moderate
Sentinel-3B/SLSTR	1 km	1-2 days	2018 - To date	Sea and land surface temperature	Moderate
Landsat 4-5/TM	120 m	16 days	1982-2013	Global land areas in HR	High
Landsat 7/ETM	60 m	16 days	1999 - To date	Global change and land cover	High
Terra & Aqua/ASTER	90 m	16 days	2000 - To date	Land surface climatology	High
Landsat 8/TIRS	100 m	16 days	2013 - To date	Global climate surface	High
ECOSTRESS	70 m	4-5 days	2019 - To date	The temperature of plants/Evapotranspiration	High
Landsat 9/TIRS	100 m	16 days	2022 - To date	Global climate surface	High
TRISHNA	60 m	3-5 days	2025	Surface temperatures all over the globe	High
SBG	60 m	Sub-monthly	2028	Inland and coastal aquatic ecosystems	High
LSTM	50 m	1-3 days	2028	Land and coastal regions in support of agriculture	High

Table 1. *Standard Thermal Infrared Instruments and Future Missions*

Several algorithms exist linked to the different products derived from the TIR sensors to retrieve the LSWT. However, the performance of these algorithms is based on different factors, such as the spectral and spatial characteristics of the sensors, required accuracy, computational time, the atmospheric conditions and the availability of the atmospheric profiles, the land surface emissivity (Jimenez-Munoz et al., 2009; Li et al., 2017; Zheng et al., 2019). The most used algorithms for measuring LSWT are:

- The single channel algorithms use a single TIR band to estimate LWST, assuming a constant surface emissivity and do not consider atmospheric changes, leading to results with less accuracy (Cristóbal et al., 2018; Jiménez-Muñoz, 2004; Jimenez-Munoz et al., 2009; Jiménez-Munoz et al., 2003). These algorithms were used for Landsat 8 imagery from 2019.

- Split window algorithms (SWA) use two TIR bands (typically around 10 and 12 µm) to estimate the LSWT(Becker et al., 1990). This algorithm considers the atmospheric correction and the atmospheric transmittance of thermal radiation and surface emissivity. The SWA has been used for several sensors, such as Landsat, MODIS, Sentinel-3, and AVHRR, and has shown a good level of accuracy for water bodies, such as lakes, rivers, and coastal regions (Rongali et al., 2018; Sobrino et al., 1993; Sobrino et al., 1994; Yu et al., 2014). As well as in the single channel, these algorithms were performed to retrieve LSWT for Landsat 8 from 2019 and Landsat 9 from 2022.

- The Temperature and Emissivity Separation algorithm (TES) is a physics-based algorithm that estimates the land surface temperature from at least three TIR channels within 10 and 12 µm (Gillespie et al., 1998; Schmugge et al., 2002). Firstly, atmospheric corrections are applied to transform the TOA (Top of Atmosphere) into BOA (Bottom of Atmosphere) radiances. Then an iterative process allows to separate the temperature and emissivity (Payan et al., 2004; Wang et al., 2015). The key to this algorithm is an empirical relationship, carried out on various laboratory samples, which links minimum emissivity to the difference between maximum and minimum emissivity (Gillespie et al., 1999).

Compared with the land surface temperature, the emissivity of the water surface is relatively known. However, the temperature and emissivity of the water surface can vary depending on the surface reflection (change of the viewing and illumination angles), depth, currents, and spatial and temporal gradient, leading to errors in the TES algorithm performance (Schneider et al., 2010).

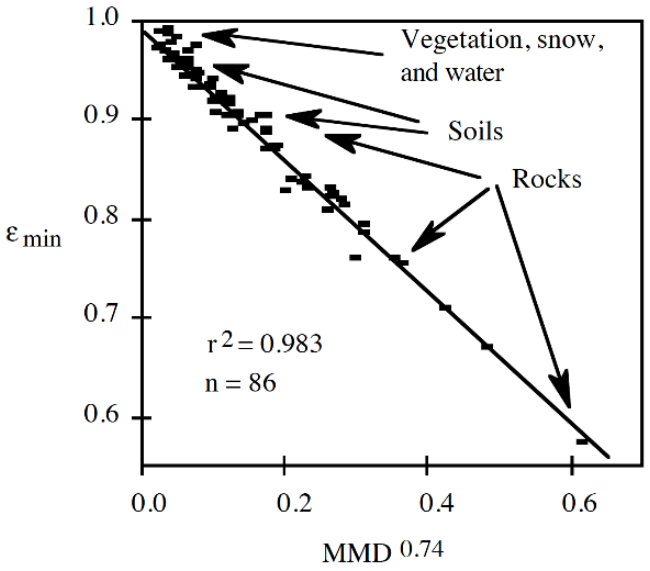

Figure 4. *The empirical relationship between $\mathcal{E}_{min}$ and MMD (spectral contrast), based on 86 laboratory reflectance spectra of rocks, soils, vegetation, snow, and water (Gillespie et al., 1998). 95% of the samples fall within ±0.02 emissivity units of the regression line, corresponding to an error in T of about ±1.5 K at 300 K. The $\mathcal{E}$min-MMD relationship follows a simple power law: $\mathcal{E}_{min}$=0.994-0.687*MMD0.737*

.

Previous studies have discussed the sensitivity of these methods considering the input parameters, like water emissivity, near-surface air temperature, and atmospheric water vapor content, which could impact the estimation of temperatures significantly (Tavares et al., 2019).

While the SWA and TES have advantages and limitations in deriving surface temperatures from inland water bodies, the SWA has improved accuracy in long-term temperature retrievals. Therefore, it can be considered better suited for this specific application than TES (Hulley et al., 2011).

2.1 Algorithms to retrieve LSWT from Landsat 8-9

For this thesis, imagery from the surface temperature products using Split Window Algorithms for MODIS and Sentinel-3 and the TES algorithm for ECOSTRESS are obtained from their platforms. However, for Landsat 8 and 9, available products atmospherically corrected to analyze the LSWT are only offered for one channel – B10 (Single Channel method). Hence, imagery at level 1 (radiance values) for both TIRS bands (B10 and B11) was used to retrieve the LSWT using methods such as Split Window Algorithms. In addition, Mono Window, Single Channel, and Practical Single Channel Algorithms validated the best approach suitable for using Landsat 8 and Landsat 9 applied to the study regions considered.

2.1.1 Mono Window Algorithm (MWA)

Due to the stray light effect, which is more present in band 11 for Landsat 8, the MWA correction method is considered to work with band 10 instead. This algorithm is the improved mono-window algorithm, as shown in the following equation (Wang et al., 2015):

$$LSWT = \frac{a_{10}(1-C_{10}-D_{10})+[b_{10}(1-C_{10}-D_{10})+C_{10}+D_{10}]T_{10}-D_{10}T_a}{C_{10}} \quad (1)$$

Where

a_{10} and b_{10} : coefficients for Landsat 8 band 10 (Table 2) (Wang et al., 2019)

C_{10} and D_{10} : functions of LSE (water emissivity value ε_{10} = 0.991)

τ_{10} : atmospheric transmittance

T_{10} : the Brightness Temperature at the Sensor for band 10 in K

T_a : the effective mean atmospheric temperature in K

$LSWT$: Lake Surface Water Temperature

C_{10}, D_{10}, τ_{10} , T_{10} and T_a are given by the following equations:

$$C_{10} = \varepsilon_{10} \times \tau_{10} \quad (2)$$

$$D_{10} = (1 - \tau_{10}) \times [1 + (1 - \varepsilon_{10}) \times \tau_{10}] \quad (3)$$

τ_{10}= *−0.0735wvc + 0.9228 (for Mid-latitude winter atmosphere)* (4)

τ_{10}= *−0.1146wvc + 1.0286 (for US Standard atmosphere)* (5)

T_a = *19.2704 + 0.9112 T_0 (for mid-latitude Winter atmosphere)* (6)

T_a = *25.940 + 0.8805 T_0 (for USA 1976 Standard atmosphere)* (7)

Temperature Range	a_{10}	b_{10}	R^2
20 - 70 °C	-70.1775	0.4581	0.9997
0 - 50 °C	-62.7182	0.4339	0.9996
-20 – 30 °C	-55.4276	0.4086	0.9996

Table 2. *Coefficients a_{10} and b_{10} for the Landsat 8 TIRS Band 10 and associate Root Mean Square*

The wvc present in the study area will determine the standard atmosphere to choose the suitable parameter when performing atmospheric correction. The standard atmospheres range and classification are as follows (About standard atmospheres, 2020):

Standard Atmosphere	Values of wvc (g/cm^2)
Dry	0.75
Fall	1.14
Spring	1.14
Mid-latitude winter	0.85
Mid-latitude summer	2.92
Subarctic summer	2.08
Tropical	4.11
US Standard	1.42

Table 3. *Values of wvc for Standard atmospheres*

Thus, this algorithm was performed for Landsat 8 imagery from 2019 in the region of the Issyk-Kul Lake.

2.1.2 Single Channel Algorithm (SCA)

This algorithm was used for Landsat 8 band 10 for 2019 images over Issyk-Kul and is called an improved single-channel algorithm with the following equation (Wang et al., 2019):

$$LSWT = \gamma\left[\left(\frac{1}{\varepsilon}\right) \times (\psi_1 L_{sen} + \psi_2) + \psi_3\right] + \delta \quad (8)$$

Where

$LSWT$: Lake Surface Water Temperature

ε*=0.991* is LSE (water emissivity in band 10).

γ and δ (values in K): two parameters depending on the Planck function, and which can be calculated by equations (9) and (10) (Wang et al., 2019):

$$\gamma \approx \frac{(T^2 sen)}{(b_\gamma L_{sen})} \quad (9)$$

$$\delta \approx (T_{sen}) - (\frac{T^2 sen}{b_\gamma}) \quad (10)$$

Where:

L_{sen} : is the at-sensor registered radiance $[\frac{W}{(m^2 \cdot sr \cdot \mu m)}]$

T_{sen} : is the at-sensor brightness temperature (K)

b_γ *: 1324* is a constant for Landsat 8 band 10 (K^{-1})

ψ_1, ψ_2, and ψ_3 : are the atmospheric function parameters (unitless) calculated from the wvc:

$$\begin{bmatrix}\psi_1\\ \psi_2\\ \psi_3\end{bmatrix} = \begin{bmatrix}0.04019 & 0.02916 & 1.01523\\ -0.3833 & -1.50294 & 0.20324\\ 0.00918 & 1.36072 & -0.27514\end{bmatrix}\begin{bmatrix}wvc^2\\ wvc\\ 1\end{bmatrix} \quad (11)$$

2.1.3 Practical Single-Channel Algorithm (PSC_{wvc})

Previous studies found that the SCA has shown primary error sources in the linearization of Planck's function and atmospheric correction. Thus, this Practical Single-Channel (PSC_{wvc}) algorithm, used for the same Landsat 8 band 10 imagery in 2019 over Issyk-Kul Lake, aims to reduce the mentioned errors, and LSWT can be calculated with the following equation (Wang et al., 2019):

$$LSWT = \left[\frac{(\frac{c2}{\lambda})}{Ln(\frac{c1}{\lambda 5}\times B(T_S)_{wvc}+1)}\right] \quad (12)$$

With

$$B(T_s)_{wvc} = a_0 + a_1 wvc + (a_2 + a_3 wvc + a_4 wvc^2)\frac{1}{\varepsilon} + (a_5 + a_6 wvc + a_7 wvc^2)\frac{1}{\varepsilon} L_{sen} \quad (13)$$

Where:

$c1$: 1.19104x10^8 W·µm^4 ·m^{-2} ·sr^{-1} is a Planck function constant

$c2$: 1.43877 × 10^4 µm·K is a Planck function constant

λ: *10.904 µm* Effective wavelength Band 10

$B(T_s)$: represents Planck's radiance with a temperature of T_s

$B(T_s)_{wvc}$: represents the wvc-dependent B(Ts) model

a_0, a_1, a_2, a_3…a_7: Coefficients of the PSC method for wvc dependent model given in g/cm^2 (values in Table 4)

ε: *0.991* LSE (water emissivity)

L_{sen}: At-sensor registered radiance $[\frac{W}{(m^2 \cdot sr \cdot \mu m)}]$

wvc: Water vapor content datasets from the ECMWF in g/cm^2

wvc (g/cm^2)	a_0	a_1	a_2	a_3	a_4	a_5	a_6	a_7
[0,2.0]	-0.2801	1.2574	0.2751	-1.3288	-0.1696	0.9991	0.0335	0.0152
[2.0,4.0]	-0.6034	1.6135	-4.9899	2.7727	-1.0427	1.7396	-0.5498	0.1290
[4.0,7.0]	2.2805	0.9182	-38.3363	13.8258	-1.7546	5.0039	-1.6283	0.1967
Full range	-0.4107	1.4936	0.2783	-1.2250	-0.3107	1.0220	-0.0197	0.0360

Table 4. *Coefficients a_k in $B(T_s)_{wvc}$ Model for Landsat 8 TIRS1 Data for Different wvc subranges*

2.1.4 Split Window Algorithm (SWA)

The SWA operates by correcting atmospheric and emissivity effects for different land cover types with known band emissivity. It uses different coefficients for different humidity and temperature ranges to address the non-linearity problem caused by high water vapor contents. The method calculates the LST by analyzing thermal radiance values in two specific TIR bands. By optimizing the parameters for viewing angle and water vapor content ranges, the method can achieve accuracy better than 1 °K for land cover types with known emissivity (Becker et al., 1990; Wan et al., 1999; Tormos et al., 2017).

The same imagery used for the previous algorithms over Issyk-Kul Lake in 2019, now by using the SWA, can provide more accurate LSWT and is one of the standard methods used due to its simplicity of operation. Hence, this atmospheric correction was based on the LSWT inversion method, firstly, without considering the variation of the atmospheric wvc (Du et al., 2015):

$$LSWT = a_0 + a_1 B_{10} + a_2 B_{11} + a_3 (B_{10} - B_{11})^2 \quad (14)$$

Where a_k are coefficients obtained by regression analysis, and Brightness Temperatures (K) from B10 and B11 were obtained from Thermal Spectral Radiance: a_0=3.228, a_1=4.072, a_2=-3.081 and a_3=0.048.

On the other hand, another SWA atmospheric correction was calculated using the LSWT inversion method mentioned before. However, the variation of atmospheric $\boldsymbol{wvc}$ was considered this time (Du et al., 2015):

$$LSWT = a_0 + a_1 B_{10} + a_2 B_{11} + a_3 (B_{10} - B_{11})^2 + a_4 wvc + a_5 wvc^2 \quad (15)$$

Where wvc is given in g/cm^2 and a_k are the coefficients obtained by regression analysis (Du et al., 2015): a_0=-0.992, a_1=3.970, a_2=-2.963, a_3=0.044, a_4=-0.328 and a_5=0.091.

2.2 LSWT from Sentinel-3 (SLSTR)

The LST product used to retrieve the LSWT (Figure 5) by using Sentinel-3 obtained using a regression-based algorithm that operates on two split-window thermal channels at 11 and 12 µm of the Sea and Land Surface Temperature Radiometer (SLSTR). The algorithm utilizes regression coefficients derived by regressing simulated brightness temperatures against a high-specification line-by-line forward model. These coefficients account for variations in surface temperature, surface spectral emissivity, atmospheric profiles of temperature and humidity, and contaminant gases. The algorithm considers nadir split-window radiance only and considers the angular effects on temperature and emissivity. The LST product is a gridded 1x1 km^2, pixel-by-pixel quantity, derived using the cloud-free top-of-the-atmosphere brightness temperatures and ancillary information to correct for water vapor absorption and spectral emissivity effects (Goryl et al., 2009).

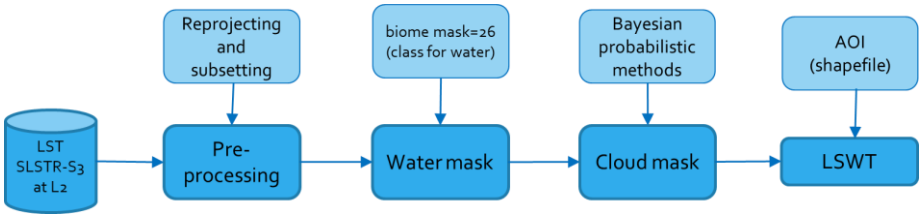

Figure 5. *LSWT retrieval process for Sentinel 3 at Level 2.*

In the split-window algorithm for this LST product, the emissivity of the water is not explicitly considered. The algorithm assumes that the emissivity factors for the land surface are sufficiently close to one for the approach to be appropriate. Therefore, there is no current intention to determine the emissivities as part of the LST product or as a separate product. Instead, the algorithm indirectly incorporates the dependence on emissivity via statistical regression coefficients that are calculated offline and translated through biome/fractional

vegetation maps for application to a particular SLSTR pixel. These regression coefficients account for atmospheric temperature and humidity variations and provide an effective atmospheric correction in clear sky conditions. The split-window method assumes linearity of the variation of atmospheric transmittance with water vapor content amount, but it does not explicitly consider the emissivity of water in the algorithm (Goryl et al., 2009).

The areas of interest were applied at different lake areas to fit the available pixels for the same date from Landsat 8-9, MODIS, and ECOSTRESS (when possible) images.

2.3 LSWT from MODIS (Terra)

The process to extract the LSWT (Figure 6) is by using the LST product (MOD11A1v006) at level 3 from MODIS Terra thermal channel data by the implementation of a generalized split-window LST algorithm, band emissivities were inferred from land-cover types based on either the MODIS land-cover data or the IGBP-type 1-km global vegetation database. For pixels with known band emissivities, the LST algorithm utilized a linear equation of the band brightness temperatures of MODIS bands 31 and 32 (10.5-12.5µm) to calculate LST. The algorithm accounted for atmospheric and emissivity effects by considering factors such as viewing angle, regional and seasonal variations in atmospheric absorption, and water vapor absorption. Additionally, a day/night LST algorithm was developed to retrieve surface band emissivities and temperatures for all cover types, including those with highly variable emissivities. This algorithm employed a statistical regression approach and χ^2 fit approach to handle emissivities that are difficult to predict. The emissivity of water was taken into account in the modeling process, including a correction for atmospheric and emissivity effects for land cover types with known band emissivities, and the values of the band average emissivities of MODIS bands 31 and 32 from the emissivity knowledge base were used as inputs to the generalized split-window LST, having that the canopy emissivity for water surfaces ranges from 0.96 to 1.0 (Wan et al., 1999).

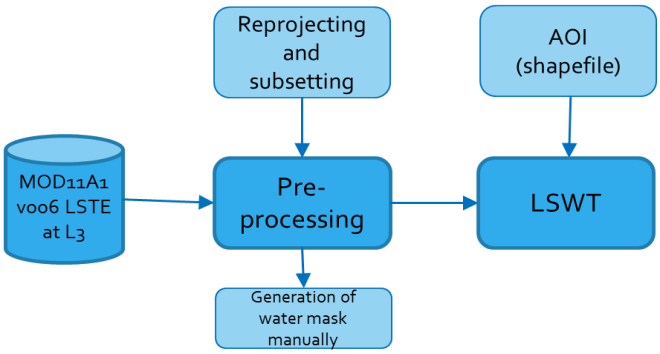

Figure 6. *LSWT retrieval process for MODIS at Level 3.*

The areas of interest were applied at different lake areas to fit the available pixels for the same date from Landsat 8-9, Sentinel-3, and ECOSTRESS (when possible) images.

2.4 LSWT from ECOSTRESS

The process to retrieve the LSWT from the ECOSTRESS products at Level 2 is described (Figure 7), where other products and algorithms were needed to follow this retrieval process:

- ECO2LSTE.001 (L2): This product is generated using the Temperature Emissivity Separation (TES) algorithm. It aims to separate the LST and spectral emissivity components from the total radiance measured by the TIR multispectral scanner onboard the ECOSTRESS mission, presenting challenges of separating these components and providing a theoretical basis for the algorithm used to generate the LST and emissivity products. The emissivity of water was measured or estimated using known values to separate the LST from the total radiance and generate the LST product (Hook et al., 2018).

- ECO1BGEO.001 (L1): This product contains geolocation due to the LSTE 70m pixels containing significant errors due to uncertainties of the ISS (International Spatial Station) positioning system. It is obtained through back-propagation of the instrument pointing model from the payload on the ISS Japanese Experiment Module Exposed Facility (JEM-EF) to the different ISS elements until it intersects with the ground topography. This

backpropagation of light from the focal plane to the ground location is achieved by assuming a straight light propagation through the atmosphere. The geolocation of each pixel is determined by iteratively intersecting the ray with a topography model, taking into account the elevation from a digital elevation model (DEM) (Smyth et al., 2018).

- ECO2CLD.001 (L2): The cloud mask product for the ECOSTRESS mission is obtained using the ECOCLOUD algorithm, which is based on previously established cloud algorithms such as the Landsat ACCAA, MODIS, and AVHRR cloud algorithms. The ECOCLOUD algorithm utilizes calibrated and geolocated L1B TIR radiance data as input and generates a cloud mask at a spatial resolution of 70 meters. The algorithm determines whether a given view of the Earth's surface is unobstructed by clouds or optically thick aerosol. It outputs an 8-bit mask that provides pixel-by-pixel information on whether the cloud was determined, along with the results of three individual thermal tests and a land/water mask. The cloud mask product is distributed as a separate additional Level-2 product. It is an 8-bit flag, where bits associated with clouds are as bit 1 = 1 and bit 3 = 1 (Hulley et al., 2018).

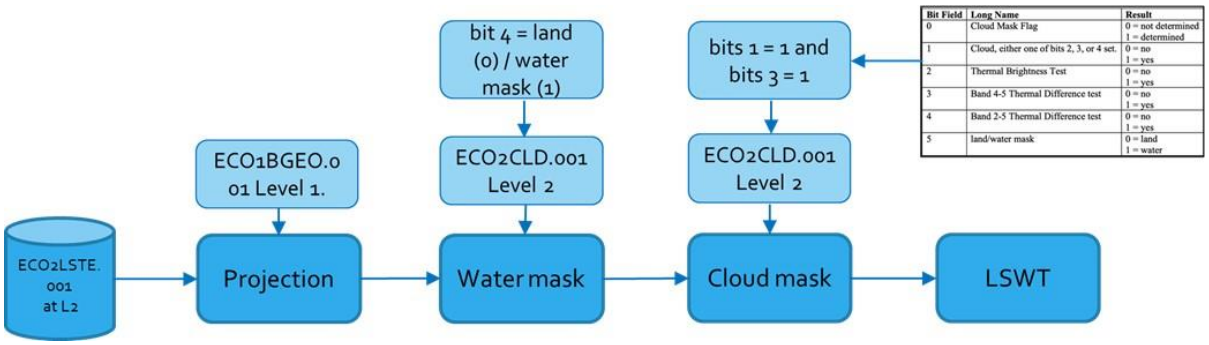

Figure 7. *LSWT retrieval process for ECOSTRESS at Level 2.*

During 2019, ECOSTRESS imagery was only available for a few dates in the second half of that year. Hence, samples were taken from 2019 to 2023.

2.5 Split Window Algorithm (SWA) for ECOSTRESS

The SWA utilizes the radiance measurements in two different spectral bands within the thermal infrared region to estimate the LST. The ECOSTRESS instrument measures radiance in five spectral bands in the thermal infrared region between 8 and 12.5 µm. The basic principle behind the SWA is that different wavelengths in the thermal infrared region are affected differently by atmospheric wvc and other atmospheric components. The algorithm can correct atmospheric effects and estimate the LST by comparing the radiance measurements in two bands. In ECOSTRESS, the LST and land surface emissivity (LSE) estimates use the SWA method in combination with the temperature and emissivity separation algorithm (TES). Separating the effects of temperature and emissivity on the observed radiance is the responsibility of the TES algorithm. The enhanced SW-TES method can concurrently extract the LST and LSE from ECOSTRESS thermal infrared data by merging the SWA and TES techniques (Ru et al., 2023).

The equation for the SWA (16) represents a mathematical model that describes the value of the LSWT (Ru et al., 2023):

$$LSWT = A_{0ij}(\theta_v)+A_{1ij}(\theta_v)T_{bi}+A_{2ij}(\theta_v)\left(T_{bi}-T_{bj}\right)+ A_{3ij}(\theta_v)(T_{bi}-T_{bj})^2 \quad (16)$$

Where:

$LSWT$: This represents the estimated ground-level brightness temperature (T_g) for a specific thermal infrared band.

A_{0ij}, A_{1ij}, A_{2ij}, and A_{3ij}: These are the VZA-dependent (view zenith angle) regression coefficients for the combination of brightness temperature at the top of the atmosphere (TOA) in two bands i and j (T_{bi} and T_{bj}), respectively. However, the VZA-independent regression coefficients were used because the ECOSTRESS sensor has near-nadir-viewing angles (±26 degrees).

θ_v: This is the view zenith angle, representing the angle between the line of sight from the sensor to the Earth's surface and the vertical direction.

T_{bi} and T_{bj}: These are the brightness temperatures at the TOA in the respective thermal infrared bands i and j used for the combination in the SWA.

The coefficients for the SWA are determined using simulation datasets to minimize the root mean square error (RMSE) between the actual and estimated ground temperature values for different band combinations.

As a part of this methodology, ground-based validations are considered one of the reliable techniques for validating temperature retrieval estimations (Li et al., 2013). Hence, validations with ground measurements were obtained in four different study areas: Lake Issyk-Kul (Kyrgyzstan), Lakes Plobsheim, Gérardmer, and Longemer (France).

Chapter 3. Study area and data

This chapter describes the location and physical characteristics of the four lakes considered in this research and the datasets used to retrieve the LSWT in those areas, from imagery derived from the TIR satellites to in-situ measurements.

3.1 Location and Characteristics of the Lakes

Lakes with different characteristics such as altitude, size, and depth have been chosen as regions of study to estimate the LSWT as follows: Issyk-Kul Lake, Kyrgyzstan (Central Asia region); Gerardmer and Longemer Lakes, France (Vosges region); and the Plobsheim Lake, France (Bas-Rhin department).

3.1.1 Issyk-Kul Lake

One of the lakes considered for this research is the Issyk-Kul Lake, which is an endorheic lake situated between the coordinates 76° and 78°15'E, and 42°40'N (Figure 8) in the Central Asia area in the eastern region of Kyrgyzstan, with a high altitude of 1,607 m, a maximum length of 178 km, and its maximum width is 60.1 km (Klerkx et al., 2002).

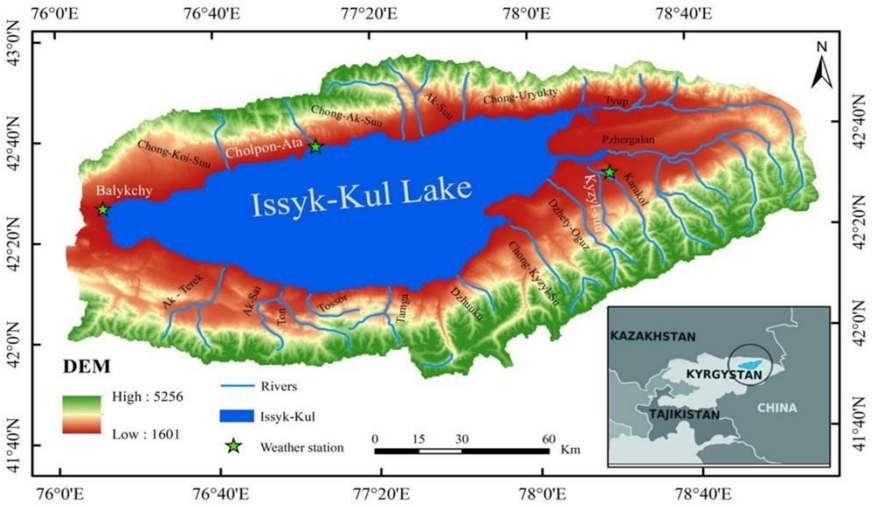

Figure 8. *Location of Issyk-Kul Lake, Kyrgyzstan, Central Asia (Alifujiang et al., 2020)*

This lake is the tenth largest (6,236 km^2) and the seventh deepest (668 m) lake in the world (Savvaitova et al., 1992; Delclaux et al., 2015), with a mean depth of 278.4 m, containing a volume of 17,738 km^3.

When considering the bathymetry of the Lake (Figure 9), the potential temperature in the Issyk-Kul Lake generally decreases with increasing depth, which is typical for all profiles measured during a study made in March 2003 in the Lake by Peeters et al. 2003. However, slight deviations from this decreasing trend were observed, especially in the upper 200 m and deeper regions just below 500 m depth. In the lake's deep water (> 600 m depth), the potential temperature ranged between 4.33°C and 4.40°C, the highest values ever observed in the deep water of Issyk-Kul. Additionally, the authors mentioned that the horizontal distribution of near-surface temperatures indicates that the central region of the lake is generally warmer than the shallow eastern region, specially during the spring season (March), where the coldest water was found in the shallow northeastern region of the lake (Peeters et al., 2003).

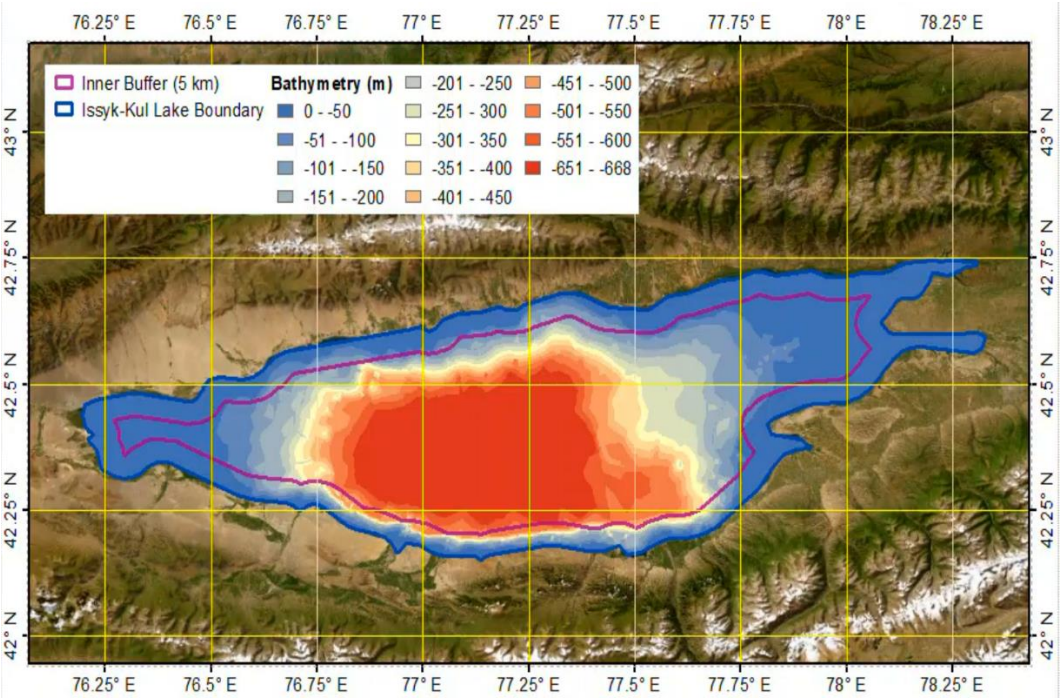

Figure 9. *Bathymetry of the Issyk-Kul Lake, Kyrgyzstan (LEGOS Laboratory)*

The Issyk-Kul Lake is located in the northern part of the Tien-Shan Mountains, with snow-topped peaks, of the Kyrgyz Republic, Central Asia. It is over an arid zone, more desert on the

west, followed by semi-desert and steppe on the east. The predominant vegetation is xerophytes. However, the vegetation type is a wetland region in certain areas where more water is found (Torgoev et al., 2013).

The importance of this water body for the region is also for touristic purposes, with some recreational centers receiving visitors annually (Savvaitova et al., 1992). The lake is affected by several environmental threats, as well as natural as anthropogenic origin: decline of the lake level resulting in a progressive increase in salinity of the water, incomplete vertical water exchange which results in eutrophication of the deep waters, risk of contamination by former or present industrial activities and uncontrolled agriculture (Klerkx et al., 2002).

Some of the atmospheric characteristics of the lake are moderate temperatures for air and water, despite the relatively low temperatures in the area around the lake, it never gets frozen during winter due to the high concentration of salt in its waters, and the sunny periods are prolonged (Peeters et al., 2003). Generally, the water in this lake is clear and transparent due to the overall salinity and the limited amount of organic life (Alifujiang et al., 2020).

Mostly, the average water surface temperatures in the lake are higher than their average air temperatures due to the different air and water thermal capacities throughout the years (Figure 10) (Alifujiang et al., 2020).

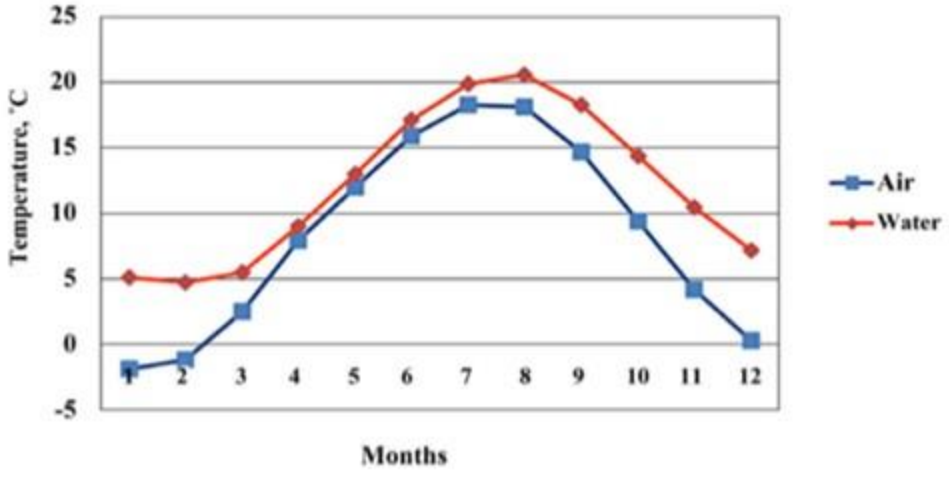

***Figure 10**. Average annual air and water temperature variations of Issyk-Kul Lake at MS Cholpon-Ata (1972-2009) (Alifujiang et al., 2020).*

More precisely, according to previous studies based on the data from the meteorological station “Cholpon-Ata” (Figure 8), located 100 m near the north side of the lake, the mean annual air temperature is 8.3 °C, and the water temperature is 12.1 °C. July and August presented the maximum mean temperatures (18.3° for air and 20.6°C for water), and minimum mean temperatures were registered in January and February (-1.9°C for air and 4.7°C for water) (Romanovsky et al., 2013).

The Issyk-Kul Lake is considered one of the sites suitable for calibration and validation due to the availability of ground measurements provided by the Cholpon-Ata meteorological station (Crétaux et al., 2018).

3.1.2 Gerardmer and Longemer Lakes

Gerardmer and Longemer Lakes, two other lakes of study, both located in the Grand-Est region, in the Vosges department of France, are two natural, dimictic lakes of glacial origin (Conseil Scientifique Plan Grands Lacs, 2023) (Figure 11).

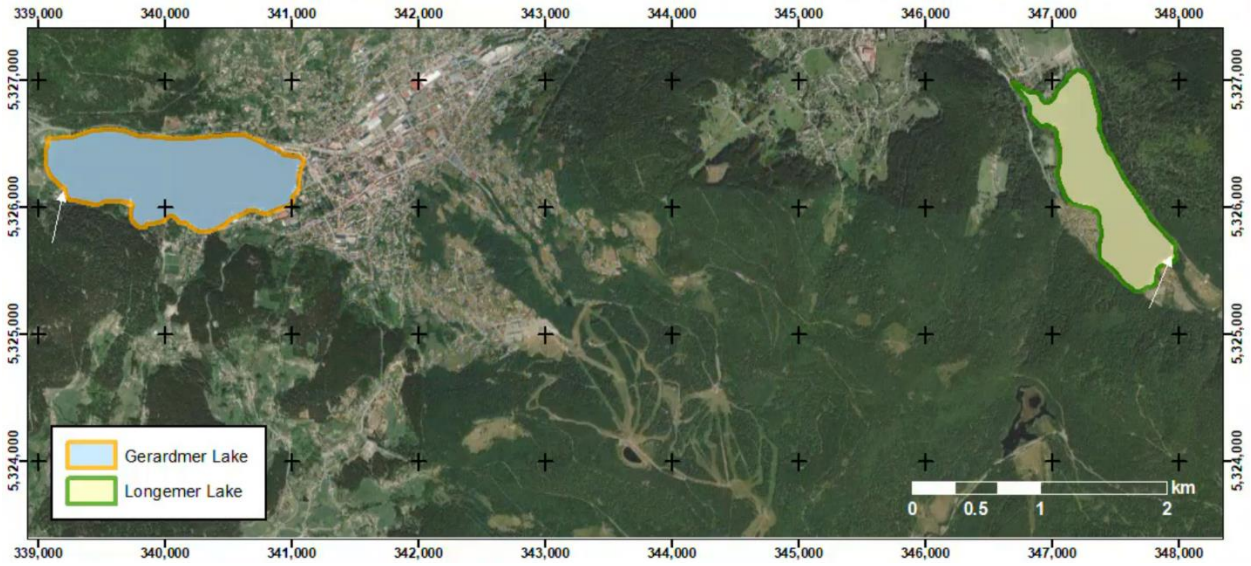

Figure 11. *Location of the Gerardmer and Longemer Lakes.*

The Gerardmer Lake is situated in the Jamagne Valley and is fed by the Jamagne River, which flows into the Vologne River. With its elliptical shape, this lake has a surface area of 1.16 km^2, a

perimeter of 5.22 km, and a depth of 36.2 m. Its Lake Biological Index (LBI) is 12.1, corresponding to average quality. It offers activities for boating, fishing, and swimming (AgroParisTech, 2017).

Figure 12. *Lake of Gérardmer (ICube, 2021).*

Longemer Lake is located as well in the Vosges region in France. The lake is classified as being in a medium ecological state. Regarding its trophic potential, Longemer Lake has a good potential for trophic productivity and high faunal biodiversity in the littoral zone. The lake is also managed by the Association Agréée de Pêche et de Protection du Milieu Aquatique (AAPPMA), which holds the fishing rights and sells fishing permits. It covers an area of 0.73 km^2, with a perimeter of 5.15 km and a depth of 29.5 m. Its LBI is 13.7, which corresponds to average quality. Its strong natural heritage is at the root of its urbanization. Like in the Gérardmer lake, this lake offers activities for boating, fishing, and swimming (AgroParisTech, 2017).

Figure 13. *Lake of Longemer (ICube, 2021).*

3.1.3 Plobsheim Lake

The Plobsheim Lake, located around fifteen kilometers south of Strasbourg, is a compensation basin designed to regulate the levels of the Rhine and Ill rivers at the entrance to the Strasbourg conurbation. It is the largest body of water in the department of Bas-Rhin, covering 6.6 km^2, with clear and shallow water, averaging 3 m in depth. This lake is known for its lush flora and is home to various fish species, such as carp, tench, perch, and catfish. Moreover, the Plobsheim lake has become a significant site for birds in Alsace. It is of great interest to avifauna throughout the year, particularly in winter. It is also crucial for nesting, summering, and the migration of various species. 234 bird species have been recorded on the lake and its banks over the last 15 years. Also, this lake is an essential habitat for waterbirds, leading to the implementation a biotope protection order for the site (Plans d'eau - Fédération de Pêche Du Bas-Rhin, n.d.). Several activities occur on the lake: professional and recreational fishing, boating, and windsurfing. Fishing competitions and regattas are held here every year. Recreational and tourist activities are also carried out along the water's edge.

Figure 14. *Lake of Plobsheim (Plans d'eau - Fédération de Pêche Du Bas-Rhin, n.d.).*

3.2 Imagery data

For this study case, in regards to the availability and access of the latest missions, the sensors and products considered for this research are imagery from the TIRS sensors onboard Landsat 8 and 9 missions, LST products derived from the MODIS sensors of Terra satellite; LST products from the SLSTR onboard the Sentinel 3 satellite; and imagery products from the ECOSTRESS sensor.

The radiometric features of some of the exploited satellite imagery with moderate and high spatial-spectral within TIR sensors and the future mission bandwidth are shown (Figure 15).

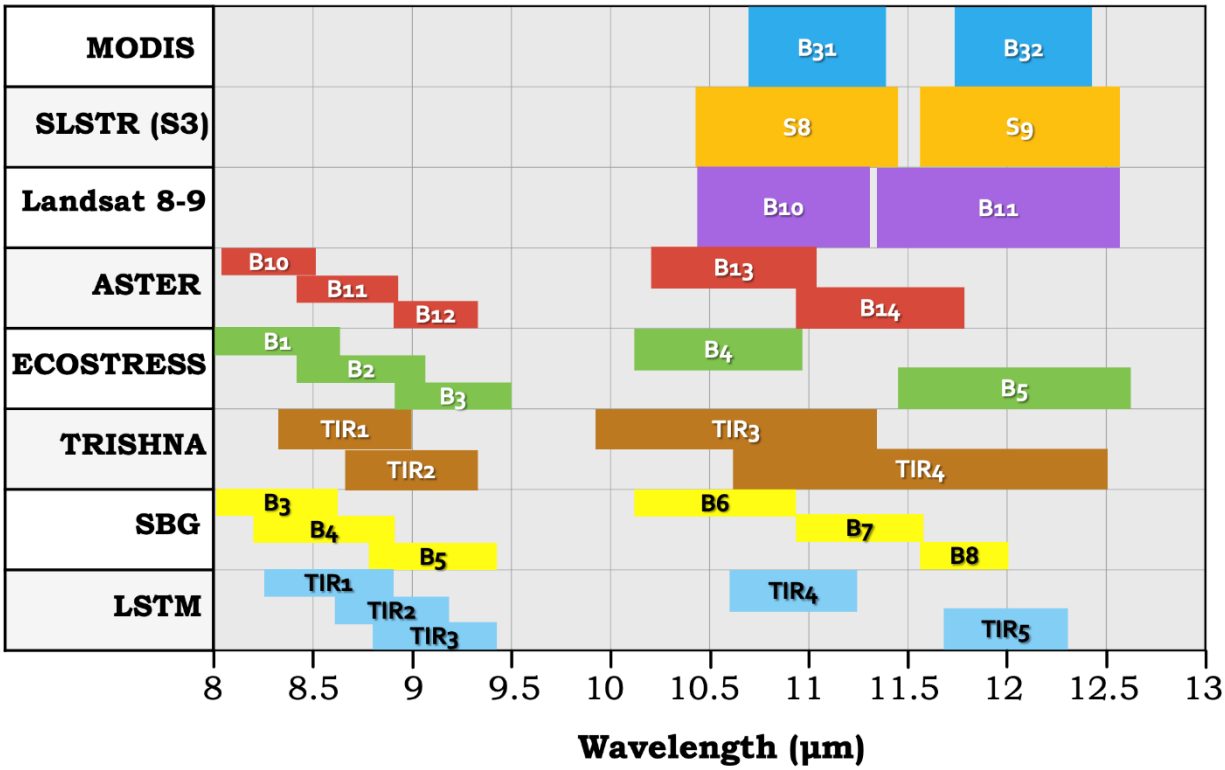

Figure 15. *Bandwidth of the exploited data and new future sensors for TIR imagery.*

Access and availability for each of these satellites were considered, having at least one image per month at the exact date and around the same time for Landsat 8-9, MODIS, Sentinel-3, and ECOSTRESS as possible, from 2019 to 2023 in the regions of Issyk-Kul, Gerardmer, Longemer, and Plobsheim Lakes.

3.2.1 Landsat 8-9 (TIRS)

Landsat 8, with its thermal infrared images, has been widely used to retrieve surface water temperatures (Dyba et al., 2022; Herrick et al., 2023; Jimenez-Munoz et al., 2009; Prats et al., 2018; Sharaf et al., 2019; Simon et al., 2014; Vanhellemont, 2020). This mission launched in 2013, including two thermal infrared bands (TIR) with a spatial resolution of 100 m and a range spectral resolution from 10.6 to 11.2 µm (Band 10) and 11.5 to 12.5 µm (Band 11) (Khalil et al., 2017).

The performance of the TIRS instrument from Landsat 8 has shown stability and less noise circumstances specially in the Band 10 for Collection 1. However, two side effects could not be corrected after its launch: non-uniform banding and error in the absolute radiometric variation. These adverse effects are correlated to the radiance magnitude outside the instrument view range and caused by a problem in a stray light, where radiance out of view range interferes with the optical system, adding noise in the signal for the focal plane detector (Gerace et al., 2017).

The solution to these problems has been through the performance of the stray light correction algorithm, based on using near-coincident thermal data (i.e., Terra/MODIS) to obtain functional relationships between out-of-field radiance and stray light signal on TIRS bands, reducing the banding from 2% or higher in terms of radiance (before correction) to under 0.5% (after correction). The artifact absolute error is reduced as high as 9% in radiance (for Band 11) to 0.5% (in both bands). With the validation of this algorithm, it is possible to enhance the Band 10 and even the Band 11 performances, allowing the LST retrieving process by the split-window approach (Gerace et al., 2017).

However, Landsat-9 as the latest satellite carrying TIRS instruments from NASA, released in September 2021 and publicly available for access to data in February 2022, has changed the design of the optical system to improve the stray light problem given in the Landsat 8 by adding baffles placed within the optical telescope to block the stray light paths. As a preliminary result of TIRS-2, total stray light has been reduced by approximately 1% (Mccorkel et al., n.d.; Montanaro et al., 2018). Landsat-9 provides a higher radiometric resolution (increased the quantization in 14-bit instead of 12-bits for its predecessor) and can still be complemented with Landstat-8 to improve the revisit time, as they still share the exact temporal and spatial resolution, showing a similar spectral response function between Landsat 8 and 9 (Figure 16).

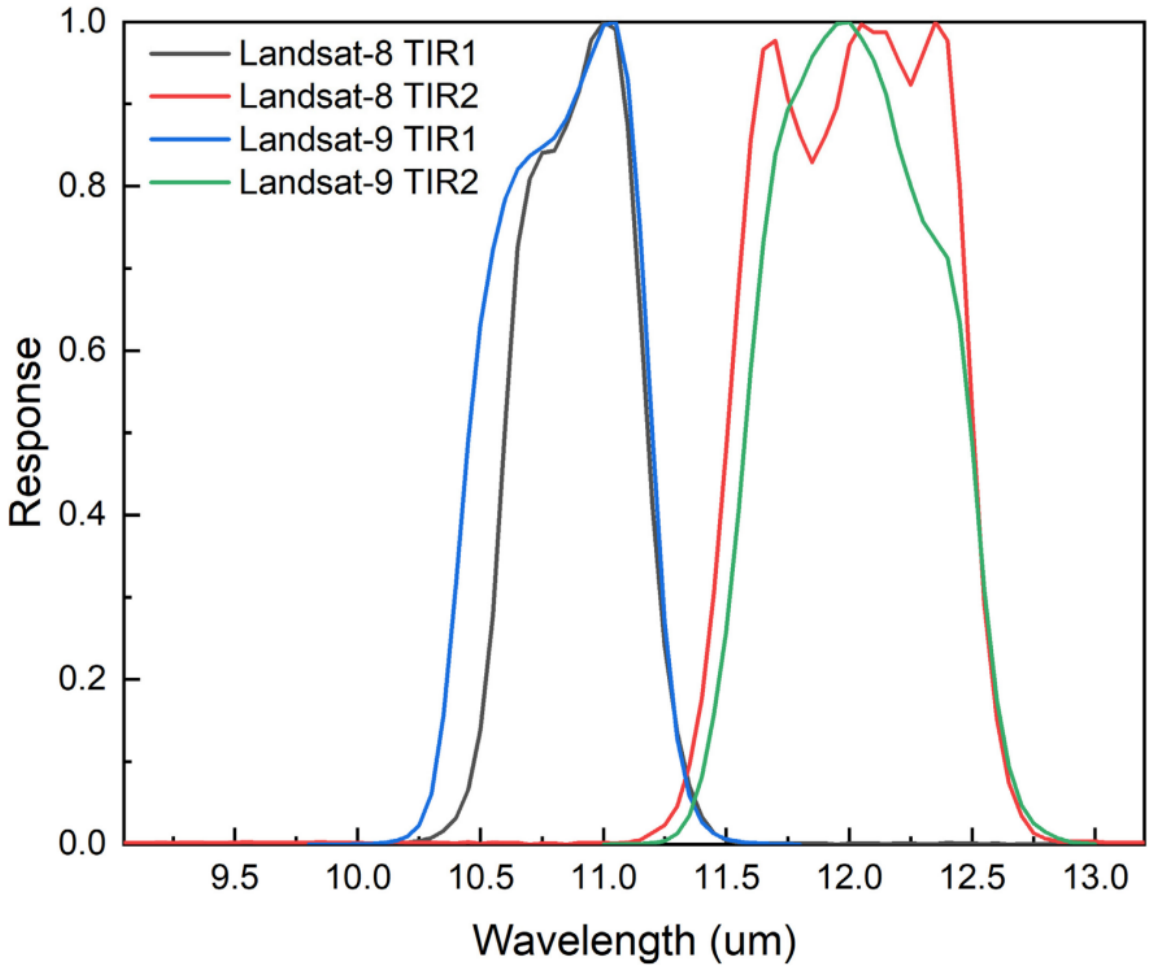

Figure 16. *Spectral Response Functions (SRFs) of Landsat-8 and Landsat-9 bands (Ye et al., 2022b).*

The Landsat 8-9 images were analyzed from 2019 to 2023 in Issyk-Kul, Gerardmer, Longemer, and Plobsheim Lakes.

3.2.2 MODIS (Terra)

The Moderate Resolution Imaging Spectroradiometers (MODIS) onboard the satellite Terra of NASA launched in 1988, have an extensive spectral range of 36 channels from 0.415 to 14.235 µm, where its thermal bands are the band 31 (10.78-11.28 µm) and 32 (11.77-12.27 µm) with a spatial resolution of 1 km in this range; this sensor has been helpful to study the water temperature of lakes providing daily-basis monitoring capable of collecting information on atmosphere, land, and water, (Lazhu et al., 2022; Reinart et al., 2008b).

The analyzed images were collected from 2019 to 2023 in the Issyk-Kul and Plobsheim Lakes regions.

3.2.3 Sentinel-3 (SLSTR)

The Sentinel-3A and 3B satellites by the European Commission's Copernicus program, launched on February 16, 2016, and April 25, 2018, respectively, carrying the Sea and Land Surface Temperature Radiometer (SLSTR) sensor, have been designed to provide information on the land and water temperature. It has channels in the middle-infrared (MIR) and TIR ranges (centered at 3.74, 10.85, and 12.02 μm), providing 1 km spatial resolution for Land Surface Temperature values. The LST product is obtained using a split window algorithm (Nie et al., 2021).

Sentinel-3 (SLSTR) images were analyzed from 2019 to 2023 in the Issyk-Kul and Plobsheim Lakes regions.

3.2.4 ECOSTRESS

The ECOsystem Spaceborne Thermal Radiometer Experiment on Space Station (ECOSTRESS), one of the modern missions, was launched at the International Space Station (ISS) in June 2018. This satellite collects thermal data over both land and water with a spatial resolution of 70 m and a revisit period of 4–5 days. It carries 5 thermal channels, with a spectral resolution from 8.29 to 12.09 μm, providing data for land surface temperature and emissivity (L2_LSTE). The orbit of the ISS is irregular (non-geostationary) or geosynchronous with earth, which means it is syncrhronized with earth's rotation. The ISS collects measurements continuously between approximately 52°N and 52°S at different times of the day. The overpass return frequency for any same spot on Earth is 1-5 days, depending on latitude, with some areas measured multiple times in a single day, particularly at higher latitudes where the ISS orbital direction shifts. This irregular orbit of the ISS provides a unique opportunity for the ECOSTRESS to capture thermal infrared radiation data with good spatial and temporal resolutions, including diurnal cycle sampling (Fisher et al., 2020).

The LST data in the ECOSTRESS mission is obtained using the Temperature and Emissivity Separation (TES) retrieval algorithm. The L2_LSTE product is generated from the ECOSTRESS instrument and L1 products. The ECOSTRESS L2 product incorporates additional data from numerical weather prediction for atmospheric correction and the generation of LST and broadband emissivity (Fisher et al., 2020).

The collection of ECOSTRESS images analyzed was from the second half of 2019 to 2023 in the regions of Issyk-Kul, Gerardmer, Longemer, and Plobsheim Lakes.

3.2.5 Datasets from CCI Lakes

An external database of surface water temperatures of lakes called CCI Lakes products, conducted on the framework of the Climate Change Initiative of the European Space Agency (ESA), has been exploited as a reference set. This dataset, recently developed (updated in July 2022 – v.2.0.2), contains global lake products for the following five thematic climate variables derived from global satellite data: Lake Water Level (LWL), Lake Water Extent (LWE), Lake Surface Water temperature (LSWT), Lake Ice Cover (LIC) and Lake Water-Leaving Reflectance (LWLR). This data presents a spatial coverage of over 2,000 relatively large lakes worldwide, with a 1/120 degree grid (≈1 km) spatial resolution and a daily temporal resolution. It provides one file (NetCDF format) per day, containing all parameters listed above, with a temporal coverage from 1992 to 2020. The LSWT combines sensors (ATSR-2, AATSR, AVHRR-3) (Carrea et al., 2023; Crétaux et al., 2018).

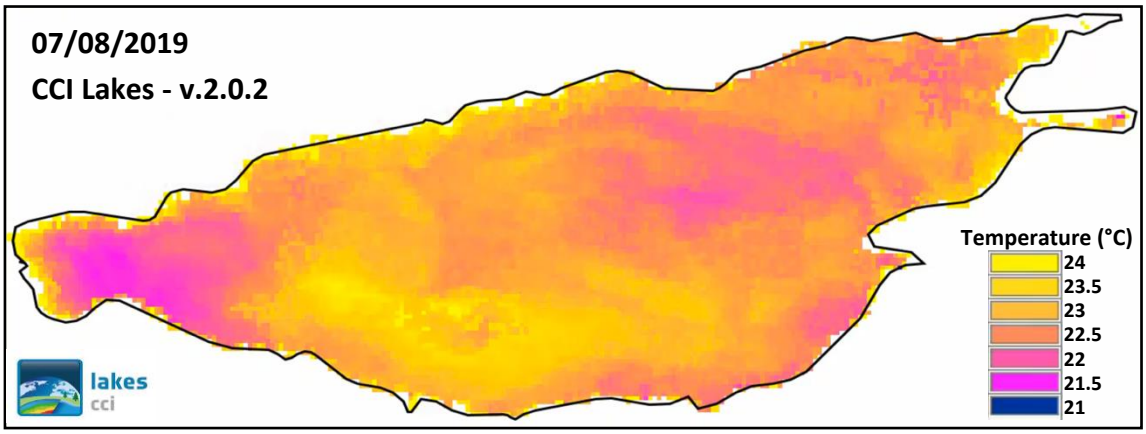

Figure 17. *CCI Lakes v.2.0.2 sample for 07 August 2019.*

3.2.6 Atmospheric water vapor content (wvc) and near-surface air temperature (T_0).

Atmospheric water vapor content (wvc), like a primary variable in the hydrological cycle, is essential when retrieving land surface temperatures from Landsat 8 (TIRS) algorithms (Ren et al., 2015). The wvc values were obtained from the ECMWF datasets at every 0.25 degrees (www.ecmwf.int) for each analyzed date, averaging the latitude and longitude (Figure 18) array values where the lake is located and at each hour according to the acquisition time of the Landsat images for each of the considered dates:

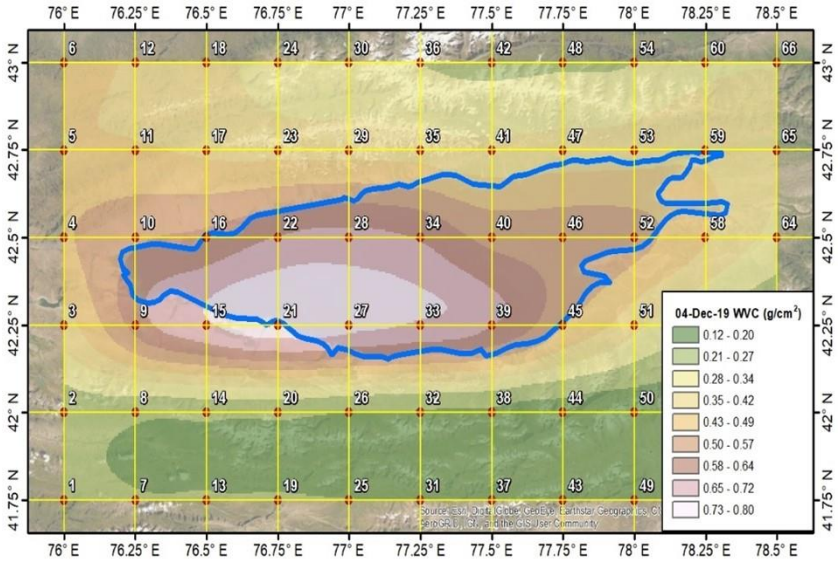

Figure 18. *GRID values for water vapor content from ECMWF.*

The surface air temperature (T_0) values were taken from ECMWF datasets at every 0.25 degrees (www.ecmwf.int) and averaging the values of the latitude and longitude (Figure 19) array where the lake is located and at each hour according to the acquisition time of the Landsat images for each of the considered dates.

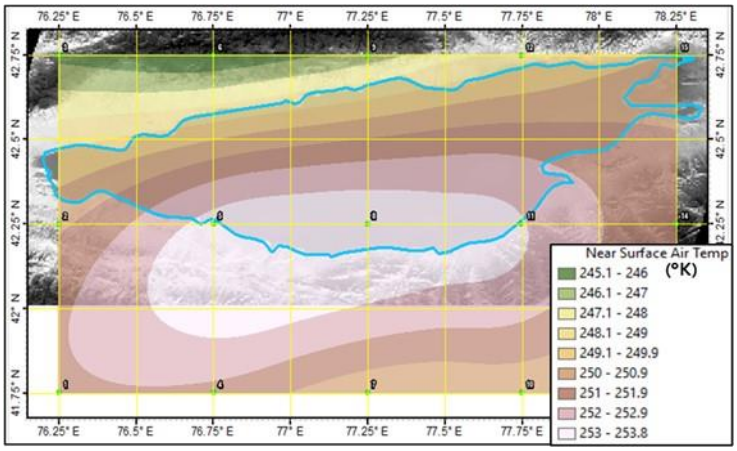

Figure 19. *GRID values for air temperature from ECMWF.*

3.3 Ground data

There were different sources considered within the in-situ observations provided and obtained in the field, listed as follows:

- Meteorological datasets (Issyk-Kul Lake) and in-situ measurements from buoys (Plobsheim, Gérardmer, and Longermer Lakes).
- Ground measurements were obtained with thermal sensors from a torrent board.
- Datasets from a radiometer (CIMEL CE 312-2) and a FLIR thermal camera.
- CCI Lakes datasets product.
- Atmospheric profiles (water vapor content and near-surface air temperature) help to retrieve the LSWT from Landsat 8 and 9.

3.3.1 Datasets from Meteorological Stations

The meteorological station datasets at Cholpon-Ata, located a few meters from the Issyk-Kul Lake, were provided by the LEGOS Laboratory from Toulouse, France, led by Jean François Crétaux. The availability of these datasets was from January 2008 until September 2021. However, some values were missing in the water and air temperatures in some months of each

year. Therefore, assumptions like interpolation and retrieving temperatures from other years as a reference were considered to fulfill these datasets.

Over this period, water temperatures in the Issyk-Kul Lake varied from 4.8 to 21.8 °C, with a mean temperature of 12.9 °C. The highest monthly water temperature was recorded in August, with an average temperature of 20.7 °C, and the lowest in February, with an overall temperature of 5.5 °C. The highest variability of water temperatures was observed generally in May and the lowest in February (Figure 20).

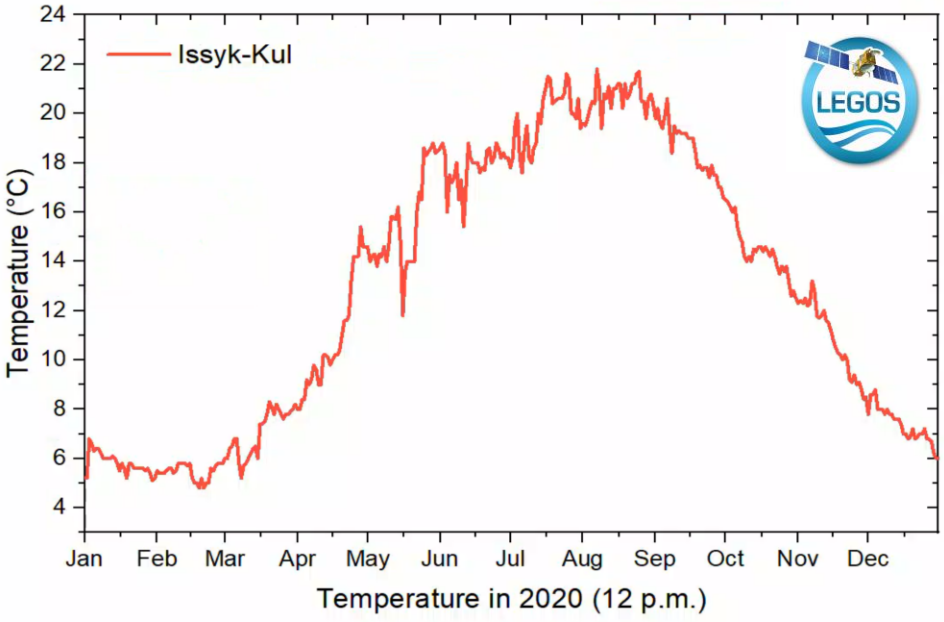

Figure 20. *Dataset example of the Cholpon-Ata Meteorological Station in 2020.*

3.3.2 In-situ datasets from buoys

Data collected locally using buoys will be used to validate the process. These temperature data were collected for lakes Gérardmer and Longemer for some months in 2021 and 2022 through three data acquisition campaigns (Plan Grands Lacs - Communauté de Communes Gérardmer Hautes Vosges, n.d.).

As well as the temperature, the buoy provides the time of acquisition. The buoys record a new temperature for each hour. Under the buoys, probes are placed at several depths in the lake (Figure 21). They provide the temperature at different lake levels to determine the thermocline.

The first temperature is collected at 50 cm. Temperatures are then measured every 1 meter down to 10.5 m, and from this level onwards, measurements are taken every 4 meters. The last measurement is taken at 34 m for Gérardmer and 29 m for Longemer (Suivi Climatique National & Fonctionnement Des Lacs : Une Bouée Installée Sur Le Lac de Gérardmer - Gerardmer Info, n.d.).

Figure 21. *Buoy in Gérardmerd Lake is used to measure the temperature at various levels of the lake (Suivi Climatique National & Fonctionnement Des Lacs: Une Bouée Installée Sur Le Lac de Gérardmer - Gerardmer Info, n.d.).*

Other data from the buoys, but this time in the lake of Plobsheim, is provided, and measurements are taken using multi-parameter loggers attached to 7 buoys approximately 1 m below the water surface, distributed from north to south in the lake (Figure 22). The acquisition frequency is every 30 minutes, and measurements of the temperature gradient were taken from the surface to the bottom of the water, with a 50 cm increment up to 3 m depth. These measurements have enabled us to observe the absence of temperature gradient in the water

(only a few tenths of a degree difference between the surface and the bottom of the water body).

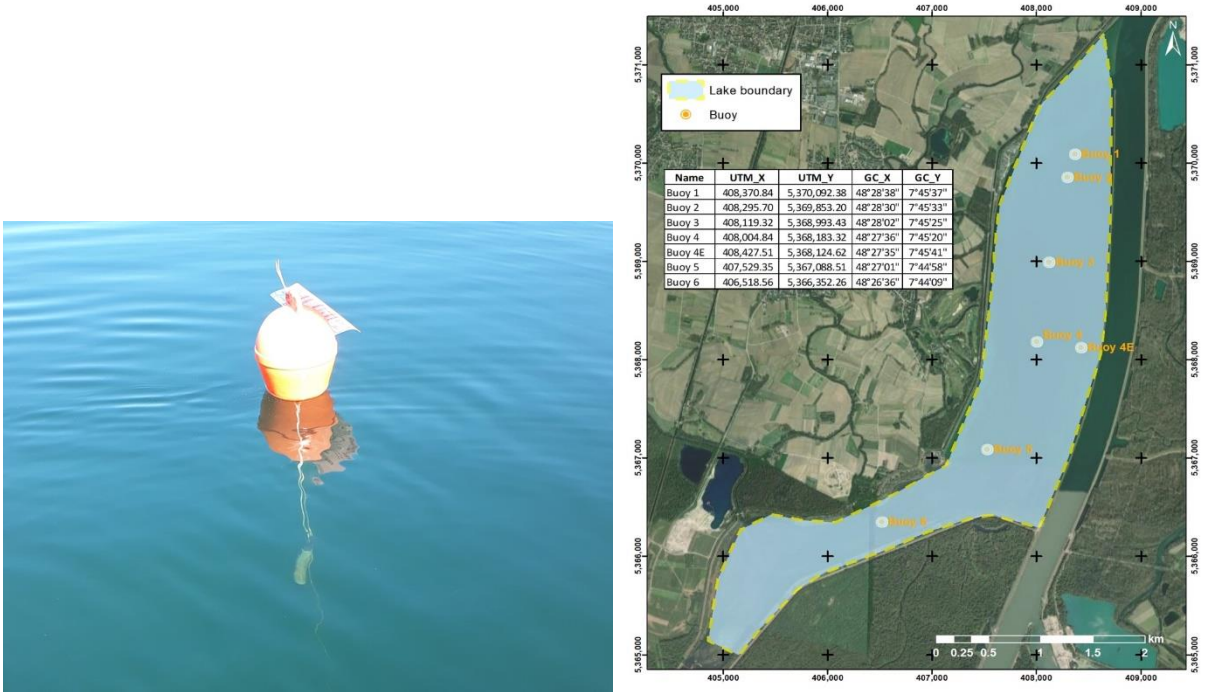

Figure 22. *On the left, a buoy in Lake of Plobsheim used to measure the temperature at various levels of the lake (Plans d'eau - Fédération de Pêche Du Bas-Rhin, n.d.); on the right, a map of the location of the seven buoys in the Plobsheim lake.*

3.3.3 Torrent Board

The instrumentation used for this device consisted of sensors to measure humidity, water, and air temperature, which were set up on a floating platform called a Torrent board (Figure 23). It contains four thermal immersion probes for measuring the surface temperature up to 35 centimeters of depth; 1 thermal probe set on the top of the buoy to measure the air temperature and humidity; a GPS and a gyroscope. The ensemble of this device was made with the collaboration of one of the TRIO team engineers from the ICube laboratory. The description of the sensors and items carried out on the torrent board is as follows:

- The Torrent Board characteristics:

- The dimensions are 105 x 65 x 25 cm3 (L x W x H).
- 4.7 kg weight (not considering the sensors).
- The material of this device can support temperature storage from -10 up to 70 °C (Torrent Board, 2020).
- A large and heavy traveling wood/metallic case and a light-carrying bag.

- Water temperature
  - A thermal immersion probe, PT100/Class A type, measuring the water temperature on the first centimeters (35) of water depths.
  - 4-wire connection with a range measuring from -50 to 200 °C.
  - Reaction time (T05/T09) of 2.5/6.5 s, 6 mm probe diameter, and 20 mm length made of stainless-steel material.
  - IP67 protection and a 1.5 silicone cable.
  - Air temperature and humidity.
  - A thermal probe SHT85 is set on the top of the buoy.
  - High-accuracy RH& T sensor for demanding measurement and test applications.
  - Typical accuracy of ±1.5 %RH and ±0.1 °C.
  - Pin-type packaging for easy integration and replacement, fully calibrated, linearized, and temperature-compensated digital output.
- GPS
  - 165 dBm sensitivity, 10 Hz updates, 66 channels 5V friendly design and only 20mA current draw breadboard friendly + two mounting holes.
  - RTC battery compatible.
  - Built-in data logging.
  - PPS output on a fix.
  - 25 km altitude.
  - Internal patch antenna + u.FL connector for external active antenna.
  - Fix status LED.
- Datalogger

    - Lopy4 - ESP32, a transmitter towards a data logger based on radio frequencies.
- Accelerometer
    - Attitude system for roll, pitch, and yaw for water roughness measurement.
- Pack of energy
    - Batteries with 5100mAh Li-Ion.

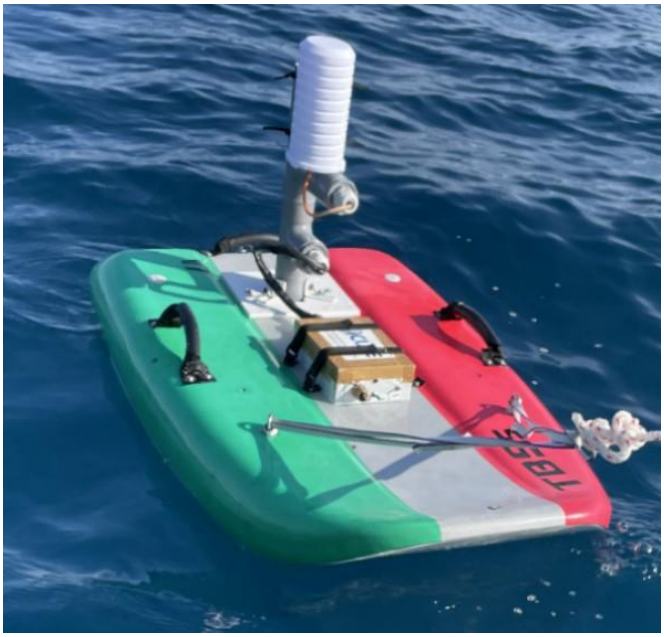

Figure 23. *Torrent Board*

The results for this research concerning the Cal/Val of the skin water surface and near-surface temperatures to study the spatial variability over the lake, and thus, compared to Sentinel-3/MODIS satellite imagery.

3.3.4 Radiometer CIMEL 312-2

The CIMEL CE 312-2 radiometer (Figure 24) is a six-band radiometer used to measure the thermal infrared radiances of distant objects. It features five LWIR bands with a 10-degree field of view comparable to the ASTER bands. It also features one wide band. The portable CIMEL CE 312-2 radiometer has a 10-degree field of view, supports automated acquisitions, and measures the radiances of distant objects. In multi-band research, emissivity spectra are interpolated and integrated using the spectral response of the CIMEL 312-2 radiometer. This instrument's radiance measurement calculates the target's effective radiance. The device uses a thermopile sensor with particular coefficients for the sensor's spectrum response (Payan et al., 2004).

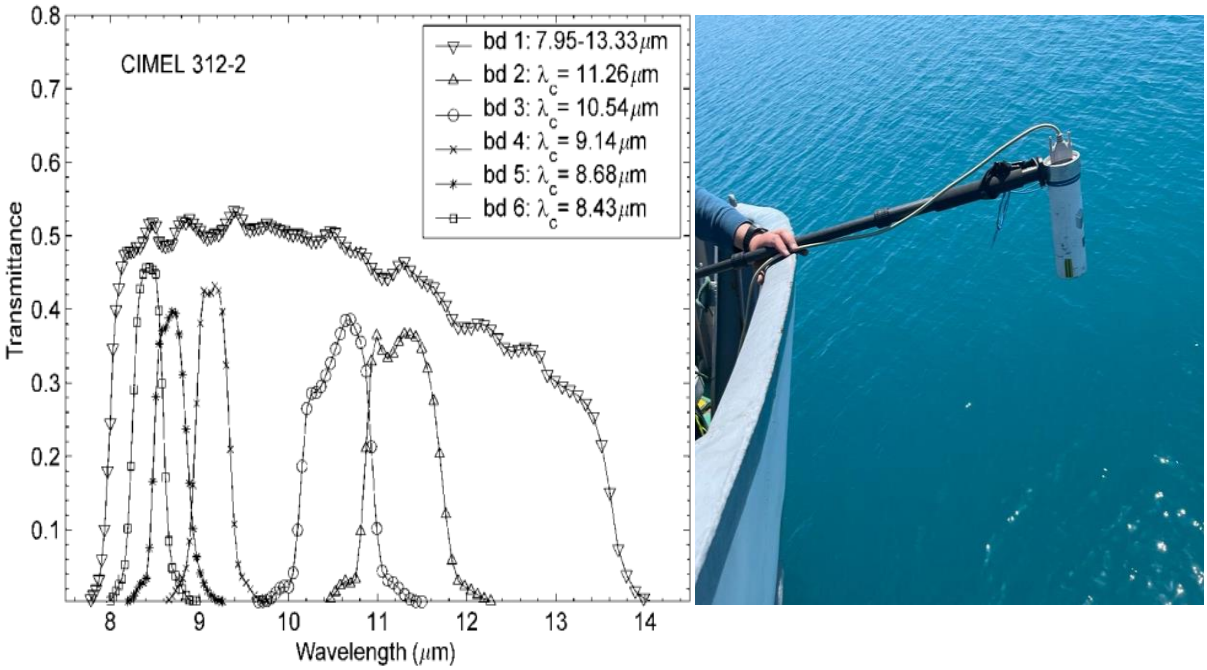

Figure 24. *On the left are the Spectral responses of the CIMEL 312-2 at the central wavelength of each band (Payan et al., 2004); on the right, the CIMEL-312-2 is in operation in the field.*

3.3.5 Infrared Camera FLIR T-560

The FLIR T-560 (Figure 25) is an infrared camera type produced by FLIR Solutions, a firm recognized for its thermal imaging cameras. The FLIR T-560 is intended for industrial and research applications requiring precise temperature monitoring and thermal imaging. This device has the following major features and characteristics:

- Thermal Sensitivity/NETD: <40 mK @ 30°C (86°F).
- Accuracy: ±2°C (±3.6°F) or ±2% of reading.
- Digital Camera 5 MP, with built-in LED photo/video lamp.
- Display4", 640 × 480-pixel touchscreen LCD with autorotation.

Figure 25. *FLIR Camera T-560*

Chapter 4. LSWT Retrieval Results and Discussion

This chapter shows the results from comparing the moderate and high-resolution TIR sensors, the results derived from the retrieval analysis of the algorithms applied for Landsat 8-9, and the results between those TIR sensors and the in-situ datasets. Besides, an explanation of the obtained results and comparison of the LSWT estimations to previous studies gives place to the discussion of its implications or consequences by describing the limitations and the contributions of this research to the previous literature.

Two standard metrics are used to assess the reliability of the results derived from the intercomparison of the sensors and the sources considered in this research: the mean absolute error (MAE) and the root-mean-squared error (RMSE). These methods are helpful in models, data analysis, and evaluation, and they provide measures of the accuracy of data predictions or estimates compared to the actual values of the data. The MAE and RMSE are for a sample of *n* observations y (y_i, i = 1, 2,…, n) and n associated model predictions $\hat{y}$, their equations are expressed as follows (Hodson, 2022):

$$MAE = \frac{1}{n}\sum_{i=1}^{n}|y_i - \hat{y}_i| \quad (17)$$

$$RMSE = \sqrt{\frac{1}{n}\sum_{i=1}^{n}(y_i - \hat{y}_i)^2} \quad (18)$$

The MAE measures a model's typical or average error and is calculated by taking the mean of the absolute differences between predicted and reference values. The MAE is represented in equation (17), where the fundamental differences are obtained by subtracting the predicted values from the values of reference, taking the absolute value of the result, and then averaging these absolute differences across all the observations in the dataset. On the other hand, the RMSE conveniently represents the typical or standard error for normally distributed errors. It is calculated by determining the difference between each predicted value ($\hat{y}_i$) and the corresponding reference value (y_i). The differences are then squared and summed up. Next, the mean of the squared differences is calculated by dividing the sum by the total number of

observations (n). Finally, the RMSE is obtained by taking the square root of the mean squared difference, represented in the equation (18) (Hodson, 2022; Use Excel to Calculate MAD, MSE, RMSE & MAPE - Dawn Wright, Ph.D., n.d.).

In the graphs of the results showing the LSWT estimates, the upward and downward error lines/bars (positive and negative) represent the standard deviation of the LSWT mean for each point, where the standard deviation values considered to show our estimates are from 0 to 1 °C. With this, we can observe the uncertainty associated with each data point.

4.1 Sensors Intercomparison

This validation method is sensitive to temporal and spatial resolutions between the LST products considered. Hence, for this first set of images, the acquisition time for each date in 2019 over the Issyk-Kul Lake was relatively close to each other, considering the temperatures from the meteorological station as the values of reference for the rest of the sources. The acquisition time for each of the sources is given in local time as follows:

Source	Acquisition time
Meteorological station	**Noon**
Landsat 8	**Between 11:00 a.m. and noon**
Sentinel-3	**Between 10:30 a.m. and noon**
MODIS	**Between 11:00 a.m. and 1:00 p.m.**
CCI Lakes	**Daily aggregation interval pinned to 6:00 p.m. (12:00 UTC)**

Table 5. *The acquisition time for the sources to compare.*

Areas of interest of 100 km^2 (identified as the light blue squares – Figure 26) are located at different regions (East or West region of the lake) by date according to the availability of pixels after retrieving to extract the LSWT over these regions.

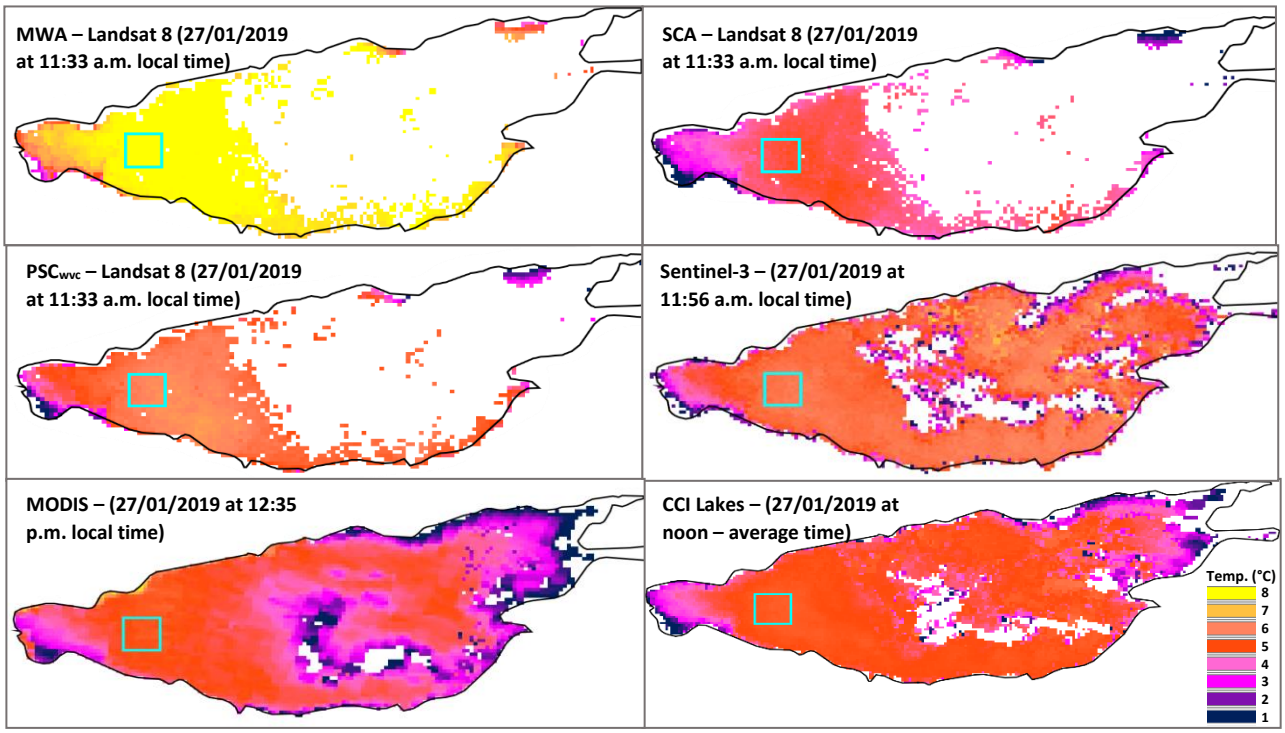

Figure 26. *Samples of LSWT in the Issyk-Kul Lake in 2019 derived from the Landsat 8 mono-channel algorithms and multi-sensors in °C*

For this LSWT estimation, one Landsat 8 image per month in 2019 is chosen to be compared with the values from the exact date and closest time from other sources, such as the meteorological station, which are the values of reference for this comparison, and the CCI Lakes product, Sentinel-3, and MODIS.

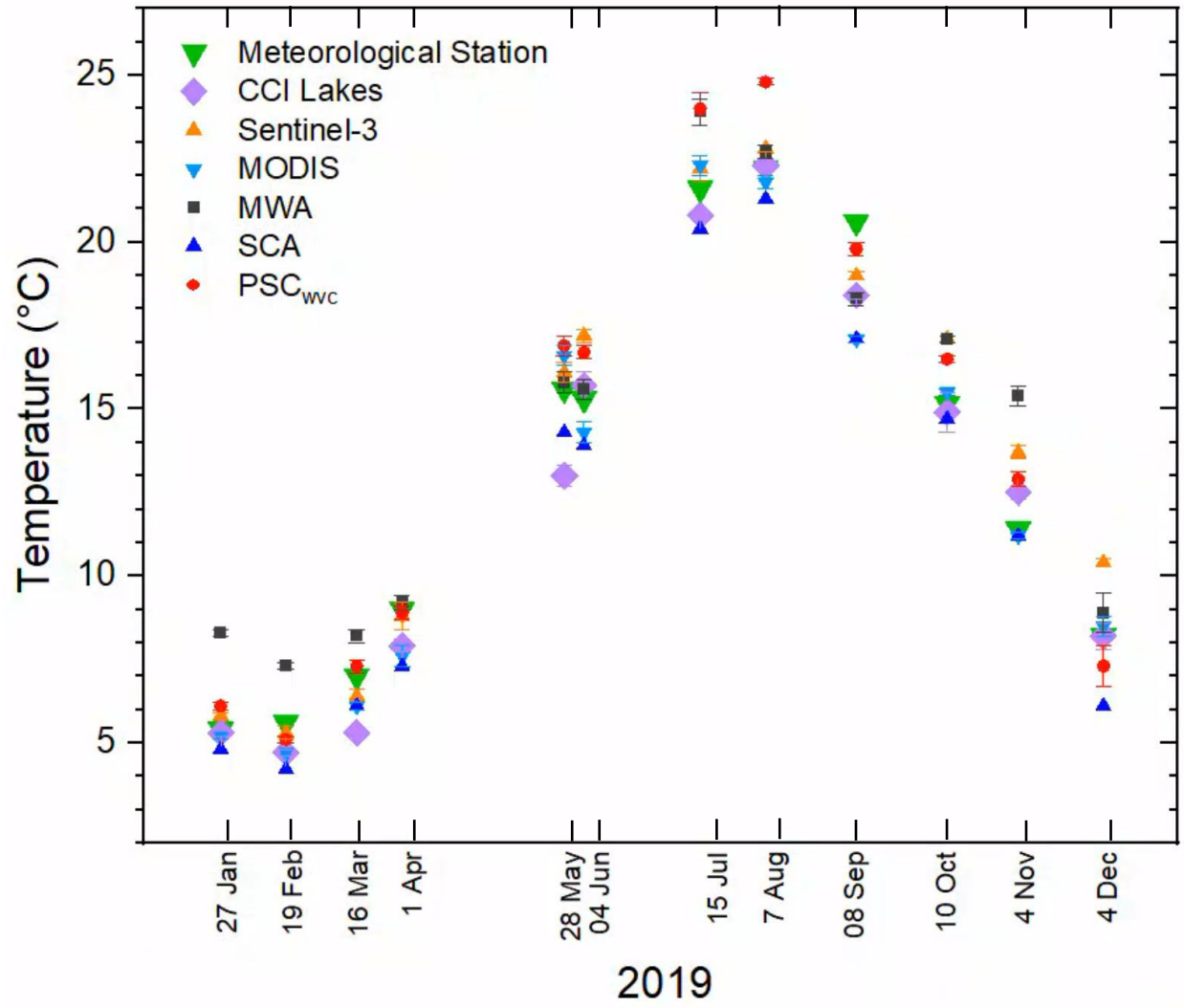

Figure 27. *Sensors intercomparison (Landsat 8 mono-channel algorithms, Sentinel-3, MODIS, Meteorological Station, and CCI Lakes) in the Issyk-Kul Lake in 2019*

Generally, all the sensors follow a similar seasonal temperature trend throughout the year (Figure 27). The SCA retrieval method underestimates the LSWT values on most dates compared to the rest of the sources.

2019	27/Jan	19/Feb	16/Mar	01/Apr	28/May	04/Jun	15/Jul	07/Aug	08/Sep	10/Oct	04/Nov	04/Dec	MAE	RMSE
Station-S3 (°C)	-0.40	0.30	0.60	0.20	-0.50	-1.90	-0.60	-0.60	1.60	-1.94	-2.30	-2.20	**1.10**	**1.34**
Station-MODIS (°C)	0.20	0.90	0.90	1.40	-1.00	1.00	-0.70	0.40	3.50	-0.34	0.20	-0.30	**0.90**	**1.25**
Station-CCI Lakes (°C)	0.10	0.90	1.70	1.10	2.60	-0.40	0.80	-0.10	2.20	0.26	-1.10	0.00	**0.94**	**1.25**
Station-(PSC_{wvc}) (°C)	-0.70	0.50	-0.30	0.10	-1.30	-1.40	-2.40	-2.60	0.80	-1.34	-1.50	0.90	**1.15**	**1.37**
Station-SCA (°C)	0.60	1.40	0.90	1.70	1.30	1.40	1.20	0.90	3.50	0.46	0.20	2.10	**1.31**	**1.55**
Station-MWA (°C)	2.90	1.70	1.20	0.20	0.20	0.30	2.30	0.50	-2.30	1.94	4.00	0.70	**1.52**	**1.91**

Table 6. *Differences in temperatures in the Issyk-Kul Lake in 2019 between the meteorological station and all the sensors with their respective MAE and RMSE*

SCA retrieval is the least corresponing algorithm to the in-situ data, with 1.55 °C of RMSE, and also presents the more significant differences in temperatures concerning the in-situ data (MAE of 1.31 °C). While the PSC_{wvc} shows more correspondence when compared to the SCA, with 1.37 °C of RMSE. Besides, Sentinel-3 estimates show LSWT values consistent with in situ data, with a RMSE of 1.34 °C to that from PSC_{wvc}. However, for these data sets, the nearest sources to the in-situ data are the MODIS sensor and the CCI Lakes product, as they provide 1.25 °C of RMSE for both of them (Table 6).

4.2 LSWT Retrieval Analysis from Sensors

The findings of the retrieval study of the methods used for Landsat 8–9, the comparison between the LSWT estimates from moderate sensors (Sentinel-3 and MODIS) and high-resolution (Landsat 8 and ECOSTRESS) TIR sensors are displayed in this section.

4.2.1 Landsat 8

At Issyk-Kul Lake, as the first study case, LSWT obtained with the MWA, SCA, PSC_{wvc}, and SWA were retrieved using Landsat 8 imagery. Using Landsat 8 Collection 1, after performing the SWA

method, it was corroborated that a stray light effect caused banding or stripping (Figure 28) mainly from the band TIR2 – B11 for most of the dates using this method. Thus, bias could be generated when estimating LSWT values for intercomparison with the other sensors and the Landsat 8 mono-channel algorithms. Hence, this method has been excluded for the rest of the dates in 2019 in the Issyk-Kul Lake region, and no further comparison has been executed using this algorithm from the Landsat 8 Collection 1.

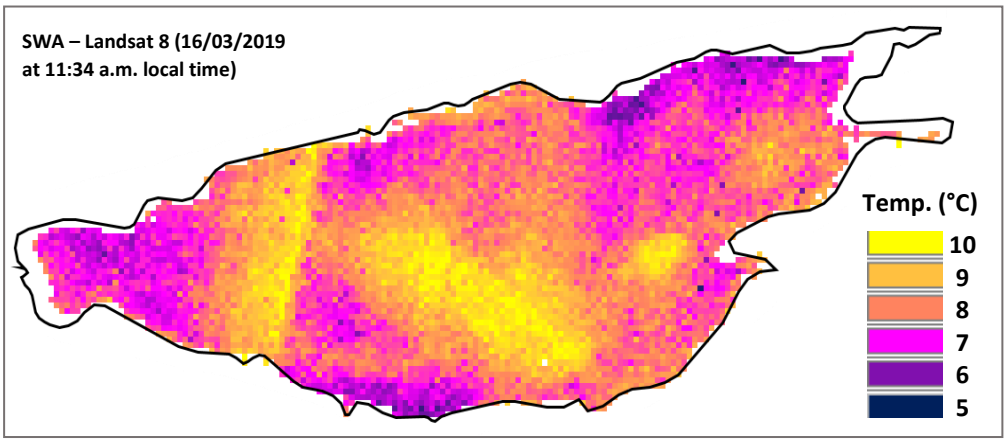

Figure 28. *A sample from the Issyk-Kul Lake in 2019 of the SWA method showing the Banding/stripping effect.*

For those algorithms using a single channel (MWA, SCA, PSC_{wvc}), the considered band is the B10 (TIR-1) from the Landsat 8 satellite. Areas of interest of 100 km^2 (identified as the light blue square – Figure 29) are located at different regions (East or West region of the lake) by date according to the availability of pixels after retrieving to extract the LSWT over these regions. The differences in temperatures between MWA, PSC_{wvc}, and SCA could be inferred until 4 °C between them (Figure 30). However, SCA and PSC_{wvc} showed closer values between each other (differences of 2 °C).

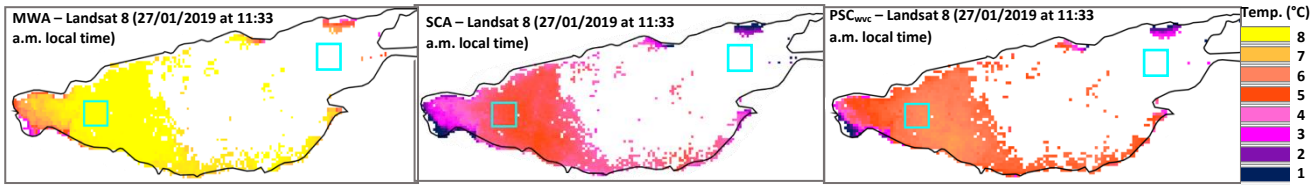

Figure 29. *Samples of LSWT in the Issyk-Kul Lake in 2019 derived from the Landsat 8 mono-channel algorithms*

For this LSWT estimation, one Landsat 8 image per month in 2019 was chosen to be compared with the values from the exact date and closest time from other sources, such as the meteorological station, which are the values of reference for this comparison, and the CCI Lakes product (Figure 30).

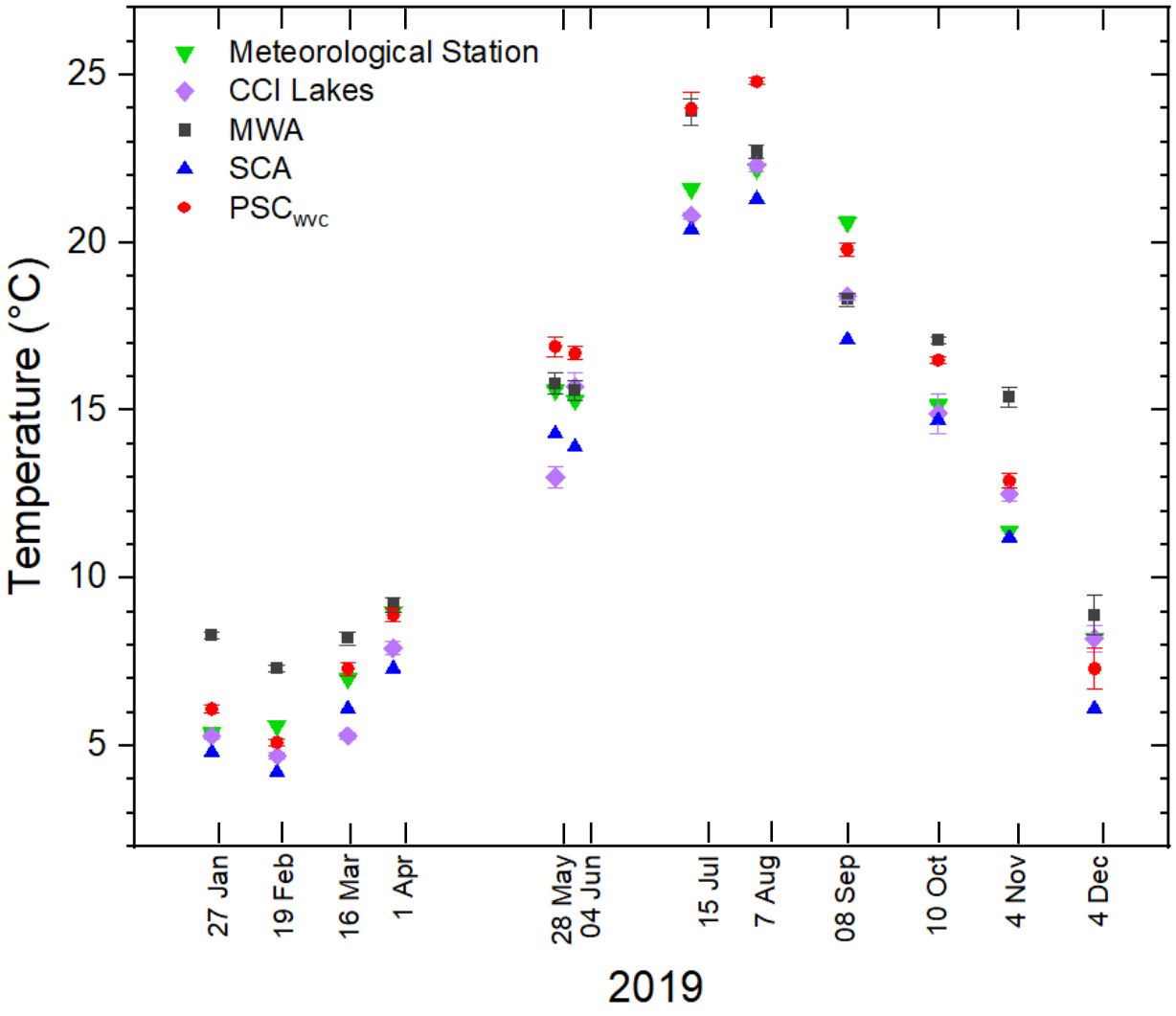

Figure 30. *LSWT estimates in the Issyk-Kul Lake in 2019 derived from Landsat 8 mono-channel algorithms, compared to in-situ data and CCI Lakes product.*

The meteorological station at Cholpon-Ata guides the region's variability and it corresponds to the rest of the sources. After this comparison, in terms of Landsat 8 mono-channel algorithms, the PSC_{wvc} is more agreed than the other two algorithms (SCA and MWA) to the meteorological

station values, showing the lowest MAE (1.15 °C) and RMSE (1.37 °C) values (Table 7). On the other hand, the least corresponding method, in this case, is the MWA, as it presents the more significant differences, 1.52 °C of MAE, between the station and this method, and 1.91 °C of RMSE. However, the CCI Lakes product estimates good results compared to the meteorological station values, with a MAE of 0.94 °C and a RMSE of 1.25 °C.

2019	27/Jan	19/Feb	16/Mar	01/Apr	28/May	04/Jun	15/Jul	07/Aug	08/Sep	10/Oct	04/Nov	04/Dec	**MAE**	**RMSE**
Station-MWA (°C)	2.90	1.70	1.20	0.20	0.20	0.30	2.30	0.50	-2.30	1.94	4.00	0.70	**1.52**	**1.91**
Station-PSC$_{wvc}$ (°C)	0.70	-0.50	0.30	-0.10	1.30	1.40	2.40	2.60	-0.80	1.34	1.50	-0.90	**1.15**	**1.37**
Station-SCA (°C)	-0.60	-1.40	-0.90	-1.70	-1.30	-1.40	-1.20	-0.90	-3.50	-0.46	-0.20	-2.10	**1.31**	**1.55**
Station-CCI Lakes (°C)	0.10	0.90	1.70	1.10	2.60	-0.40	0.80	-0.10	2.20	0.26	-1.10	0.00	**0.94**	**1.25**

Table 7. *Differences of temperatures in the Issyk-Kul Lake in 2019 between the meteorological station and the Landsat 8 mono-channel algorithms and CCI Lakes with their respective MAE and RMSE*

Derived from these results, one of the advantages of the PSC$_{wvc}$ and the SCA methods is that they require only two input parameters: the land surface emissivity (ε) and the atmospheric water vapor content (*wvc*). By not considering the effective mean atmospheric temperature (T_a) parameter and directly using the *wvc*, these methods reduce the error of the final retrieved LSWT caused by the errors in T_a. On the other hand, the MWA requires the effective mean atmospheric temperature (T_a) and the atmospheric transmittance (τ), where the T_a can significantly impact the retrieved LSWT (Wang et al., 2019).

4.2.2 LSWT for Sentinel-3 (SLSTR)

The estimates of the LSWT using the Sentinel-3 satellite are derived from the product provided by the SLSTR instrument (Level 2 Land Surface Temperature product). It is retrieved using a split-window basic algorithm as described previously in the description of the data chapter.

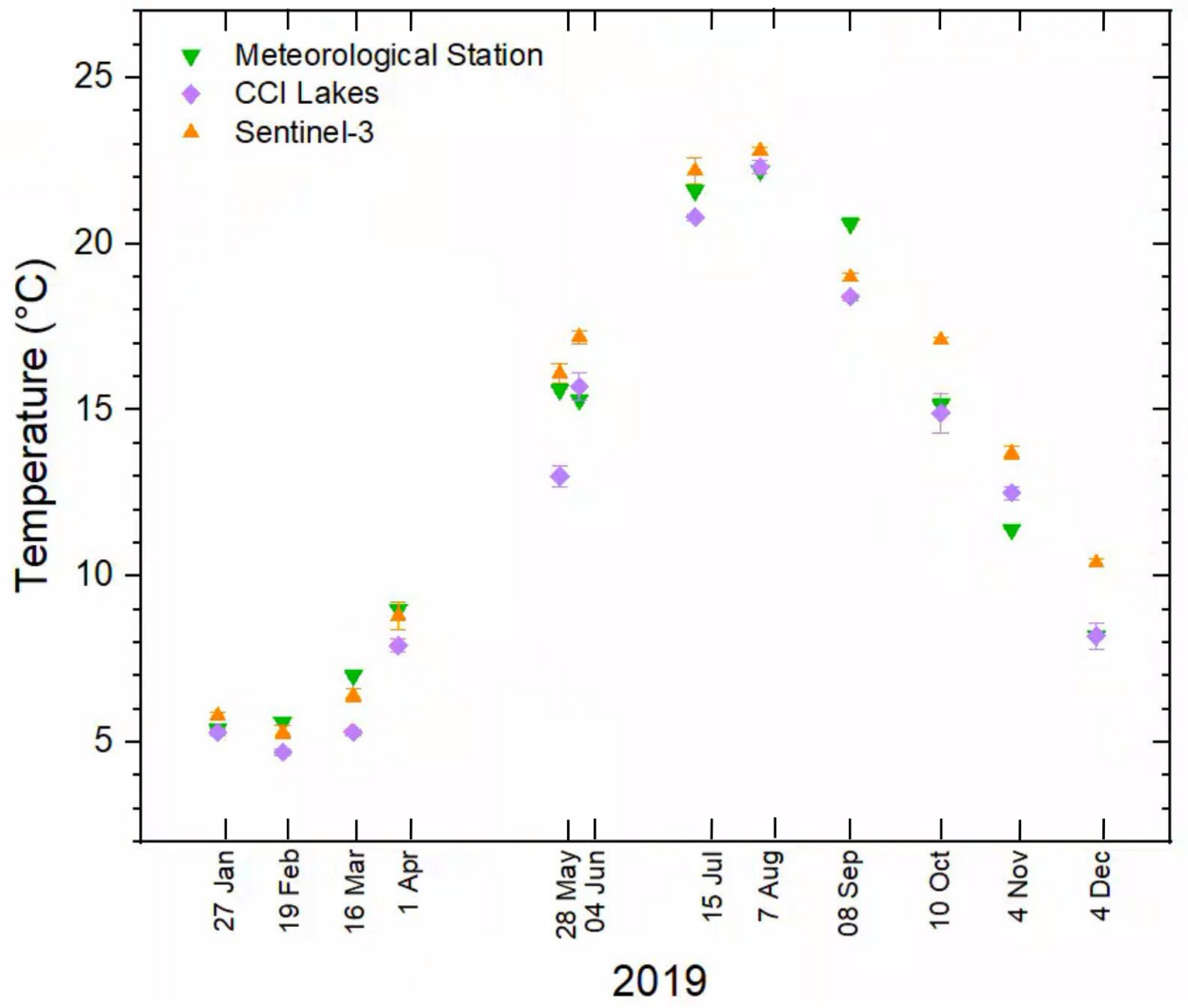

Figure 31. *LSWT estimates in the Issyk-Kul Lake in 2019 from Sentinel-3, CCI Lakes, and in-situ data.*

The area of interest of 100 km^2 is located at the East or West region of the Lake, according to the availability of pixels, after applying the cloud mask for Sentinel-3, which is based on a Bayesian probabilistic method. The images were selected according to the exact dates in 2019 with the meteorological station as reference values at noon, while the closest acquisition time for Sentinel-3 images is between 10:30 a.m. and noon in local time. Besides, the CCI Lakes product was added as another source of comparison (Figure 31).

2019	27/Jan	19/Feb	16/Mar	01/Apr	28/May	04/Jun	15/Jul	07/Aug	08/Sep	10/Oct	04/Nov	04/Dec	MAE	RMSE
Station-S3 (°C)	-0.40	0.30	0.60	0.20	-0.50	-1.90	-0.60	-0.60	1.60	-1.94	-2.30	-2.20	**1.10**	**1.34**
CCI Lakes-S3 (°C)	-0.50	-0.60	-1.10	-0.90	-3.10	-1.50	-1.40	-0.50	-0.60	-2.20	-1.20	-2.20	**1.32**	**1.53**
Station-CCI Lakes (°C)	0.10	0.90	1.70	1.10	2.60	-0.40	0.80	-0.10	2.20	0.26	-1.10	0.00	**0.94**	**1.25**

Table 8. *Differences in temperatures in the Issyk-Kul Lake in 2019 between the in-situ data, CCI Lakes, and Sentinel-3 with their respective MAE and RMSE*

From the results derived after this comparison with other sources in 2019 (Table 8), temperature differences from Sentinel-3 are more notable when compared to the CCI Lakes source (MAE of 1.32 °C). Still, they were showing good agreement to the meteorological station values with 1.10 °C of MAE and 1.34 °C of RMSE. On the other hand, CCI Lakes shows good correspondence to the in-situ values, with the slightest differences (MAE of 0.94 °C) compared to the other sources.

A time series analysis in 2020 was also estimated (Figure 32). Sentinel-3 shows a similar seasonal tendency with values from the meteorological station and the CCI Lakes sources, where temperatures during summer and fall show better correspondence between the presented sources.

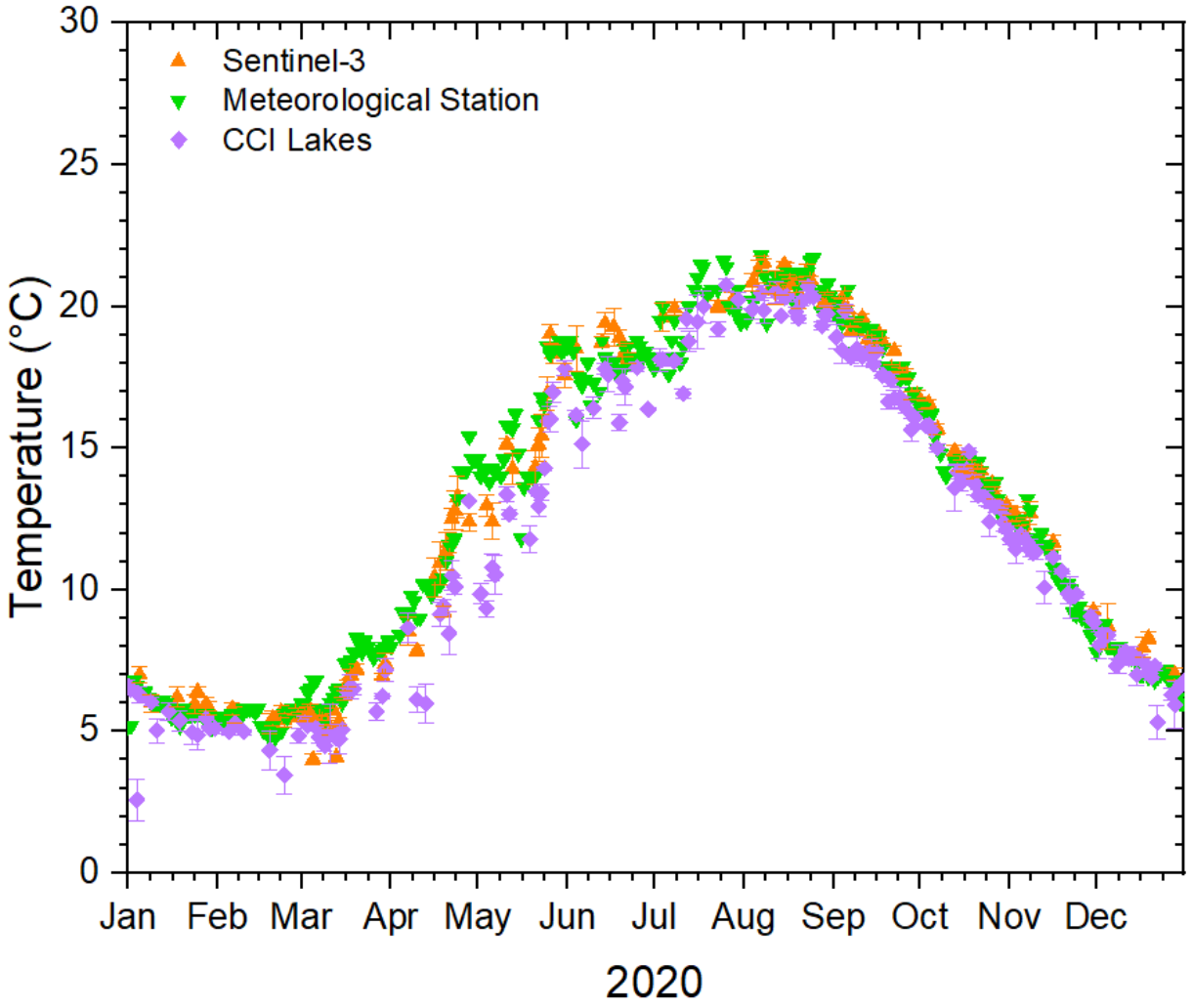

Figure 32. *LSWT time series estimates in the Issyk-Kul Lake in 2020 derived from Sentinel-3, in-situ data, and CCI Lakes*

CCI Lakes and Sentinel-3 showed good agreement between them (0.98 °C of MAE), mainly in summer and fall, where CCI Lakes product is the least corresponding to in-situ data (1.05 °C of MAE). The values between Sentinel-3 and the meteorological station agreed, with 0.79 °C of RMSE, showing the slightest differences throughout the year (0.59 °C of MAE) (Table 9).

2020	MAE	RMSE
Station-S3 (°C)	**0.59**	**0.79**
CCI Lakes-S3 (°C)	**0.98**	**1.21**
Station-CCI Lakes (°C)	**1.05**	**1.37**

Table 9. *MAE and RMSE derived from the differences in temperatures in the Issyk-Kul Lake in 2020 between the in-situ data, CCI Lakes, and Sentinel-3*

4.2.3 LSWT for MODIS (Terra)

The estimates of the LSWT using the MODIS sensor are derived from the LST product (MOD11A1v006) at Level-3 derived from the MOD11 Level-2; this product is retrieved by using the algorithm a generalized split-window. The area of interest of 100 km^2 is located in the East or West region of the lake according to the availability of pixels; besides, their acquisition time is generally between 11:00 a.m. and 1:00 p.m. in the region of Issyk-Kul Lake local time in 2019. Also, the reference values for this comparison are those from the meteorological station (registered at noon), adding the CCI Lakes as another reference source, showing a similar tendency throughout 2019 when comparing these three sources (Figure 33).

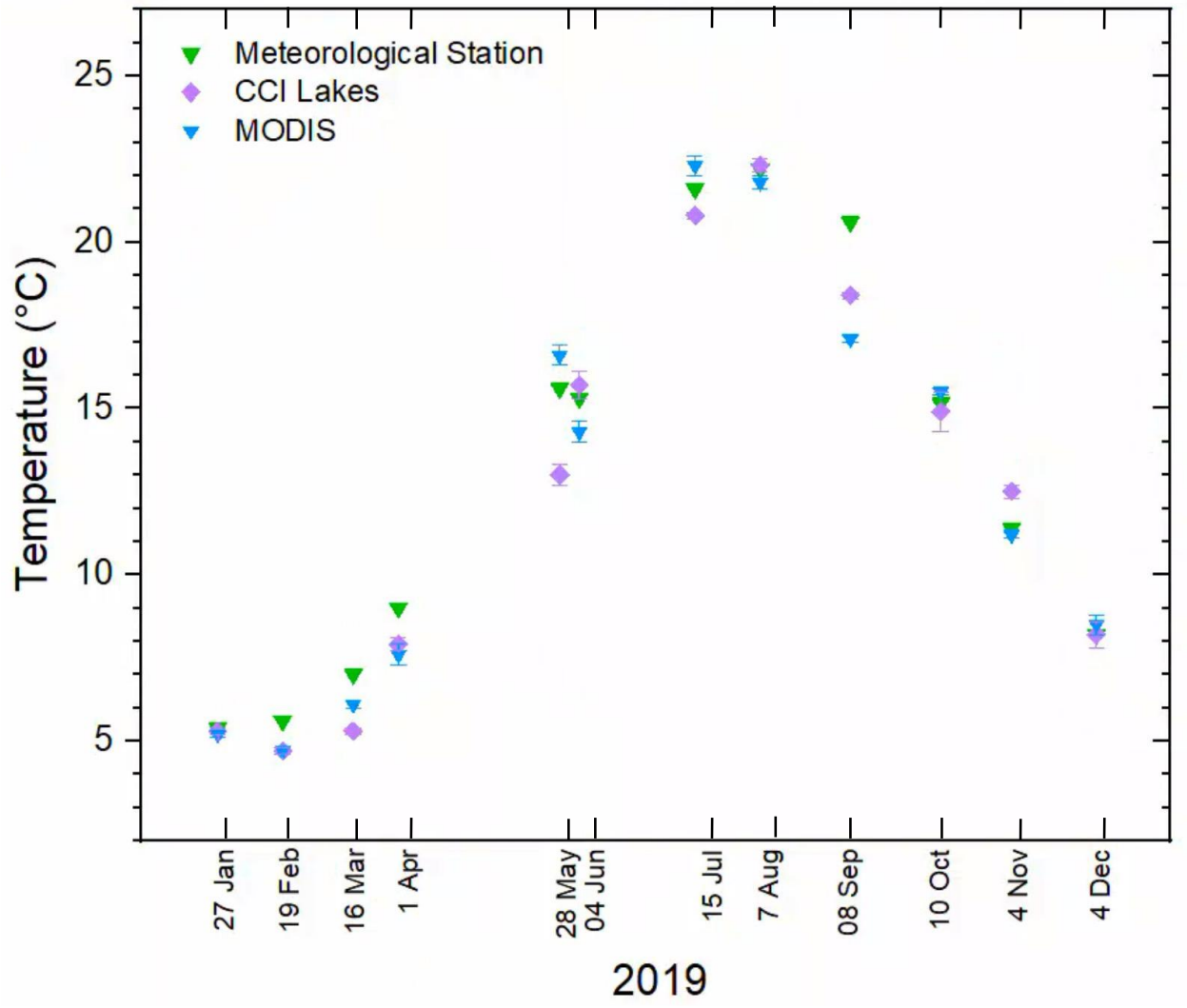

Figure 33. *LSWT estimates in the Issyk-Kul Lake in 2019 derived from MODIS, in-situ data, and CCI Lakes*

The product MODIS presents relatively good approximations between in-situ measurements (1.25 °C of RMSE) and the CCI Lakes to in-situ data with the same accuracy as MODIS. Besides, MODIS and the CCI Lakes product show little difference, with 0.98 of MAE and 1.35 °C of RMSE, even when they differ in their acquisition time (Table 10).

Date	27/Jan	19/Feb	16/Mar	01/Apr	28/May	04/Jun	15/Jul	07/Aug	08/Sep	10/Oct	04/Nov	04/Dec	**MAE**	**RMSE**
Station-MODIS (°C)	0.20	0.90	0.90	1.40	-1.00	1.00	-0.70	0.40	3.50	-0.34	0.20	-0.30	0.90	**1.25**
CCI Lakes-MODIS (°C)	0.10	0.00	-0.80	0.30	-3.60	1.40	-1.50	0.50	1.30	-0.60	1.30	-0.30	0.98	**1.35**
Station-CCI Lakes (°C)	0.10	0.90	1.70	1.10	2.60	-0.40	0.80	-0.10	2.20	0.26	-1.10	0.00	**0.94**	**1.25**

Table 10. *Differences in temperatures in the Issyk-Kul Lake in 2019 between in-situ data, CCI Lakes, and MODIS with their respective MAE and RMSE*

A time series analysis of 2020 using this MODIS LST product was also estimated. For this case, MODIS follows similar tendencies as the meteorological station and CCI Lakes throughout this year (Figure 34).

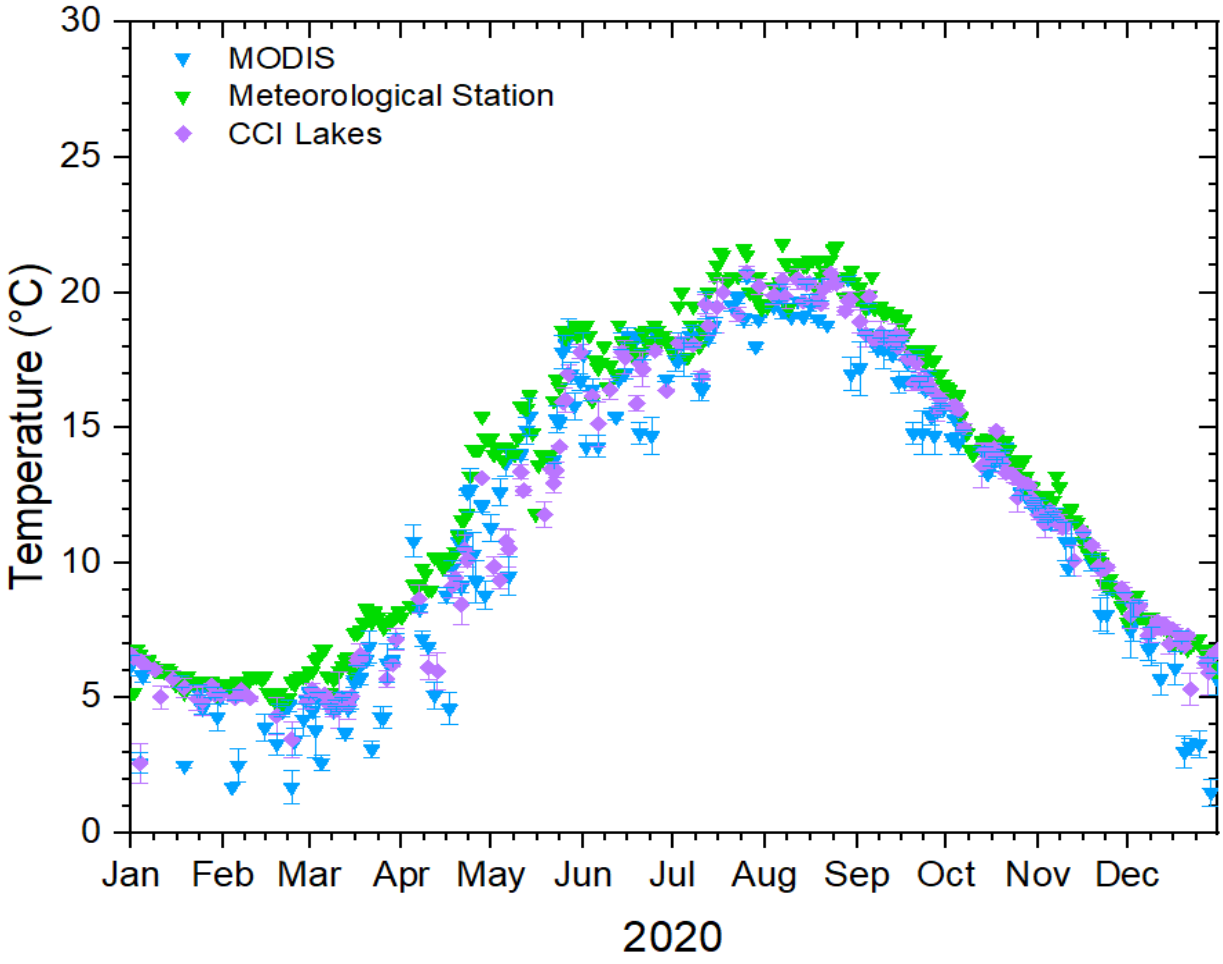

Figure 34. *LSWT time series estimates in the Issyk-Kul Lake in 2020 derived from MODIS, in-situ data, and CCI Lakes*

However, in terms of agreement, MODIS does not show good performance compared to the in-situ data with 1.93 °C of accuracy (Table 11), which could be attributed to the different acquisition times in MODIS, as well as for CCI Lakes product, as they presented differences of 0.73 °C between them, but CCI Lakes is closer to in-situ values (1.05 °C of MAE); besides, clouds are present in most of the dates in 2020.

2020	MAE	RMSE
Station-MODIS (°C)	**1.51**	**1.93**
CCI Lakes-MODIS (°C)	**0.73**	**1.04**
Station-CCI Lakes (°C)	**1.05**	**1.37**

Table 11. *MAE and RMSE derived from the differences in temperatures in the Issyk-Kul Lake in 2020 between the in-situ data, CCI Lakes, and MODIS*

4.2.4 LSWT for ECOSTRESS

During 2019, ECOSTRESS imagery was only available for a few dates in the second half of that year due to its recent mission launch. Hence, samples are taken from June to December 2019. The results for these ECOSTRESS images provide underestimated temperatures on each date compared with temperatures provide by the meteorological station and CCI Lakes (Figure 35). The acquisition time for each date of ECOSTRESS images is different at each overpassing date due to its non-geostationary orbit (from the ISS), and the overpassing time for the same region will not always be the same. Hence, more significant variations in the acquisition time could have derived greater differences when compared to the rest of the sources.

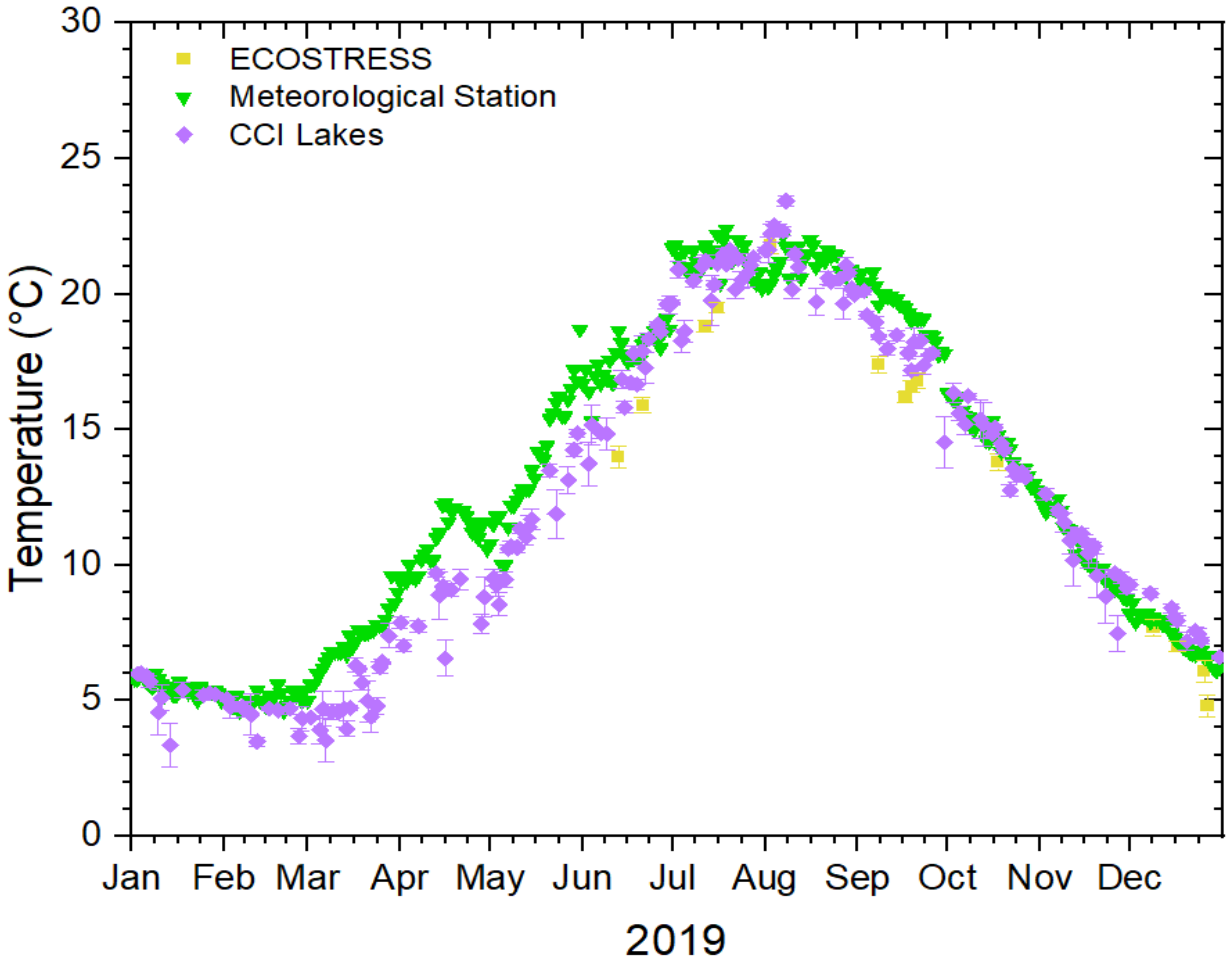

Figure 35. *LSWT time series estimates in the Issyk-Kul Lake in 2019 derived from ECOSTRESS, in-situ data, and CCI Lakes*

Results after this comparison were identified with a low correspondence of ECOSTRESS to the in-situ datasets, presenting a RMSE of 2.33 °C and differences of 2.00 °C between them. On the other hand, the ECOSTRESS estimates are closer to the values provided by the CCI Lakes, with differences of 1.29 °C of MAE, and 1.46 °C of RMSE; besides, CCI Lakes is also near to the values of the meteorological station, with 1.42 °C of RMSE, and MAE of 1.08 °C.

2019	MAE	RMSE
Station-ECOSTRESS (°C)	**2.00**	**2.33**
CCI Lakes-ECOSTRESS (°C)	**1.29**	**1.46**
Station-CCI Lakes (°C)	**1.08**	**1.42**

Table 12. *MAE and RMSE derived from the differences in temperatures in the Issyk-Kul Lake in 2019 between the in-situ data, CCI Lakes, and ECOSTRESS*

In 2020, LSWT estimates with the ECOSTRESS sensor provide again underestimated temperatures on each date compared to the temperatures from the meteorological station and CCI Lakes product (Figure 36). They present a similar tendency throughout 2020 between the sources.

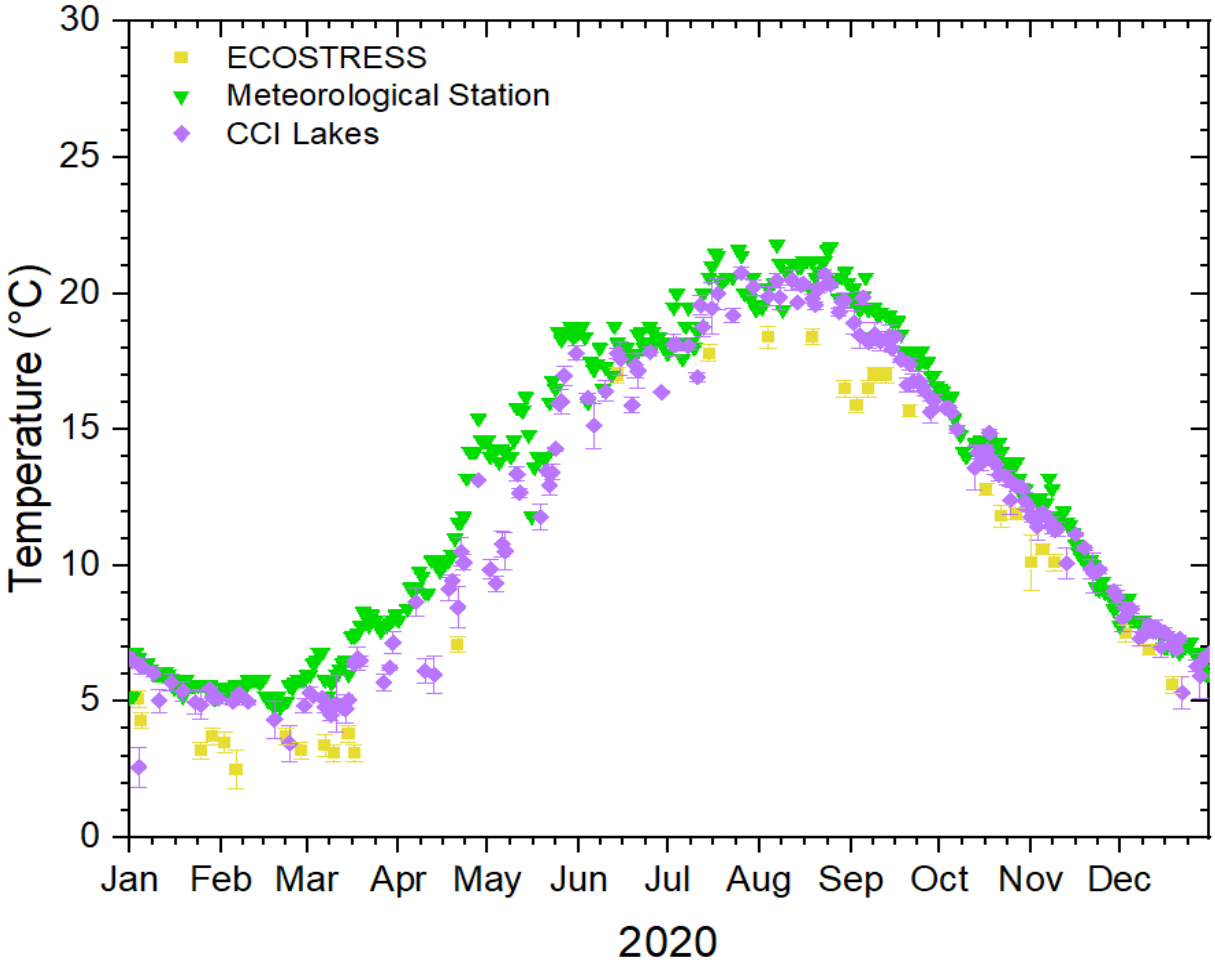

Figure 36. *LSWT time series estimates in the Issyk-Kul Lake in 2020 derived from ECOSTRESS, in-situ data, and CCI Lakes*

ECOSTRESS shows differences in temperatures of 2.30 °C, presenting a RMSE of 2.47 °C to in-situ data, where these differences are similar to those in 2019. On the other hand, values from CCI Lakes product are near to the in-situ data with a MAE of 1.05 °C and a RMSE of 1.37 °C (Table 13).

2020	MAE	RMSE
Station- ECOSTRESS (°C)	**2.30**	**2.47**
CCI Lakes- ECOSTRESS (°C)	**1.60**	**1.71**
Station-CCI Lakes (°C)	**1.05**	**1.37**

Table 13. *MAE and RMSE derived from the differences in temperatures in the Issyk-Kul Lake in 2020 between the in-situ data, CCI Lakes, and ECOSTRESS*

4.2.5 SWA for ECOSTRESS

After performing the SWA for ECOSTRESS, the estimations were retrieved by considering the spectral signature for two bands (typically the bands 2 and 5). The variability of temperatures in 2019 increases these values by 1 °C in most of the dates relatively, compared to the original LST product of ECOSTRESS (retrieved with the TES algorithm), which usually underestimates the temperatures throughout the year when comparing to in-situ data and CCI Lakes (Figure 37).

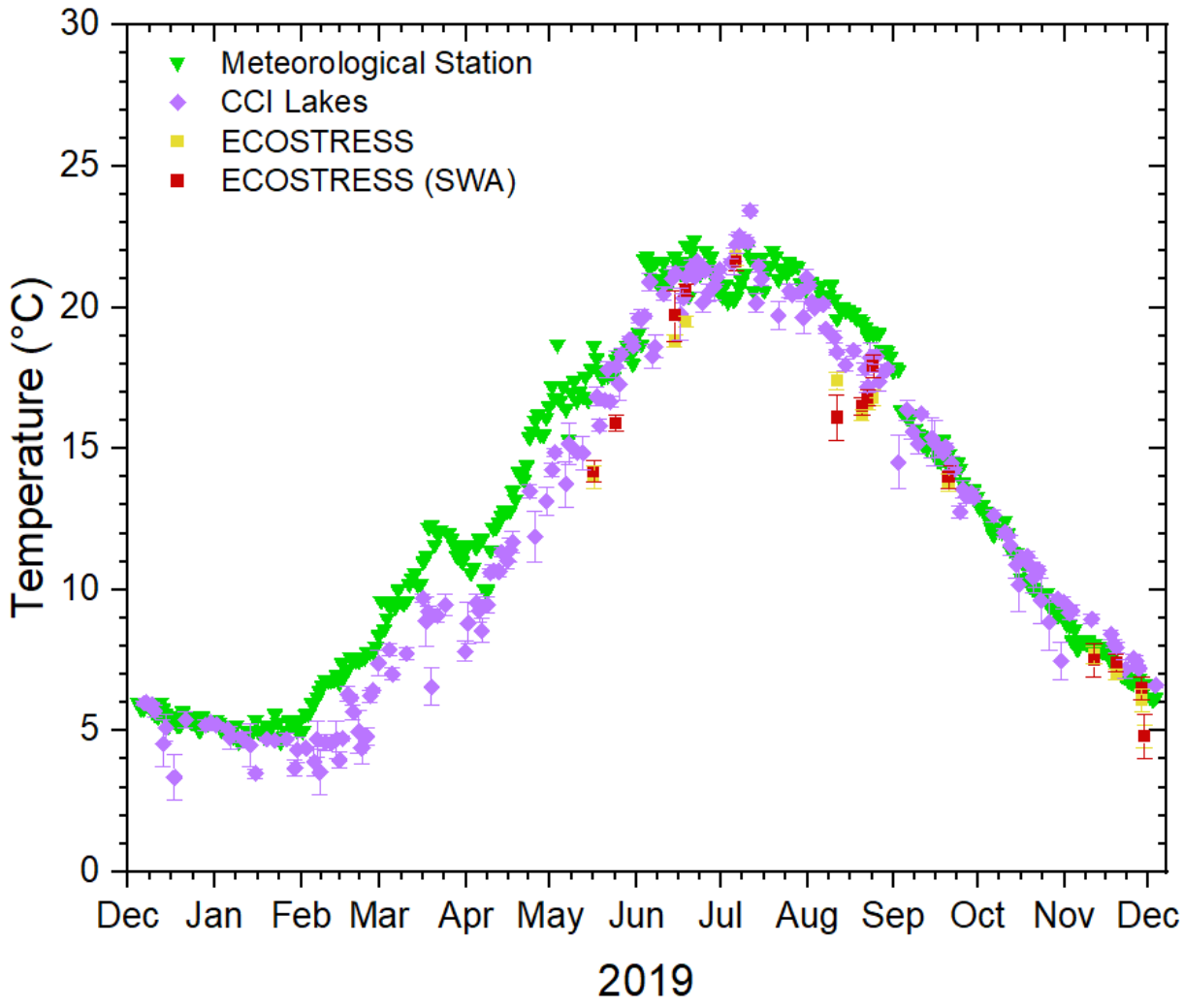

Figure 37. *LSWT time series estimates in the Issyk-Kul Lake in 2019 derived from ECOSTRESS (SWA), in-situ data, and CCI Lakes*

With this SW algorithm, the RMSE of the LSWT values from ECOSTRESS slightly decreased from 2.33 °C to 2.15 °C in 2019 (Table 14). Consequently, the temperature differences to in-situ data also decrease by 1.78 °C (MAE).

2019	MAE	RMSE
Station-ECOSTRESS (SWA) (°C)	**1.78**	**2.15**
Station- ECOSTRESS (°C)	**2.00**	**2.33**
CCI Lakes-ECOSTRESS (SWA) (°C)	**1.13**	**1.35**

Table 14. *MAE and RMSE derived from the differences in temperatures in the Issyk-Kul Lake in 2019 between in-situ data, CCI Lakes, ECOSTRESS, and ECOSTRESS (SWA)*

4.3 Ground Validation

Ground validations were carried over the four lakes considered for this research. Two campaigns for in-situ measurements were performed in the Issyk-Kul Lake region (October 2021 and May 2023). Then, ground validation was derived from the buoys located in the lakes of Gerardmer and Longemer, where datasets were provided from 2021 and 2022. Lastly, two validation campaigns were performed in the region of Plobsheim Lake during the summer of 2023. The instrumentation used for the validation campaigns included sensors to measure humidity, water, and air temperatures, installed on a floating platform called the Torrent board, an instrument assembled in the Icube laboratory (TRIO team). For some of these campaigns, a radiometer CIMEL CE-312 and a camera FLIR-T560 were used.

4.3.1 Validation campaign in Issyk-Kul in October 2021

A multidisciplinary, international mission, led by Jean François Crétaux (LEGOS -Toulouse), was done in October 2021 in the Issyk-Kul Lake area for 10 days to acquire in situ measurements and obtain good correspondence datasets for validation. The Laboratory ICUBE (Unistra) has participated in the Cal/Val of the skin water surface temperature to study its spatial variability over the lake, and thus, compared to Sentinel-3/MODIS satellite imagery.

The instrumentation used for this activity consisted of sensors that measured water and air temperatures and humidity values, which were set up on a floating geolocalized dragged board.

During the field survey, Sentinel-3 and MODIS were overpassing over the lake. Despite the cloud coverage, field measurements taken by the sensors of the Torrent board could be compared with these two sensors on one of the dates, where sensors at 5 cm (wT1) to 10 cm (wT2) depth showed slightly lower values than deeper temperatures (15 cm – wT3 and 35 cm – wT4), the difference between these two ranges being less than around 0.2 °C. Air temperature did not strongly correlate with water temperatures, or at least there was not easy to categorize them for most of the samples, except for the sample 1, which air temperatures were in between the water temperature values in this sample, ranging between 14.5 and 16.5°C. The LSWT of Sentinel-3 was closest to the LSWT of the Torrent board (0.3 °C), and the difference in LSWT from MODIS compared to the Torrent board was 1.3 °C. Consequently, the most good correspondence sensor was Sentinel-3, which provided the closest values retrieved by the Torrent board sensors.

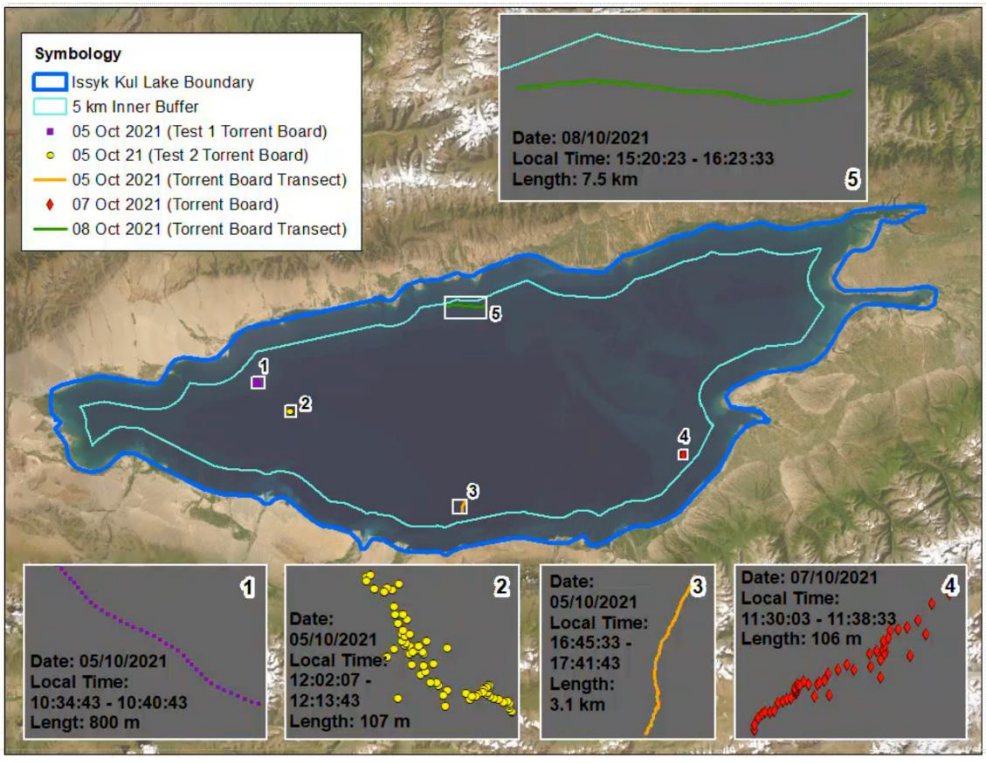

Figure 38. *Spatial distribution of the collection of the data in the field campaign in Issyk-Kul October 2021*

A general description of the samples measured from the 5 to the 8 of October 2021 at different times is presented (Figure 38), with a gap in the 6 of October, as due to the stormy weather conditions, activities in the lake were stopped, spending the day near the coast.

- **Sample 1:** The first measurements were taken on the 5 of October 2021 from 10:34 a.m. to 10:40 a.m. Temperatures at the skin surface (wT1) of the lake are around 13 °C, while the deeper temperatures at 35 cm (wT4) are around 15 °C. Air temperature shows a similar tendency for the sensor wT3 (at 15 cm).

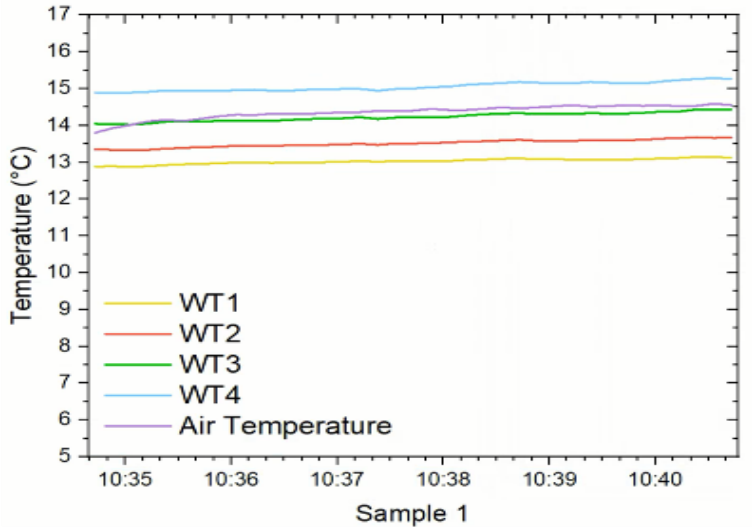

Figure 39. *LSWT and air temperature measurements in the Issyk-Kul Lake by sensors on the Torrent Board on 05/Oct/2021 from 10:34 a.m. to 10:40 a.m. (local time)*

- **Sample 2:** These measurements were taken on the 5th of October 2021 from 12:03 p.m. to 12:12 p.m. Temperatures from the four different depth sensors show similar values around 16.0 °C. Air temperature does not strongly correlate with water temperature sensors, with temperatures from 14.5 to 15.5 °C.

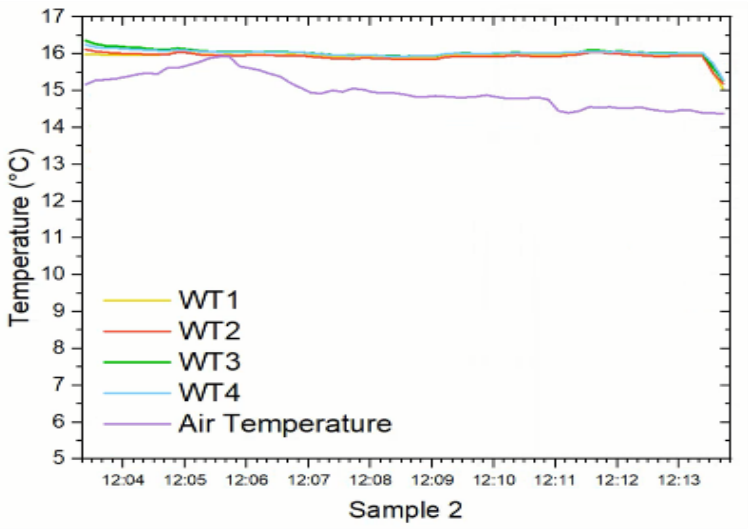

Figure 40. *LSWT and air temperature measurements in the Issyk-Kul Lake by sensors on the Torrent Board on 05/Oct/2021 from 12:03 a.m. to 12:12 p.m. (local time)*

- **Sample 3:** The first transect measurements were taken on the 5th of October 2021 from 4:45 p.m. to 5:40 p.m. Temperature variations are from 16.1 to 16.3 °C, where at skin surface temperatures (wT1 and wT2) are slightly lower values than the deeper temperatures at 15 cm and 35 cm (wT3 and wT4 respectively) by less than 0.2 °C. Air temperature does not strongly correlate with water temperature sensors, with temperatures from 13.0 to 17.0 °C.

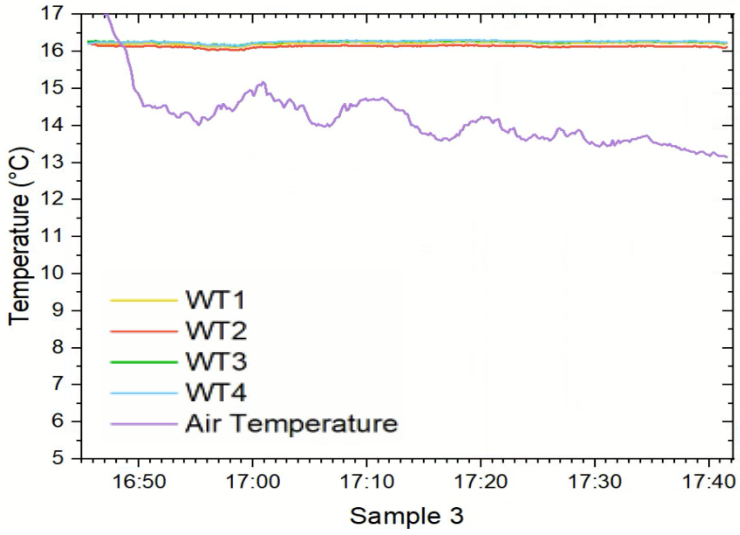

Figure 41. *LSWT and air temperature measurements in the Issyk-Kul Lake by sensors on the Torrent Board on 05/Oct/2021 from 4:45 p.m. to 5:40 p.m. (local time)*

- **Sample 4:** The measurements were taken on the 7 of October 2021 from 11:30 p.m. to 11:38 p.m. temperatures variations are from 14.8 to 15.6 °C, where at skin surface (wT1 and wT2) sensors are lower values than the deeper temperatures at 15 cm and 35 cm (wT3 and wT4). The difference between them is less than 0.4 °C. Again for this sample, the air temperature does not strongly correlate with water temperature from the sensors, with temperatures from 6.0 to 6.6 °C.

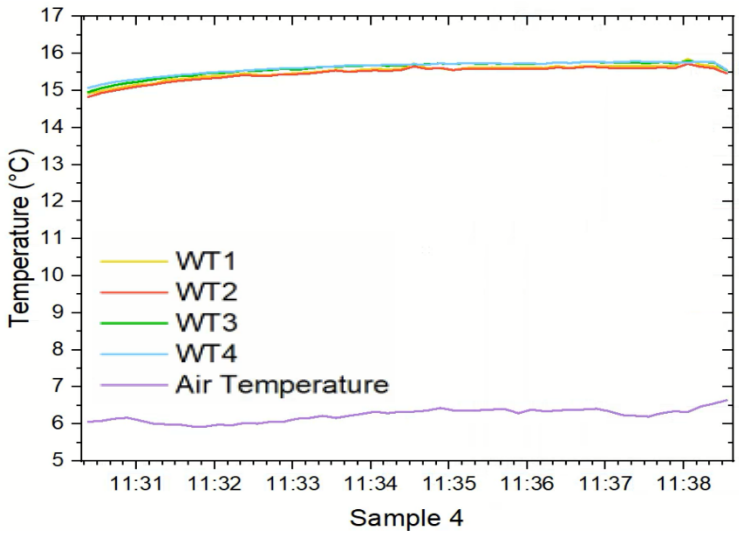

Figure 42. *LSWT and air temperature measurements in the Issyk-Kul Lake by sensors on the Torrent Board on 07/Oct/2021 from 11:30 a.m. to 11:38 a.m. (local time)*

After acquiring these measurements, there was no overpassing for any of the satellites of interest (Landsat 8-9, MODIS, Sentinel-3, or ECOSTRESS), or the image quality is poor on those dates due to the cloud coverage.

- **Sample 5:** The last transect measurements were taken on the 8th of October 2021 from 3:20 p.m. to 4:23 p.m. Temperature variations are from 16.1 to 16.3 °C, where at skin surface (wT1 and wT2) sensors are slightly lower values by less than 0.2 °C than the deeper temperatures at 15 cm and 35 cm (wT3 and wT4). Air temperature does not strongly correlate with water temperature sensors, with temperatures from 14.5 to 16.5 °C (see Figure 43).

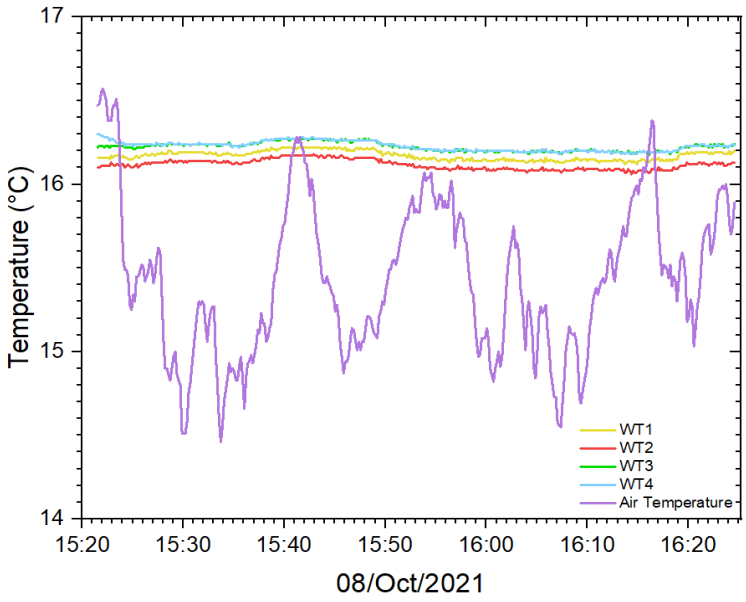

Figure 43. *LSWT and air temperatures were measured in the Issyk-Kul Lake by sensors on the Torrent Board on 08/Oct/2021 from 3:20 p.m. to 4:23 p.m.*

The local weather during the measurements was partially cloudy, and a bit windy with some waves. Over the transect measurements retrieved by the torrent board on this date on the North region of the lake, identified as a light blue line on the temperatures maps of Sentinel-3 and MODIS (Figure 44), Sentinel-3 temperature estimates are of 16.4 °C, and MODIS of 15.0 °C.

The LSWT by Sentinel-3 (11:19 a.m.) is the nearest value to the LSWT from the Torrent Board (3:22 p.m.), with a difference of 0.3 °C. LSWT by MODIS (10:50 a.m.), compared with Torrent board values (3:22 p.m.), is 1.3 °C. Values from the Sentinel-3 sensor provide the closest values (16.4 °C) to those retrieved by the Torrent board sensors (16.1 °C). However, differences in acquisition time, when in-situ measurements were taken, are around 4 hours for Sentinel-3 and around 5 hours for MODIS.

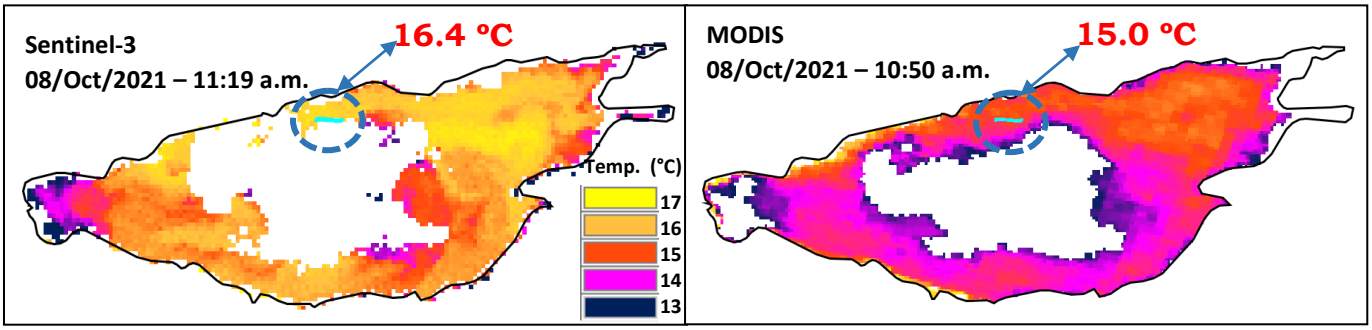

Figure 44. LSWT derived from Sentinel-3 (left) and MODIS (right) in the Issyk-Kul Lake on 08/Oct/2021

4.3.2 Validation campaign in Issyk-Kul in May 2023

The Icube Laboratory participated in a second mission over Issyk-Kul Lake, invited by the LEGOS team. This time, the source to retrieve LSWT in situ was made using the radiometer CIMEL CE-312. Over three days, from 10th to 12th May, at the time of the satellite overpass, temperatures were measured over the lake's East region (Figure 45). The acquisition was also made on the 14th, but some technical incidents spoiled the data.

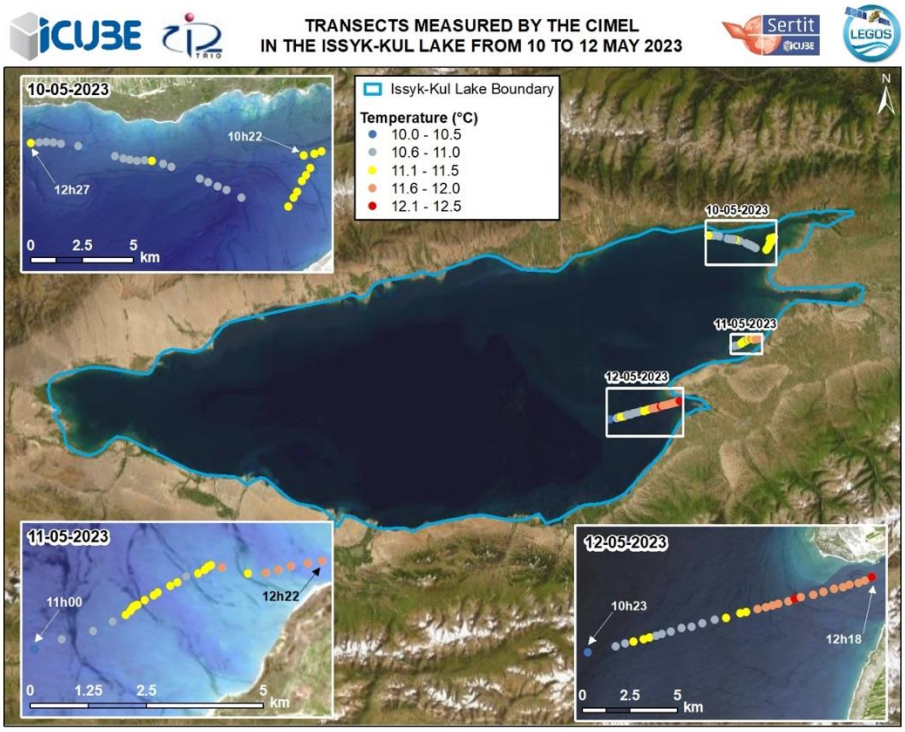

Figure 45. *Spatial distribution of the data collection in the field campaign in the Issyk-Kul Lake on May 2023*

The coincidence of satellite overpasses in this region during the data acquisition dates derived from the CIMEL CE-312-2 radiometer is only for two dates. For the 10th of May, Sentinel-3 passes at 11:55 a.m. and MODIS at 12:12 p.m., while the CIMEL registered data from 11:18 a.m. to 1:23 p.m., all in local time. On the 11th of May, Sentinel-3 overpasses at 11:56 a.m. and MODIS at 12:55 p.m., when the CIMEL acquired measurements from 11:56 a.m. to 1:18 p.m., as

well in local time (Figure 46). On the 12th of May, no overpassing satellites were to be validated with the measurements registered with the CIMEL. These results represent the values of temperatures from the radiometer with a maximum 1 °C of standard deviation.

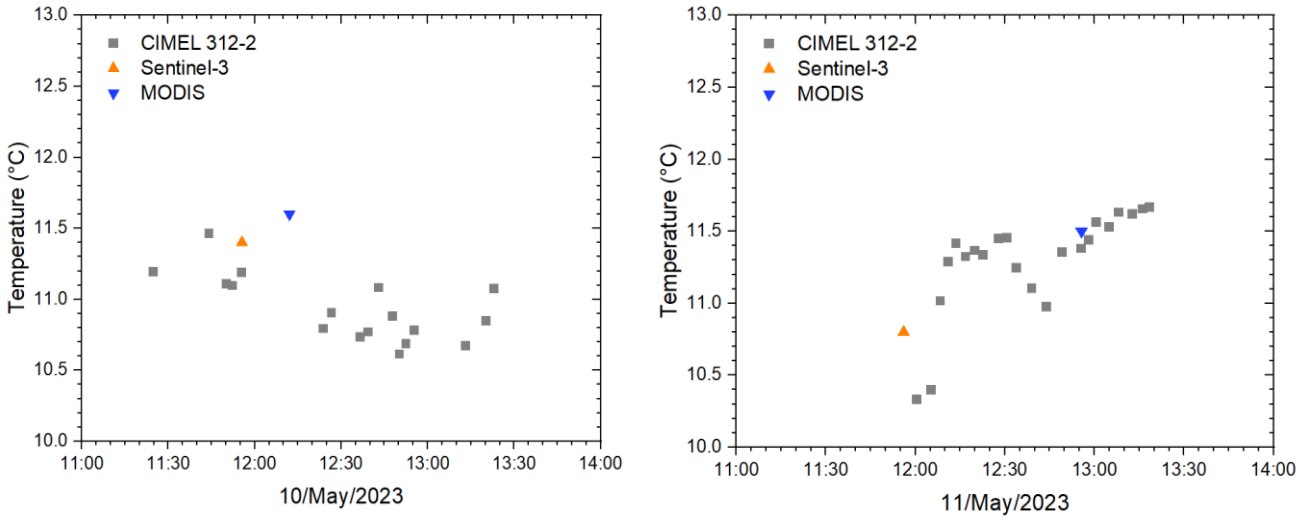

Figure 46. *Temporal distribution of the data collection in the field campaign in the Issyk-Kul Lake on May 2023*

On the 10th of May, the local weather on was sunny, and it was not windy and not wavy. Sentinel-3 estimates a temperature of 11.4 °C; MODIS estimates 11.6 °C; and the CIMEL registers 11.2 °C at 11:55 a.m. On the 11th of May, the local weather was partially cloudy, no windy and calm waters. Sentinel-3 estimates a temperature of 10.8 °C, and MODIS estimates a value of 11.5 °C, while the CIMEL registers 10.3 °C and 11.4 °C for each satellite, respectively. Hence, the measurements from the CIMEL are a good source of comparison for both satellites (MODIS and Sentinel-3) with differences of less than 1.0 °C in both dates.

Date	**CIMEL 312-2** *(°C)*	Sentinel-3 *(°C)*	**CIMEL 312-2** *(°C)*	MODIS *(°C)*
10/May/23	**11.2**	**11.4**	**11.2**	**11.6**
11/May/23	**10.3**	**10.8**	**11.4**	**11.5**

Table 15. *Measurements obtained in the Issyk-Kul Lake on the 10th and 11th of May 2023 with the Sentinel-3 and MODIS satellites and comparison at the same time with the CIMEL 312-2*

4.3.3. Ground validation in Gerardmer and Longemer Lakes

For the Gerardmer and Longemer Lakes study areas, Landsat 8-9 and ECOSTRESS images were processed from January 2021 to May 2022 to observe the temperature variations and compare these results with in-situ measurements. Temperatures from Landsat 8-9 Collection 2 were estimated using the SWA algorithm.

Firstly, LSWT estimates from ECOSTRESS and Landsat 8-9 were compared to in-situ data (used as references) from Gerardmer Lake registered with a buoy in this lake, provided from June 2021 to April 2022. However, some values were missing from August 2021 to November 2021 for these datasets (Figure 47).

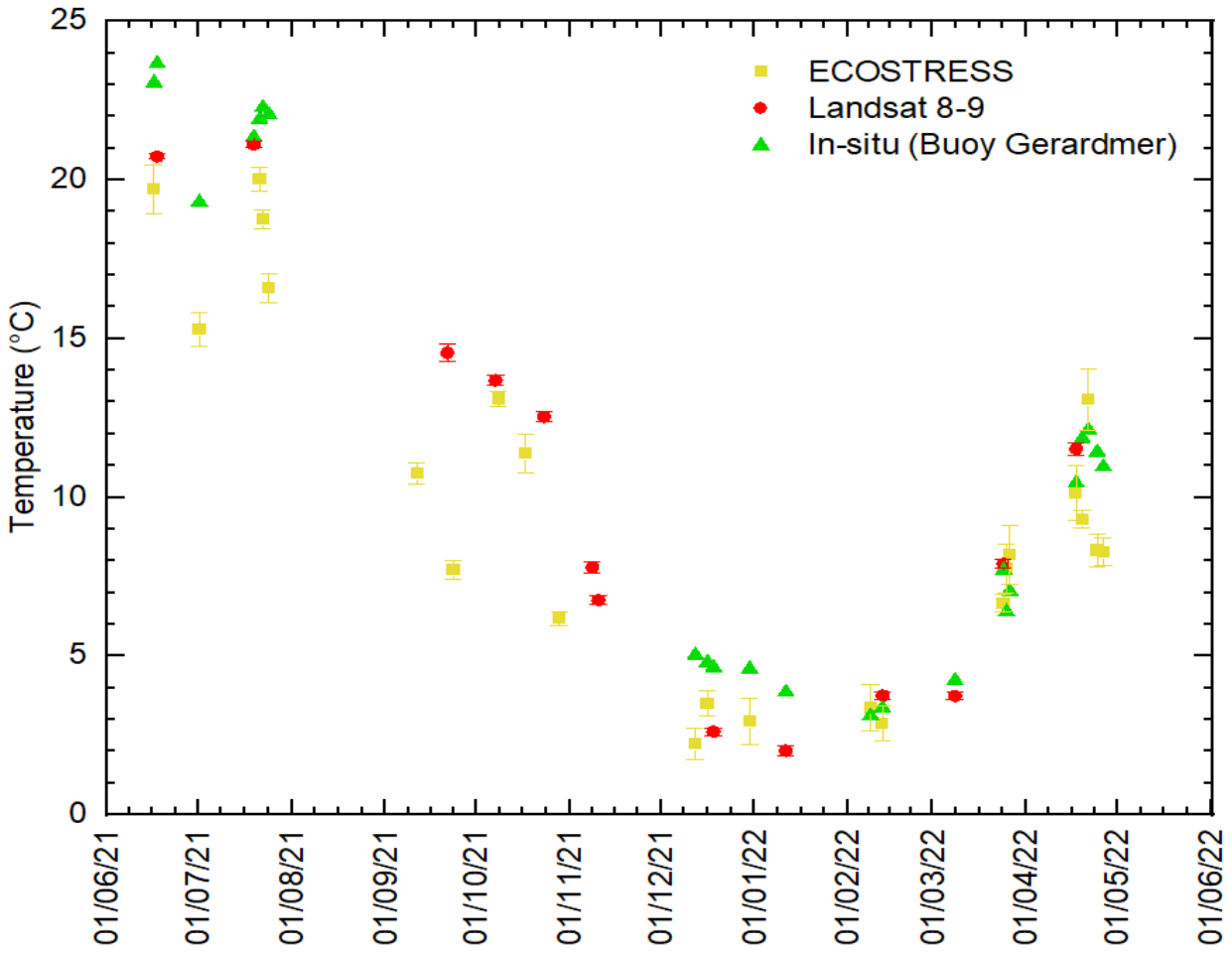

Figure 47. *LSWT estimates in the Gerardmer Lake from 2021 to 2022 derived from in-situ data, ECOSTRESS, and Landsat 8-9 (SWA)*

Landsat 8-9 values estimates in the Gerardmer Lake are closer to the in-situ measurements with the slightest differences in temperatures of 1.15 °C (MAE) than those from ECOSTRESS. More significant differences are presented in most retrieved dates with ECOSTRESS (2.10 °C of MAE), where temperatures are generally underestimated, which could be associated with clouds over the region. Thus, the RMSE is better from estimates with Landsat 8-9 (RMSE of 1.40 °C) than those from ECOSTRESS (RMSE of 2.52 °C).

Gerardmer (2021-2022)	MAE	RMSE
Buoy-ECOSTRESS (°C)	2.10	2.52
Buoy- Landsat 8/9 (SWA) (°C)	**1.15**	**1.40**

Table 16. *MAE and RMSE derived from the differences in temperatures in the Gerardmer Lake from 2021 to 2022 between in-situ data, ECOSTRESS, and Landsat 8-9 (SWA)*

On the other hand, regarding the imagery collection results in the Grand-East lakes, there were more datasets in the Longemer region than in Gerardmer, even for the in-situ measurements, as the datasets from the buoy in Longemer (considered as the values of references) were provided from June 2021 to May 2022 (Figure 48).

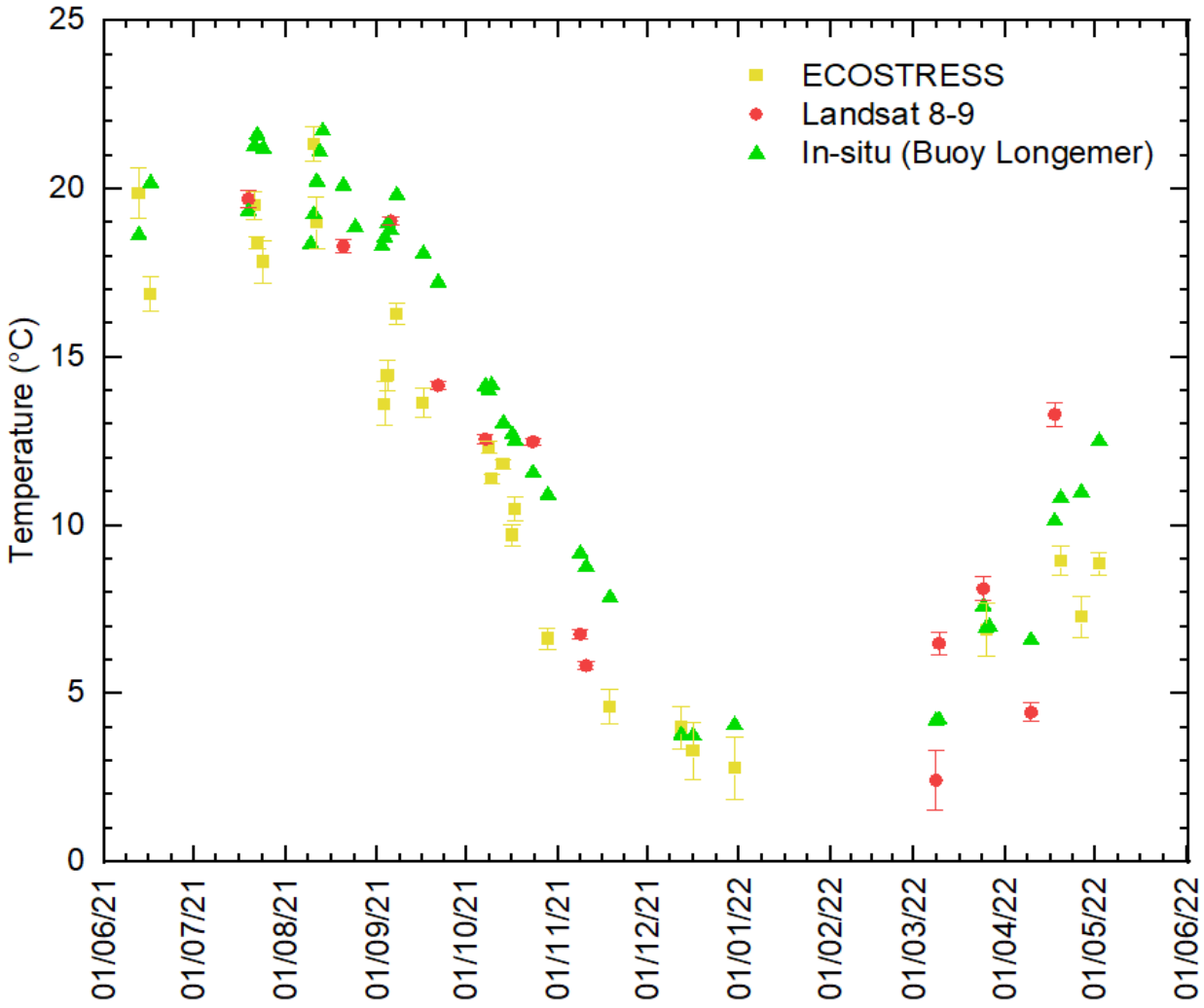

***Figure 48**. LSWT estimates in the Longemer Lake from 2021 to 2022 derived from in-situ data, ECOSTRESS, and Landsat 8-9 (SWA)*

The values from Landsat 8-9 are more related to the in-situ measurements, contrary to values from ECOSTRESS, where temperatures are generally underestimated on most dates. For the LSWT estimates in Longemer Lake, the MAE from Landsat 8-9 is lower (1.79 °C) than those from ECOSTRESS (2.53 °C). LSWT values drop to deficient levels, as in the Gerardmer Lake, which could also be associated with clouds over the region. Thus, the RMSE is not optimal from any of the sources in this case, as Landsat 8-9 presents a RMSE of 2.04 °C and 2.87 °C for ECOSTRESS (Table 17).

Longemer (2021-2022)	MAE	RMSE
Buoy-ECOSTRESS (°C)	**2.53**	**2.87**
Buoy- Landsat 8/9 (SWA) (°C)	**1.79**	**2.04**

Table 17. *MAE and RMSE derived from the differences in temperatures in the Longemer Lake from 2021 to 2022 between in-situ data, ECOSTRESS, and Landsat 8-9 (SWA)*

4.3.4 Validation campaign in Plobsheim Lake in April 2023

In the context of comparison using in-situ datasets, within the Plobsheim Lake, seven buoys distributed from North to South of the lake provide temperature values every 30 minutes (Figure 49).

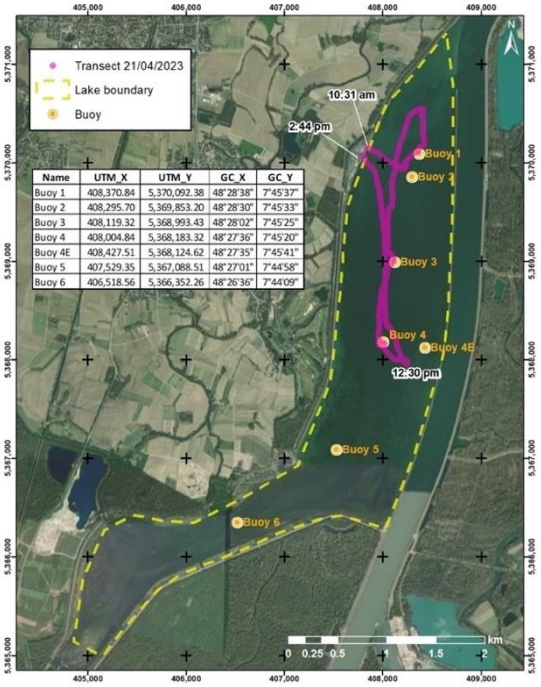

Name	UTM_X	UTM_Y	GC_X	GC_Y
Buoy 1	408,370.84	5,370,092.38	48°28'38"	7°45'37"
Buoy 2	408,295.70	5,369,853.20	48°28'30"	7°45'33"
Buoy 3	408,119.32	5,368,993.43	48°28'02"	7°45'25"
Buoy 4	408,004.84	5,368,183.32	48°27'36"	7°45'20"
Buoy 4E	408,427.51	5,368,124.62	48°27'35"	7°45'41"
Buoy 5	407,529.35	5,367,088.51	48°27'01"	7°44'58"
Buoy 6	406,518.56	5,366,352.26	48°26'36"	7°44'09"

Figure 49. *Spatial distribution of the data collection in the field campaign in Plobsheim Lake on April 2023*

Datasets from these buoys were provided from May to November 2022, with some missing values at different dates between the buoys. Datasets from buoys 2 and 4 are considered as the values of reference to validate the estimates from ECOSTRESS (SWA), Landsat 8-9 (SWA), and MODIS, where a similar tendency is followed throughout 2022 by all the sources (Figure 50).

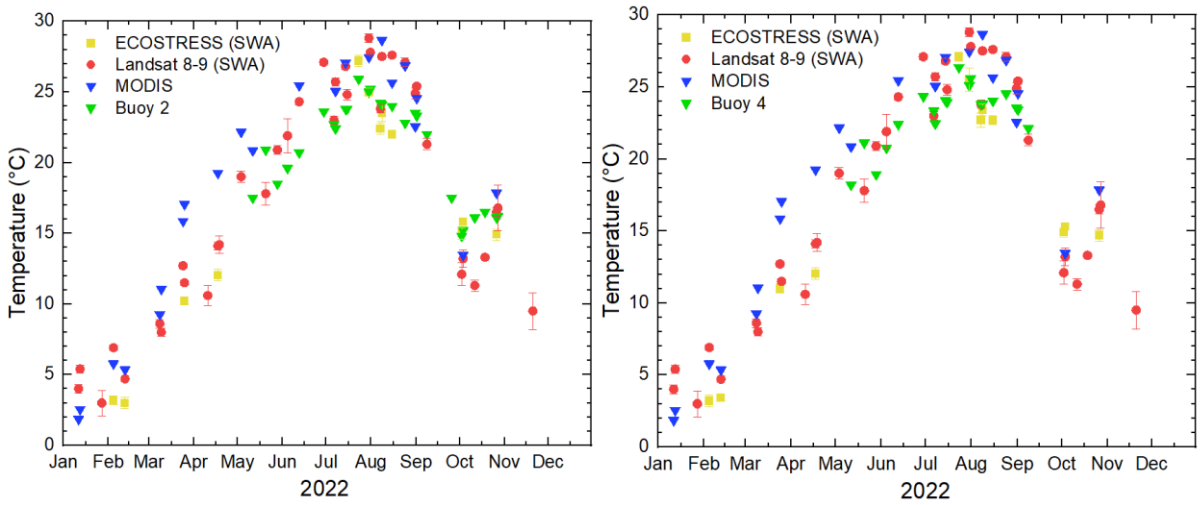

Figure 50. *LSWT estimates in the Plobsheim Lake in 2022 from in-situ data (buoys 2 and 4), MODIS, ECOSTRESS (SWA), and Landsat 8-9 (SWA)*

The LSWT values in 2022 derived from buoys 2 and 4 are closer to estimates from ECOSTRESS (SWA) (1.10 and 0.79 °C of MAE, respectively) than to those from MODIS (2.70 and 2.46 °C of MAE, respectively), and those to Landsat 8-9 (2.54 and 2.17 °C respectively). Hence, the lower amount of RMSE is achieved with ECOSTRESS (SWA), especially when it validates with the values from buoy 4 in the lake (a RMSE of 0.87 °C) (Table 18).

Plobhseim 2022	MAE	RMSE
Buoy 2-ECOSTRESS (SWA) (°C)	**1.10**	**1.18**
Buoy 2- Landsat 8/9 (SWA) (°C)	**2.54**	**2.95**
Buoy 2- MODIS (°C)	**2.70**	**2.97**
Buoy 4-ECOSTRESS (SWA) (°C)	**0.79**	**0.87**
Buoy 4- Landsat 8/9 (SWA) (°C)	**2.17**	**2.55**
Buoy 4- MODIS (°C)	**2.46**	**2.67**

Table 18. *MAE and RMSE derived from the differences in temperatures in the Issyk-Kul Lake in 2022 between in-situ data, ECOSTRESS (SWA), and Landsat 8-9 (SWA)*

Regarding the validation campaign made on the 21st of April 2023, where the local weather during measurements had temperatures from 11 to 16 ºC, partially cloudy, steady waters, with winds of 5 km/h from the N. The measurements with the radiometer CIMEL 312-2 and with the sensors on the Torrent board were acquired over the location of the first five buoys in the lake,

with a trajectory starting from North to South, and returning to the same location where we started the measurements acquisition (Figure 49). The datasets from the buoys on this date show good correspondence with the measurements from the Torrent board, followed by the CIMEL.

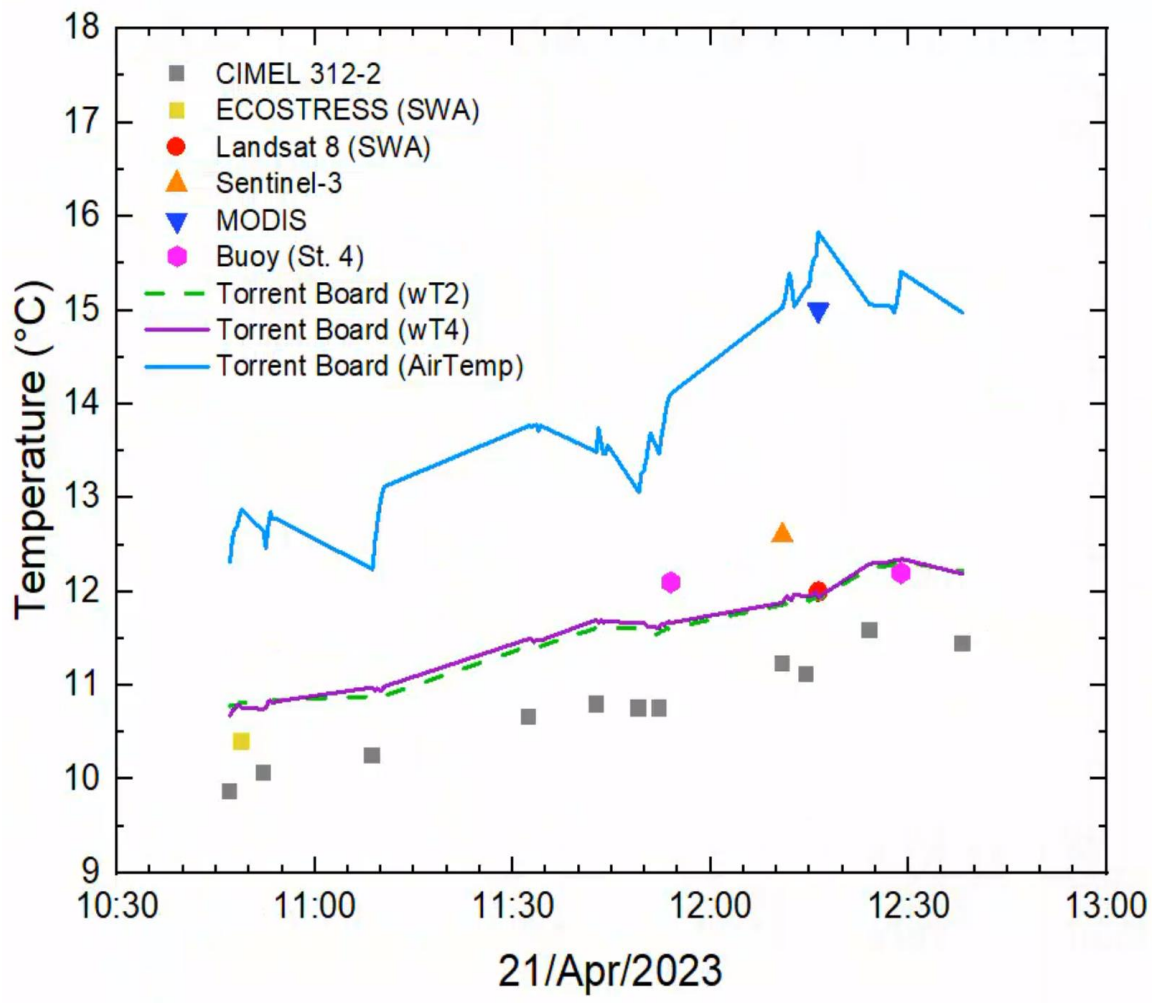

Figure 51. *Multi-sensors validation in the Plobsheim Lake on 21/04/2023*

The temperatures in this lake from the first measurements with the Torrent board start at 10.5 °C at 10:47 a.m. and increase until 12.0 °C at 12:40 p.m., considering two sensors from the Torrent board (wT2 and wT4). While the temperatures registered from the CIMEL 312-2 follow a similar tendency within the same time range. However, the temperatures are underestimated generally at 1.0 °C or even less than that, starting from 9.8 °C and increasing until 11.6 °C at the

end of the measurements. The satellites validated in this campaign were the ECOSTRESS, Landsat 8, Sentinel-3, and MODIS sensors (Figure 51).

The LSWT values extracted from the different images, identified as the light blue marks (Figure 52), are spotted according to the measurements derived from the Torrent board's sensors and each satellite's acquisition time (local time).

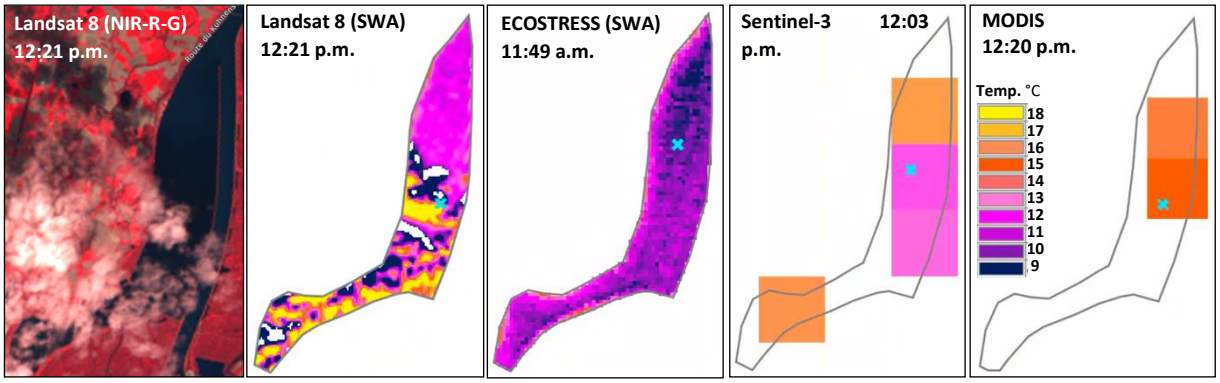

Figure 52. *Spatial variability from multi-sensors in the Plobsheim Lake on 21/04/2023*

Concerning estimates from these satellites, differences in temperatures at similar acquisition times for the same date with the Torrent board are as follows: 1.0 °C for ECOSTRESS, 0.1 °C for Landsat 8, 0.7 °C for Sentinel-3, and MODIS a more significant difference of 3.2 °C is observed (Table 18). From these results, it can be inferred that the nearest values are the LSWT estimates with Landsat 8 regarding the measurements from the sensors on the Torrent board and the radiometer CIMEL 312-2, followed by Sentinel-3 and Landsat 8. However, the spatial resolution from the Sentinel-3 and MODIS (1 km) must be considered, having only a few representative pixels due to the size of this lake (area of 6.6 km^2).

Acquisition Time	**CIMEL 312-2** (°C)	**wT2** (°C)	**wT4** (°C)	**ECOSTRESS (SWA)** (°C) 11:49 a.m.	**Sentinel-3** (°C) 12:03 p.m.	**MODIS** (°C) 12:20 p.m.	**Landsat 8 (SWA)** (°C) 12:21 p.m.
11:49 a.m.	**10.8**	**10.8**	**10.8**	**9.8**	-	-	-
12:03 p.m.	**11.2**	**11.9**	**11.9**	-	**12.6**	-	-
12:20 p.m.	**11.6**	**11.9**	**11.9**	-	-	**15.1**	-
12:21 p.m.	**11.6**	**11.9**	**11.9**	-	-	-	**12.0**

Table 19. *Measurements validation in the Plobsheim Lake on 23 April 2023 with the Torrent Board, CIMEL 312-2, ECOSTRESS, Landsat 8, Sentinel-3 and MODIS*

4.3.5 Validation campaign in Plobsheim Lake in June 2023

Another validation campaign was performed on the 16th of June in the region of Plobsheim Lake, with fair conditions as a local weather, sunny and slight waves, with winds up to 21 km/h from the N. For this occasion, the radiometer CIMEL CE-312 was replaced, due to technical problems with this device, with a thermal infrared camera (FLIR-T560) and the Torrent board. The transect of the measurements follows the location of the seven buoys in the lake for validation with them in the future (Figure 53).

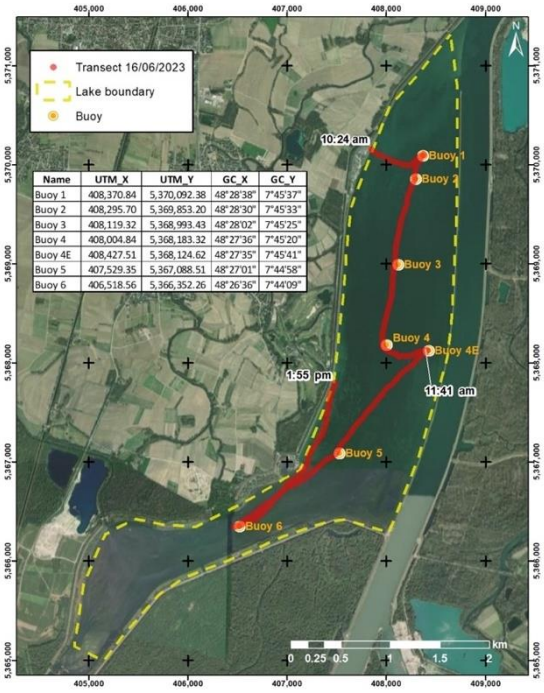

Name	UTM_X	UTM_Y	GC_X	GC_Y
Buoy 1	408,370.84	5,370,092.38	48°28'38"	7°45'37"
Buoy 2	408,295.70	5,369,853.20	48°28'30"	7°45'33"
Buoy 3	408,119.32	5,368,993.43	48°28'02"	7°45'25"
Buoy 4	408,004.84	5,368,183.32	48°27'36"	7°45'20"
Buoy 4E	408,427.51	5,368,124.62	48°27'35"	7°45'41"
Buoy 5	407,529.35	5,367,088.51	48°27'01"	7°44'58"
Buoy 6	406,518.56	5,366,352.26	48°26'36"	7°44'09"

Figure 53. *Spatial distribution of the data collection in the field campaign in the Plobsheim Lake on June 2023*

The temperatures in the lake from the first measurements with the Torrent board start from 23.0 °Cat 10:30 a.m. and increase until 25.0 °C at 1:55 p.m., considering two sensors from the Torrent board (wT2 and wT4). In contrast, the temperatures registered from the camera FLIR T-560 follow a similar tendency within the same time range. However, the temperatures were underestimated at around 1.5 °C, starting from 21.5 °C and increasing until 23.5 °C at the end of the measurements. The in-situ data from the buoys agree with the sensors from the Torrent

board, followed by the FLIR camera. The satellites validated in this campaign were the Landsat 9, Sentinel-3, and MODIS sensors (Figure 54).

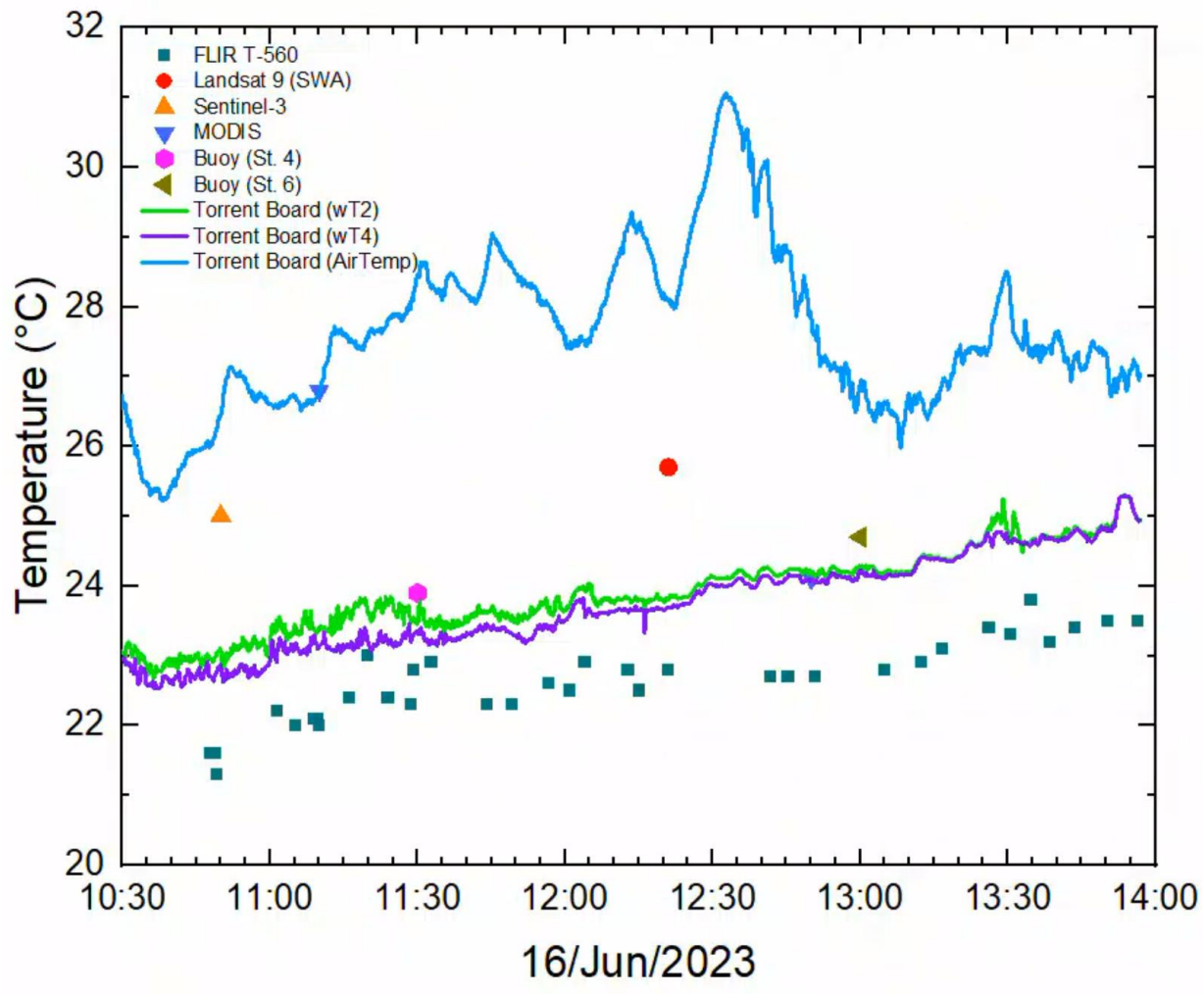

Figure 54. *Multisensors validation in the Plobsheim Lake on 16/06/2023*

The LSWT values extracted from the different images, identified as the light blue marks (Figure 55), are spotted according to the measurements derived from the Torrent board's sensors and each satellite's acquisition time (local time).

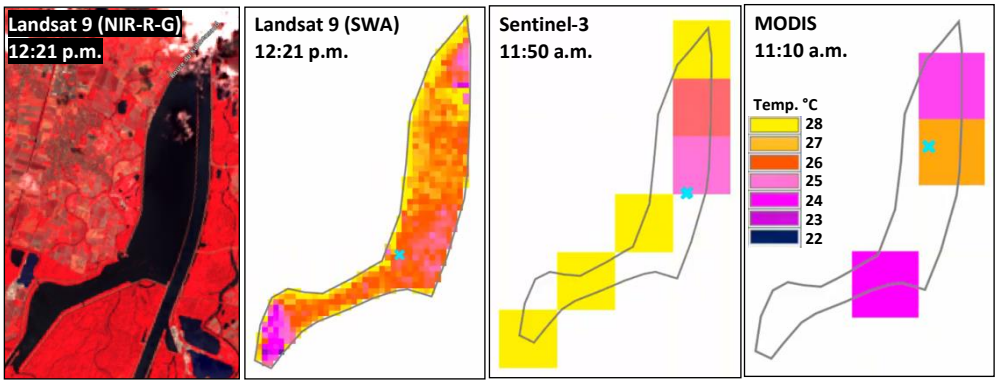

Figure 55. *Spatial variability from multi-sensors in the Plobsheim Lake on 16/06/2023*

Regarding sensor intercomparison (Figure 54), Sentinel-3 is agreed to the measurements acquired with the instruments from the Torrent board simultaneously (11:50 p.m.) with a 1.4 °C difference. On the other hand, values derived from the FLIR-T560 camera show differences of 1.26 °C with the wT2 and 1.07 °C with the wT4 from Torrent Board, with RMSE of 1.29 and 1.12, respectively (Table 20).

For the overpassing of Sentinel-3 and Landsat 9, some clouds were present at the time of the measurements. Thus, it could explain the more significant differences (around 2.0 °C) between the Torrent board sensors and the FLIR camera values.

16/Jun/2023	MAE	RMSE
wT2-FLIR-T560 (°C)	**1.26**	**1.29**
wT4-FLIR-T560 (°C)	**1.07**	**1.12**

Table 20. *MAE and RMSE derived from the differences in temperatures in the Plobsheim Lake in 2022 between in-situ data (Torrent Board) and the Camera FLIR-T560.*

4.4 Discussions

This section describes the limits and contributions of this research to the prior literature, followed by an explanation and comparison of the acquired results with the LSWT estimations to earlier studies, leading to a discussion of its implications or repercussions.

4.4.1 Sensors Intercomparison

The results in the first part of this study derive from the intercomparison between multi-sensors: Landsat 8 mono-channel algorithms, Sentinel-3, MODIS, and CCI Lakes, considering as values of reference the datasets from the meteorological station. The methodology consisted of taking at least one image per month 2019 for each sensor to compare at the same day and time or the closest time available. An area of interest of 100 km^2 is set on the East or West region of the Issyk-Kul Lake, according to the availability of the pixels in each image. This comparison shows the highest correspondence of the PSC_{wvc} method (Landsat 8), CCI Lakes, and MODIS LSWT products when validating with in-situ data (values from the meteorological station). However, MODIS shows the best correspondence, following a study by Wan et al. (2002), who evaluated the absolute radiometric accuracy of the MODIS (TIR) data by comparing it with in situ measurements collected in Lake Titicaca in Peru and Bolivia. These authors suggest good agreement between MODIS TIR data and in situ measurements, particularly in bands 31 and 32, with an accuracy within 0.4% in the daytime overpass. Thus, MODIS, like in our study, could be suggested as a good agreement source for estimating the LWST. Another study accords with our research; Tavares et al. (2019) retrieved the LSWT using MODIS (MOD11 product), retrieved using the Generalized Split-Window algorithm, and considered the difference in emissivity between specific bands to estimate the LSWT.

Regarding the closest values to the in-situ measurements, the study found that MODIS obtained the highest accuracy for LSWT estimation. The RMSE for the measurements from this sensor was 1.05 °C, and our study's results (1.25°C) are within the same range of RMSE.

Therefore, MODIS is recommended for LSWT studies. However, other sources with higher spatial resolution are suggested for small lakes.

Another study by Liu et al. (2015) found that MODIS was reliable after validating and mapping surface water temperatures in Lake Taihu, China. The study used MODIS level 3, 1-km nominal resolution daily products called MOD/MYD11A1 (Collection 5) derived from MODIS TIR bands 31 and 32 and employ a generalized split-window land surface temperature (LST) algorithm. These products provide land surface temperature (LST) information and include quality control datasets. The validation involved comparing the MODIS-derived LSWT with the in-situ water temperature. The accuracy was assessed using RMSE and a linear correlation analysis, which showed a significant correlation with a coefficient of determination higher than 0.96. The RMSE between MODIS-derived LSWTs and in situ water temperatures ranged from 1.2 °C to 1.8 °C, indicating a lower accuracy (as the accuracy requirement for MODIS LST products is within 1 °C at 1 km resolution), which was not achieved in this study. Due to the differences in the measurements (bulk temperature in each depth vs. surface temperature) and the significant spatial variation in LSTs. Thus, this study provided similar results compared to our time series analysis with MODIS for 2020, as the in-situ data does not correspond well to in-situ values on this year, with RMSE of 1.93 °C.

In the case of the mono-channel algorithms for Landsat 8, a study by Wang et al. (2019) comparing the PSC algorithm to the general single channel (SC) found that the PSC algorithm provides a more accurate estimation of land surface temperature (LST) compared to the SCA algorithm, with RMSE of 1.77 °C for the PSC algorithm when validating with measurements from the U.S. surface radiation budget network as actual values. However, the difference between this last study was that the validation method was not made with field measurements, as we validated using in-situ measurements over the Issyk-Kul Lake in 2019. Despite that, accuracy was similar to our study (RMSE of 1.37 °C).

Based on the same LSWT estimates process as MODIS over the Issk-Kul Lake, where the LST product from Sentinel-3 is obtained with the SWA method, these LSWT estimates with Sentinel-3 correspond well overall to in-situ temperatures. Sentinel-3 shows RMSE of 0.79 °C derived

from the time series analysis in 2020. In addition, derived from the intercomparison at the same day and similar times with other sensors in 2019, Sentinel-3 provides a RMSE of 1.34 °C. With this, overall, Sentinel-3, with its moderate resolution, provides a good correspondence level when validated with in-situ measurements. On the other hand, in terms of comparison with previous studies using the same or similar approach to estimate LSWT using Sentinel-3, at the moment of this research, there are no current studies proposing estimates with the approach of this satellite. Therefore, Sentinel-3 is recommended for LSWT studies. However, as for MODIS, other sources with higher spatial resolution are suggested for smaller lakes.

The case of the results from CCI Lakes surprisingly shows good agreement to in-situ measurements during 2019 over Issyk-Kul Lake, considering one image per month on the same day as the other satellites, with RMSE of 1.25 °C and differences of 0.94 °C as MAE. On the other hand, during the time series analysis in the same year (2019) and 2020, the RMSE decreased by 1.42 °C and 1.37 °C, respectively. CCI Lakes could be considered a valuable reference source when comparing the LSWT with other sources. However, this product is inaccurate regarding temporal resolution when cross-validation, as its acquisition time is pinned at 12:00 UTC daily.

4.4.2 LSWT Retrieval

Regarding the performance using the Landsat 8 mono-channel algorithms, our study spots the PSC_{wvc} as the most stable method compared to the SCA and MWA, where this last one shows the lowest agreement. These estimates are compared to the reference values from the meteorological station 2019 in the Issyk-Kul Lake. One image per month is retrieved to perform the one-channel algorithms from Landsat 8, using areas of interest of 100 km^2 at the East or West region of the Lake according to the availability of the pixels in function of the cloud coverage. The advantage of using the SCA lies in its simplicity, requiring only two input parameters and not needing to estimate the effective mean atmospheric temperature. However, its limitations include sensitivity to atmospheric *wvc* errors and the lack of consideration for atmospheric transmittance (τ). While the PSC_{wvc} method is an improved version of the SCA, they have the same advantage: it requires only two input parameters, just

as the SCA (LSE and *wvc*). This PSC_{wvc} simplifies retrieval and reduces errors associated with other parameters, such as the effective mean atmospheric temperature (T_a). The PSC_{wvc} addresses some of the limitations and errors associated with atmospheric *wvc,* providing a more accurate retrieval of the LSWT. If there are errors in estimating the *wvc*, it can lead to more significant errors in the retrieved land surface temperature.

In terms of sensitivity, the MWA and SC method are more sensitive to error with the increase in temperature and humidity, specially in humid and hot conditions regions. On the other hand, the advantage of the MWA is that it can achieve good results in retrieving LSWT from channel TIRS-2 (B10) of Landsat. However, this method is sensitive to errors in *wvc*. When the error of *wvc* reaches the maximum of 0.3 g/cm^2, the error of the retrieved LST exceeds 1 K. Additionally, the MWA is also sensitive to errors in the effective mean atmospheric temperature (T_a) (Wang et al., 2019).

In terms of the results performance of the Practical Singe Channel (PSC) algorithm, a study showed similar results to our analysis using this retrieval method. Wang. et al. (2019) found that the better corresponding algorithm for retrieving LST was the PSC after evaluating the performance of PSC and the generalized single-channel (GSC) algorithm using both simulation data sets and satellite measurements. A previous study using these algorithms concluded, as well as in our research, that SCA and PSC_{wvc} show good agreement when compared to in situ measurements, and estimation errors have been attributed to the quality of atmospheric *wvc*. Wang et al. (2019) compared three algorithms (MWA, SCA, SWA), where SWA was found to be the most reliable method for LST retrieval compared to the MWA and SCA. The SWA had the lowest sensitivity to errors in input parameters, and its results were less affected by humid environments. The MWA and SCA were more sensitive to errors in input parameters, particularly in hot and humid conditions. These two algorithms were susceptible to errors in atmospheric *wvc*. When the error of atmospheric *wvc* reached the maximum, the error of LST exceeded 1.0 °C. On the other hand, the SWA demonstrated more stability, and the error of input parameters did not cause a significant error in LST.

Another study supports our results. Jimenez-Muñoz et al. (2014) tested the SCA and the SWA using simulated data from atmospheric profile databases and emissivity spectra. The results showed mean errors below 1.5 °C for both algorithms. The accuracy of the algorithms for LST retrieval was assessed through bias values, standard deviation, root mean square errors (RMSE), and linear correlation coefficients. Both algorithms showed promising accuracy for LST retrieval from Landsat-8 TIRS data based on simulated data, with slightly better results for the SWA method. However, further validation using ground data is necessary to determine the best correspondence and performance of these algorithms.

Results from the LSWT estimates using ECOSTRESS show low correspondence level compared to in-situ measurements, with RMSE of 2.47 °C over the Issyk-Kul Lake in 2019, and a RMSE of 2.33 °C in 2020. The temperatures throughout the year are underestimated, with MAE of 2.0 °C and 2.30 °C in 2019 and 2020, respectively. However, after using the SWA for ECOSTRESS, temperatures enhanced their results regarding their LSWT underestimation, with 2.15 °C of RMSE and a MAE of 1.78 °C in 2019. On the other hand, over the LSWT estimates in Gerardmer and Longemer Lakes during 2020 and 2021, when we compare estimates from Landsat 8-9 and ECOSTRESS, frequently they show similarity between their values and tendencies in most of the cases, with a difference of less than 1 °C. Moreover, there are periods when there is a remarkable variation between the two data, with a difference of up to 2 °C. One of the observations we can make after validating with in-situ measurements is that ECOSTRESS datasets are less stable than Landsat 8-9. In Gerardmer, for example, ECOSTRESS presents 2.52 °C of RMSE and 1.40 °C with Landsat 8-9, while in Longemer, ECOSTRESS gives 2.87 °C of RMSE and Landsat 8-9 a RMSE of 2.04 °C. Thus, temperatures estimated by SWA with Landsat data are generally very close to in-situ data compared to the estimation method with ECOSTRESS products (TES), even if the difference between the two is not very large. Knowing the performance of the SWA and TES algorithms, the discrepancies can be due to the sensors, especially for ECOSTRESS, which often presents high spatial variations. In addition, processing with ECOTRESS data has the advantage of acquiring data on several dates (revisit 1-2 days in this region in France). However, even with ECOSTRESS's cloud product, some dates were

retained with abnormal temperatures. This could be due to inconsistencies in the cloud detection.

4.4.3 Ground validation

We made different types of validations in this research work, such as sensors intercomparison, meteorological station, in-situ data derived from buoys, Torrent board equipped with temperature sensors, radiometer (CIMEL 312-2), and a FLIR camera (T-560).

In terms of validation of the retrieved LSWT from the intersensors comparison and the Landsat 8 algorithms, our results are similar to that of Wang et al. (2019), who evaluated the temperature-based method, which directly compares the satellite-derived LST with in-situ LST measurements at the satellite overpass; the cross-comparison process, which compares the retrieved LST with the MODIS LST product; and the last method to validate was to compare the retrieved LST with ground observation data. Then, compared to this research, similarities were found regarding results and validation methods. The main difference in comparison with this study was the SWA performance. Even when they recommended not to apply it due to the stray light effect implication, especially for Band 11 (TIR-2), they still used a correction algorithm called the stray light correction algorithm (SLCA); besides the application to this study was applied into the land (LST).

However, we still performed the SWA by only using collection 2 from Landsat 8-9, where the stray light effect implication is reduced significantly, especially for the TIR2 (B10). The results derived from our retrieval analysis show good correspondence level in the validation campaigns and with in-situ datasets in Issyk-Kul, Gerardmer, Longemer, and Plobsheim Lakes from 2021 to 2023. The results that the SWA method provide for Landsat 8-9, show better correspondence to in-situ measurements than those results that SWA show when applied to ECOSTRESS, Sentinel-3, and MODIS. Coincidences with a study from Ye et al. (2022), who validated results from the SWA method to Landsat 9 with an accuracy of about 1.57 K, which was better than the existing Landsat-9 LST product (mono-channel using the SCA). The retrieved LST images had similar

spatial distribution to the Landsat-9 LST products, with RMSE ranging from 0.31 to 2.87 K in different regions. Li et al. (2022) evaluated different waterbody extraction algorithms using Landsat-9 data and the Google Earth Engine (GEE) platform in the Qinghai-Tibet Plateau. After comparing Landsat-9 data with Landsat-8 data, they concluded that these two sources have great consistency and can be used collaboratively to extract water and lake areas.

For the LSWT estimates from Sentinel-3, values generally show good agreement in all the comparisons made over the different study areas and years, being a good source of reference when validating in-situ data and validation campaigns. Sentinel-3 is suitable for lakes with more significant extensions due to its spatial resolution of 1 km. Thus, the Issyk-Kul Lake Sentinel-3 is a decent source to estimate the LSWT, with RMSE of 1.34 °C or less for each comparison. However, in smaller lakes, such as Plobsheim Lake, Sentinel-3 can be helpful as an additional source of reference, and not as the main one, considering that only 4 to 5 pixels could be available in the area, which sometimes cannot be representative in this lake. In comparison with other studies, our research coincides with Pérez-Panells et al. (2021), who presented a validation through ground-based validation and comparing in-situ measurements with satellite-derived LST values for the Sentinel-3A and Sentinel-3B SLSTR LST Level-2 product, indicated that the LST product from these sensors was accurate for nighttime data, with a median accuracy of 1 °C and a precision of 1 °C for the investigated surfaces. However, for daytime data, the accuracy was determined to be 1.8 °C with a precision of 1.2 °C. The increase in daytime precision is attributed to the more considerable thermal heterogeneity of the land surface. At the same time, the rise in bias is thought to be caused by wrongly assigned biomes. The validation results for Sentinel-3A and 3B showed that the accuracy and precision of LST over water (flooded soil) were less accurate than other land covers.

From the LSWT estimates using ECOSTRESS, we could compare our research to a study from Li et al. (2021) that evaluates LST products (MODIS, ECOSTRESS, GOES-R, Landsat, and Sentinel-3) using in-situ measurements from 11 sites in the U.S. Corn Belt during the 2018 and 2019 growing seasons. The evaluation focused on the biases and accuracy of the LST products compared to ground observations. This study indicates that all the LST products have tendencies within ±2 °C during nighttime and ±3 °C during daytime. For daytime LST, the

highest agreement with ground observations is achieved by ECOSTRESS, while MODIS and MYD11A1 products slightly underestimate daytime LST. ECOSTRESS had an overall absolute bias of less than 0.9 °C, an RMSE of less than 2.15 °C, and a standard deviation of less than 1.95 °C. Contrary to our research, the ECOSTRESS satellite showed less agreement in underestimating temperatures (4 °C) against the meteorological station values. These differences could be due to the validation of the LST products, where the study of Li et al. (2021) primarily used ground observations from agricultural sites rather than water surfaces, where the performance of the LST product of ECOSTRESS retrieved by using the TES method could behave differently for water.

Another study differs from this research in terms of agreement, as Shi et al. (2021) estimated the LST by using the TES algorithm; the accuracy and reliability of the LST data were evaluated through several validation processes, including comparisons with in-situ measurements and well-calibrated MODIS measurements. The results demonstrated a high correlation between the ECOSTRESS LST and in situ LST, indicating the effectiveness of the retrieval algorithm.

In addition, Ru et al. (2023) developed an extended SW-TES algorithm (combining the SWA and TES algorithms) to retrieve LST and LSE simultaneously while considering the urban geometry effect. The results show that the retrieved LST values with the extended algorithm are generally lower than those obtained without considering the urban geometry effect. They concluded that the performance of the SWA alone, with no urban geometry, may not be as reliable for LST retrieval over urban areas using ECOSTRESS data. However, for our type of surface, the water is considered almost a flat surface, except when there is roughness, wavelets, and swell; the repercussion should not be as great on the estimates. Our comparisons with ECOSTRESS, using the LST original product (TES algorithm), show a lower accuracy and more significant differences in LSWT estimates within the different study areas. However, after performing the SWA for ECOSTRESS, the LSWT values enhanced relatively by 1.0 °C. For instance, over Issyk-Kul Lake in 2019, the RMSE values enhanced from 2.33 to 2.15 °C when validated to in-situ datasets. With this, ECOSTRESS could be a good corresponding source of LSWT estimates by using the SWA method, as when compared to Landsat 8-9, values between them rely, and they could complement each other in temporal resolution.

In the case of the results from the radiometer and the infrared camera over the Plobsheim Lake validation campaign in April 2023, they show relatively good agreement. For instance, the temperatures obtained from the sensors on the Torrent board validate the LSWT from the CIMEL CE-312-2, with differences in temperatures of less than 1 °C. In addition, ECOSTRESS shows a 1.0 °C difference, and Landsat 8 is only 0.1 °C. ECOSTRESS and Landsat 8 are good agreement sources compared to in situ values derived from the torrent board sensors and the radiometer. On the other hand, the LSWT from the camera FLIR T-560 in the validation campaign in Plobsheim Lake in June 2023 show a higher difference in temperatures between all sensors but less differences with the sensors from the values from the Torrent board sensors wT2 and wT4 (RMSE of 1.29 °C and 1.12 °C respectively). This may be due to camera difficulties when capturing the images in the field or to calibration problems of the camera. However, it was impossible to compare the FlIR camera and the radiometer during the same validation campaign due to the unavailability of these instruments at the time of each validation campaign.

Chapter 5. Conclusions and Perspectives

The Lake Surface Temperature (LSWT) indicates the temperature of the skin layer on the lake surface. However, it is an essential indicator of the lakes' state and strongly influences water chemistry and the aquatic ecosystem. At the same time, the LSWT has a driving effect on the weather and climate around the large lakes. Typically, LSWT data are collected from in-situ measurements. However, these in-situ data are often spatially rare and inaccessible. Information on water temperature with improved spatial and temporal resolutions is needed in many applications, such as climate change monitoring and hydrological cycle studies, and in the habitat of aquatic organisms, fisheries, aquaculture, and water quality management.

Remote sensing sensors, with spectral ranges between 8 and 14 µm (known as thermal infrared radiation - TIR), are one of the techniques used to study the LSWT variation. This approach provides temporal and spatial variations on different scales that help to understand the physical processes of the water cycle by enabling a finer interpretation of the LSWT dynamics. However, there is still a lack of research into data acquisition and analysis involving multiple sensors with different resolutions.

The objectives of this thesis included:

1) To obtain and analyze LSWT from multiple sensors with different spatial, temporal, and spectral resolutions, providing denser spatial and temporal measurements of LSWT is needed to understand processes and dynamics in the thermal domain and its changes in time and space.

2) To validate LSWT by comparing it with in situ measurements. Validation campaigns were carried out on the Issyk-Kul Lake (Kyrgyzstan) and three lakes in the Grand-Est region of France (Gerardmer, Longemer, and Plobsheim lakes).

Our research analyzed multi-resolution and multi-sensor satellite missions with onboard TIR sensors (MODIS, Sentinel-3, ECOSTRESS, and Landsat 8 and 9) to perform these objectives. Besides, these sensors provide valuable information in anticipation of new TIR missions such as

TRISHNA in 2025 (CNES-ISRO) and longer-term missions such as LSTM (ESA Copernicus) and SBG (NASA), both in 2028.

5.1 Conclusions

Different approaches for extracting the LSWT from high and medium-resolution satellites have been implemented, tested, and compared. The satellites and their corresponding sensors used for this research were Landsat 8-9 (TIRS), MODIS (Terra), Sentinel-3 (SLSTR), and ECOSTRESS on board the ISS. An initial series of images were selected based on criteria such as date of acquisition, clear weather, and the broadest possible coverage, with at least one image per month; however, the availability of ECOSTRESS was limited to the Issyk-Kul Lake area. On the other hand, for the rest of the regions (Gerardmer, Longemer, and Plobsheim), the imagery availability was better, however, the regular cloud coverage over these regions limited the imagery quality for their analysis, especially during autumn and winter seasons.

The first results are derived from the intersensors comparison retrieved in 2019 over the Issyk-Kul Lake. One image per month on the same day and at an exact or similar time is compared. They reveal that LSWT estimates from MODIS are nearest to the CCI Lakes product (RMSE 1.25 °C and MAE of 0.90 °C) compared to in-situ measurements. However, estimates from Sentinel-3 (RMSE 1.34 °C and MAE of 1.10 °C) and Landsat 8- PSC_{wvc} (Collection 1) (RMSE 1.37 °C and MAE of 1.15 °C) are also near to the in-situ measurements, but less than MODIS. However, derived from the time series analysis over Issyk-Kul Lake in 2019 and 2020, Sentinel-3 is a good agreement source of reference to the in-situ measurements, with RMSE of 1.34 °C and 0.79 °C, respectively.

The performance of the LSWT estimates on the Issyk-Kul Lake in 2019 with MWA, $PSC_{wvc,}$ and SCA methods after excluding SWA due to stray light in Landsat 8 collection 1, causing a band or stripping effect, evident in band 11 (TIRS-2). Thus, from the mono-channel algorithms derived from this satellite, MWA is not as consistent as PSC_{wvc} or SCA in the cross-validation method with the temperatures from the meteorological station and the CCI Lakes product. PSC_{wvc}

corresponds better to the in-situ reference values with a RMSE of 1.37 °C and 1.15 °C of MAE. The low correspondence that MWA gives, RMSE of 1.92 and MAE of 1.52 °C, could be due to MWA being sensitive to errors in *wvc*. As high as the *wvc* is, the error of the retrieved LSWT exceeds. The MWA is also sensitive to errors in the effective mean atmospheric temperature (T_a).

During the validation campaign in the Issyk-Kul Lake using the Torrent board carrying sensors for measuring humidity, air, and water temperatures (to a depth of 35 cm), the LSWTs derived from Sentinel-3 are the nearest to the LSWTs from the Torrent board, with a difference of 0.3 °C, and a difference of 4 hours regarding the acquisition time between these two sources. For the LSWTs from MODIS, compared with the temperatures from the Torrent board, temperatures differ by 1.3 °C and by 5 hours of the acquisition time difference between them. Some cloud coverage during the MODIS overpassing was perceived at the time of the validation.

On the other hand, the Gerardmer and Longemer Lakes analysis in 2021 and 2022 shows that ECOSTRESS data underestimates values by 5 °C and Landsat 8-9 data by 2 °C. The datasets are generally consistent for the same-date analysis between these two sources. However, the LSWT estimates with the Landsat 8-9 using the SWA algorithm correspond better to the in situ data. The ECOSTRESS imagery is limited to their cloud mask to present a cleaner image. However, this mask did not reduce the standard deviation of their results. ECOSTRESS products are rich in information but can be complex in the geoprocess. Each product contains multiple layers of data, including land surface temperature evapotranspiration. Moreover, to enhance the LSTE product geolocation of ECOSTRESS, due to the inaccuracy in the geolocalization derived in the ISS, it is necessary to join extra products of geolocation as well as a cloud mask product to the LSTE product, adding efforts in the LSWT retrieval.

Over the Plobsheim Lake in 2021 and 2022, the results from Landsat 8-9 are consistent, but they show higher temperature differences than those with ECOSTRESS and MODIS. This could be related to a limitation in cloud mask detection for Landsat 8-9 or a problem in the instrument due to stripping. Hence, ECOSTRESS and MODIS values correspond better to the in-

situ measurements (buoys) than those with Landsat 8-9 (SWA). On the other hand, for the validation campaign in the same lake on 2023, ECOSTRESS and Landsat 8-9 show good agreement with the in-situ measurements from the buoys and from sensors of the Torrent board and the radiometer CIMEL CE-312-2. In contrast, the FLIR-T560 camera present larger temperatures difference with ECOSTRESS and Landsat 8-9, but good agreement with the Torrent board sensors values. This may be due to camera handling difficulties over the field when capturing the images or even to calibration problems of the instrument.

Regarding the performance of the multi-sensors used to retrieve the LSWTs, those using the SWA when retrieving the temperatures, unlike those using the TES algorithm (ECOSTRESS), demonstrated better proximity to in-situ values. We can conclude that SWA requires no prior atmospheric corrections, unlike the TES algorithm, where accuracy can be affected by perturbations in atmospheric conditions. Besides, ECOSTRESS demonstrates to correct its LSWT estimates by 1 °C when implementing its SWA correction method.

To sum up these conclusions, we can list them as follows:

- MODIS and Sentinel-3 provide good agreement LSWT estimates when compared to the in-situ datasets. They are mainly proposed for greater extension lakes due to their spatial resolution (1 km). Besides, for validation campaigns, the overpassing of these satellites can be predicted.

- Sentinel-3 is a novelty in this study since, until this research, there are no previous studies where lake temperatures are estimated with this sensor. Also, something new is a comparison of Sentinel-3 with high-resolution satellites such as ECOSTRESS and Landsat 8-9, where the SWA for ECOSTRESS is tested to compare the same method of retrieval by using SWA methods.

- CCI Lakes also provides near estimates, a great reference of LSWT values product. However, its temporal resolution is a daily aggregation interval pinned to 12:00 UTC, which limits its correspondence compared to other sources at different acquisition times. Besides, its spatial resolution does not provide estimates for small lakes.

- The performance of the mono-channel algorithms for Landsat 8 (collection 1), designed for the B10 -TIR1, shows that the PSC_{wvc} provides the best agreement when compared to the in-situ measurements of MWA and SCA. It is due to MWA being susceptible to wvc errors. The obtained LSWT error exceeds as high as the wvc. Errors in the effective mean air temperature (T_a) can also affect the MWA estimates.

- Regarding collection 2 for Landsat 8-9, the SWA method corresponds well when validated with in-situ measurements. It is an excellent source to estimate LSWT for smaller lakes. However, they are still limited, with their temporal resolution set at 16 days.

- ECOSTRESS, with a better temporal resolution (3-5 days) than Landsat 8-9, in terms of high spatial resolution (70 m), shows more difficulties when retrieving LSWT due to the need to combine the LSTE product with the geolocation and cloud products. The LSTE product is produced using the TES algorithm, and their results are generally unreliable in our study regions. However, when performing the SWA method to retrieve the LSWT, estimates were enhanced by 1 °C on most dates. It can be because SWA does not require any previous atmospheric adjustments, in contrast to the TES algorithm, whose accuracy may be impacted by atmospheric circumstances.

- The LSWT estimates from the radiometer CIMEL CE 312-2 show good agreement to the Torrent board sensors, with less than 1 °C of temperature differences, unlike the FLIR-T560 camera, which shows a higher difference in temperatures between all sensors and less than 2 °C differences with the sensors from the Torrent board values. This could be due to calibration problems with the instrument.

This research considered small and medium-sized lakes such as Gerardmer, Longemer, and Plobsheim. It means that future high-resolution thermal missions (60-70 m) will be able to provide optimal regular information to study other lakes of similar size, considering that each hectare contains approximately 140 pixels with such spatial resolution. Hence, a 10-ha extension lake could provide representative valuable data of its LSWT.

Finally, ground-based reference sites such as lakes are vital in validating, calibrating, and accurately assessing satellite data collected by instruments like Trishna or LSTM missions. Those sites serve as a basis for increasing trust in satellite-derived information, allowing it to be used effectively in scientific study, environmental monitoring, and decision-making. From our experience with the lakes used to perform the validation campaings in this research, the Lakes of Gerardmer, Longemer, and Plobsheim in France and Issyk-Kul Lake in Kyrgyzstan could be considered as good references for ground-based sites.

5.2 Perspectives

To achieve optimal validation and monitoring of lake temperatures, experimental and satellite measurements must be implemented. Some recommendations could be considered to achieve this:

- Ground data (in situ) collection:
    - Deploy in situ temperature sensors, such as thermistors or data loggers, at various depths within the lake. Ensure sensors are appropriately calibrated and regularly maintained. Distribute sensors strategically to capture temperature profiles, including the lake's surface, middle, and bottom layers.

      Measure the temperature at different depths of a lake provides insights into the thermal structure and dynamics of the lake ecosystem. These measures can influence the distribution and behavior of aquatic organisms, nutrient cycling, and overall lake productivity. Additionally, understanding the vertical temperature profile of a lake is crucial for studying processes such as stratification and mixing, thermal stability, and heat exchange between the water and the atmosphere.
    - Collect high-quality in situ temperature data at frequent intervals, capturing diurnal and seasonal variations.

- Implement a continuous monitoring and update system to ensure the lake temperature dataset remains accurate. Regularly assess data quality and make necessary corrections. The approaches for this could be assessed with the help of a device carrying sensors to measure the temperature of the first layers of the lake, such as the Torrent board. Additionally, radiometers and FLIR cameras could be helpful to complement the monitoring of the LSWT.
- Validate LSWT estimates for heterogeneous and non-isothermal surfaces, by assessing the accuracy of temperature estimates against ground-based measurements and combining it with high spatial-resolution LSWT acquired from unmanned aerial vehicle (UAV) platforms – drones or planes equipped with thermal sensors can cover large areas quickly. It is especially beneficial for monitoring the surface temperature of large lakes, where traditional methods might be time-consuming and less practical.

- Satellite measurements:
  - Acquire satellite remote sensing data with suitable sensors for lake temperature monitoring. Understand the specifics of the satellite data, such as spatial and temporal resolution, spectral bands, and calibration information. As demonstrated in this research, those with better correspondence include Sentinel-3, even MODIS for great extension lakes mainly, and Landsat 8-9 and ECOSTRESS (SWA) for smaller lakes.
  - Validate satellite-derived lake temperature data against in situ measurements. Ensure that in situ measurements and satellite overpasses are well-matched in time and space.
  - Use statistical techniques like RMSE (Root Mean Square Error), MAE (Mean Absolute Error), regression analysis, and correlation coefficients to assess the agreement between satellite and in situ data.

- Regarding measuring the temperature at different depths, satellite and aerial imagery can be used to estimate lake depths as LiDAR (Light Detection and Ranging) and satellite altimetry can provide information about the surface elevation of the water, which can then be used to infer depth.

In terms of satellites temporal resolution, more in-depth image analysis could be envisaged using low-resolution sensors such as Fengyun-4 (FY-4A), equipped with the AGRI (Advanced Geostationary Radiation Imager) instrument for the LST product, with a spatial resolution of 4 km, an IR radiometric resolution of 10.3 to 13.8 µm and a temporal resolution of 15 minutes. AGRI is, therefore, the optimum tool for covering the limited temporal resolution offered by moderate and high-resolution TIR sensors. Thus, the data derived from the FY-4A satellite will provide the daily dynamics of pixel temperature at low resolution (Fan et al., 2022; Meng et al., 2019). The information from this dynamic would allow the modeling of the daily temperature cycle, which could be applied to high-resolution, such as Landsat 8-9, ECOSTRESS, and the new TIR mission TRISHNA in 2025 (CNES-ISRO), and medium-resolution (Sentinel-3 and MODIS) pixels.

Another outlook for this research would be analyzing possible synergies between the optical sensors and temperatures from passive microwaves to avoid the problem of cloud cover by applying a downscaling process. The data that could be considered for passive microwaves are the C-band (AMSR-E, ~50km; AMSR_2, ~40km) and L-band (SMOS, ~40km; SPAM, ~40km). SMOS is a multiangular mission that gives access to horizontal (TBh) and vertical (TBv) polarizations of the emitted radiation, allowing to invert the physical temperature, which is constant according to polarization and angle, knowing that for SMAP we do not have multi-angular data, only horizontal and vertical polarization. Finally, an interesting idea would be to combine Band-C (AMSR-E AMSR-2) and Band-L (SMOS/SMAP). It would minimize the effects of vegetation, such as algae, and the roughness of the water surface (wind effect); in terms of SAR and optical sensors, exogenous data of the Sentinel 1 (roughness) and Sentinel 2/3 (vegetation) types may be used to characterize the surface conditions. However, this aspect of the LSWT synergy between optical and passive microwave sensor temperatures has a more exploratory element, where research in this direction already exists, with statistical studies on IRT and

microwave surface temperature relationships showing exciting correlations (Boutin et al., 2004; Mao et al., 2007). Additionally, it could be available exclusively for large lakes due to the size of the pixels (40 km) provided by these passive microwave datasets. Thus, only a few pixels could be extracted for the downscaling process.

To sum up, optimal validation and monitoring of LSWT require a synergistic approach that leverages the strengths of both in-situ measurements and satellite observations. This integration enhances our understanding of lake dynamics, improves the accuracy of remote sensing algorithms, and provides valuable information for various scientific, environmental, and resource management applications.

References

Ades, M., Adler, R., Aldeco, L. S., Alejandra, G., Alfaro, E. J., Aliaga-Nestares, V., Allan, R. P., Allan, R., Alves, L. M., Amador, J. A., Andersen, J. K., Anderson, J., Arndt, D. S., Arosio, C., Arrigo, K., Azorin-Molina, C., Bardin, M. Y., Barichivich, J., Barreira, S., … Veasey, S. W. (2019). State of the climate in 2018. In *Bulletin of the American Meteorological Society* (Vol. 100, Issue 9). https://doi.org/10.1175/2019BAMSStateoftheClimate.1

AgroParisTech. (2017). *DIAGNOSTIC TECHNIQUE ET SOCIOLOGIQUE DES LACS DE GÉRARDMER, LONGEMER ET RETOURNEMER ET PLAN D'ACTION*.

Alifujiang, Y., Abuduwaili, J., Maihemuti, B., Emin, B., & Groll, M. (2020). Innovative trend analysis of precipitation in the Lake Issyk-Kul Basin, Kyrgyzstan. *Atmosphere*, *11*(4). https://doi.org/10.3390/atmos11040332

Alsdorf, D. E., Rodríguez, E., & Lettenmaier, D. P. (2007). Measuring surface water from space. *Reviews of Geophysics*, *45*(2). https://doi.org/10.1029/2006RG000197

Attiah, G., Kheyrollah Pour, H., & Scott, K. A. (2023). Lake surface temperature retrieved from Landsat satellite series (1984 to 2021) for the North Slave Region. *Earth System Science Data*, *15*(3). https://doi.org/10.5194/essd-15-1329-2023

Battarbee, R. W., Kernan, M., Livingstone, D. M., Nickus, U., Verdonschot, P., Hering, D., Moss, B., Wright, R. F., Evans, C. D., Grimalt, J. O., Johnson, R. K., Maltby, E., Linstead, C., & Skeffington, R. A. (2008). Freshwater Ecosystem Responses to Climate Change: The Euro-Limpacs Project. In *The Water Framework Directive: Ecological and Chemical Status Monitoring*. https://doi.org/10.1002/9780470716090.ch20

Becker, F., & Li, Z. L. (1990). Towards a local split window method over land surfaces. *International Journal of Remote Sensing*, *11*(3). https://doi.org/10.1080/01431169008955028

Boutin, J., Waldteufel, P., Martin, N., Caudal, G., & Dinnat, E. (2004). Surface salinity retrieved from SMOS measurements over the global ocean: Imprecisions due to sea surface roughness and temperature uncertainties. *Journal of Atmospheric and Oceanic Technology, 21(9)*. https://doi.org/10.1175/1520-0426(2004)021<1432:SSRFSM>2.0.CO;2

Carrea, L., Crétaux, J. F., Liu, X., Wu, Y., Calmettes, B., Duguay, C. R., Merchant, C. J., Selmes, N., Simis, S. G. H., Warren, M., Yesou, H., Müller, D., Jiang, D., Embury, O., Bergé-Nguyen, M., & Albergel, C. (2023). Satellite-derived multivariate world-wide lake physical variable timeseries for climate studies. *Scientific Data*, *10*(1). https://doi.org/10.1038/S41597-022-01889-Z

Carrea, L., Embury, O., & Merchant, C. J. (2015a). Datasets related to in-land water for limnology and remote sensing applications: distance-to-land, distance-to-water, water-body identifier and lake-centre co-ordinates. *Geoscience Data Journal*, *2*(2), 83–97. https://doi.org/10.1002/gdj3.32

Carrea, L., Embury, O., & Merchant, C. J. (2015b, July 21). *GloboLakes: high-resolution global limnology dataset v1*. Centre for Environmental Data Analysis.

Cawse-Nicholson, K., Townsend, P. A., Schimel, D., Assiri, A. M., Blake, P. L., Buongiorno, M. F., Campbell, P., Carmon, N., Casey, K. A., Correa-Pabón, R. E., Dahlin, K. M., Dashti, H., Dennison, P. E., Dierssen, H., Erickson, A., Fisher, J. B., Frouin, R., Gatebe, C. K., Gholizadeh, H., … Zhang, Q. (2021). NASA's surface biology and geology designated observable: A perspective on surface imaging algorithms. In *Remote Sensing of Environment* (Vol. 257). https://doi.org/10.1016/j.rse.2021.112349

Coll, C., Wan, Z., & Galve, J. M. (2009). Temperature-based and radiance-based validations of the V5 MODIS land surface temperature product. *Journal of Geophysical Research Atmospheres*, *114*(20). https://doi.org/10.1029/2009JD012038

Conseil scientifique Plan Grands Lacs. (2023).

Crétaux, J. F., Bergé-Nguyen, M., Calmant, S., Jamangulova, N., Satylkanov, R., Lyard, F., Perosanz, F., Verron, J., Montazem, A. S., Guilcher, G. Le, Leroux, D., Barrie, J., Maisongrande, P., & Bonnefond, P. (2018). Absolute calibration or validation of the altimeters on the Sentinel-3A and the Jason-3 over Lake Issykkul (Kyrgyzstan). *Remote Sensing*, *10*(11). https://doi.org/10.3390/rs10111679

Cristóbal, J., Jiménez-Muñoz, J. C., Prakash, A., Mattar, C., Skoković, D., & Sobrino, J. A. (2018). An Improved Single-Channel Method to Retrieve Land Surface Temperature from the Landsat-8 Thermal Band. *Remote Sensing 2018, Vol. 10, Page 431*, *10*(3), 431. https://doi.org/10.3390/RS10030431

Crosman, E. T., & Horel, J. D. (2009). MODIS-derived surface temperature of the Great Salt Lake. *Remote Sensing of Environment*, *113*(1). https://doi.org/10.1016/j.rse.2008.08.013

Dallas, H. (2008). Water temperature and riverine ecosystems: An overview of knowledge and approaches for assessing biotic responses, with special reference to South Africa. In *Water SA* (Vol. 34, Issue 3). https://doi.org/10.4314/wsa.v34i3.180634

Danis, P.-A., Tormos, T., Simon, R., Reynaud, N., Rebierre, D., Moullec, P., Cavalli, L., Sagot, C., Dubois, C., Daufresne, M., & Baudoin, J.-M. (2014). *IR-LANDSAT et lacs sentinelles*.

Dash, P. (2005). Land Surface Temperature and Emissivity Retrieval from Satellite Measurements. *Meteorologie*.

Dataset Record: GloboLakes: high-resolution global limnology dataset v1. (n.d.). Retrieved September 26, 2023, from https://catalogue.ceda.ac.uk/uuid/84d4f66b668241328df0c43f8f3b3e16

Dataset Record: GloboLakes: Lake Surface Water Temperature (LSWT) v4.0 (1995-2016). (n.d.). Retrieved September 26, 2023, from https://catalogue.ceda.ac.uk/uuid/76a29c5b55204b66a40308fc2ba9cdb3

Delclaux, F., Chevallier, P., Esgaib, L., Romanovsky, V., & Crétaux, J.-F. (2015). Un bilan hydrologique du lac Issyk-Koul (Kirghizstan). *Open Edition Journals*, *25*(Cahiers d'Asie central), 75–102.

Dokulil, M. T. (2014). Predicting summer surface water temperatures for large Austrian lakes in 2050 under climate change scenarios. *Hydrobiologia*, *731*(1). https://doi.org/10.1007/s10750-013-1550-5

Du, C., Ren, H., Qin, Q., Meng, J., & Zhao, S. (2015). A practical split-window algorithm for estimating land surface temperature from landsat 8 data. *Remote Sensing*, *7*(1). https://doi.org/10.3390/rs70100647

Dyba, K., Ermida, S., Ptak, M., Piekarczyk, J., & Sojka, M. (2022). Evaluation of Methods for Estimating Lake Surface Water Temperature Using Landsat 8. *Remote Sensing*, *14*(15). https://doi.org/10.3390/rs14153839

Fan, J., Han, Q., Wang, S., Liu, H., Chen, L., Tan, S., Song, H., & Li, W. (2022). Evaluation of Fengyun-4A Detection Accuracy: A Case Study of the Land Surface Temperature Product for Hunan Province, Central China. Atmosphere, 13(12). https://doi.org/10.3390/atmos13121953

Fiedler, E. K., Martin, M. J., & Roberts-Jones, J. (2014). An operational analysis of Lake Surface Water Temperature. *Tellus, Series A: Dynamic Meteorology and Oceanography*, *66*(1). https://doi.org/10.3402/tellusa.v66.21247

Fisher, J. B., Lee, B., Purdy, A. J., Halverson, G. H., Dohlen, M. B., Cawse-Nicholson, K., Wang, A., Anderson, R. G., Aragon, B., Arain, M. A., Baldocchi, D. D., Baker, J. M., Barral, H., Bernacchi, C. J., Bernhofer, C., Biraud, S. C., Bohrer, G., Brunsell, N., Cappelaere, B., … Hook, S. (2020). ECOSTRESS: NASA's Next Generation Mission to Measure Evapotranspiration From the International Space Station. *Water Resources Research*, *56*(4). https://doi.org/10.1029/2019WR026058

Gerace, A., & Montanaro, M. (2017). Derivation and validation of the stray light correction algorithm for the thermal infrared sensor onboard Landsat 8. *Remote Sensing of Environment*, *191*. https://doi.org/10.1016/j.rse.2017.01.029

Giardino, C., Pepe, M., Brivio, P. A., Ghezzi, P., & Zilioli, E. (2001). Detecting chlorophyll, Secchi disk depth and surface temperature in a sub-alpine lake using Landsat imagery. *Science of the Total Environment*, *268*(1–3). https://doi.org/10.1016/S0048-9697(00)00692-6

Gillespie, A., Rokugawa, S., Hook, S. J., Matsunaga, R., & Kahle, A. B. (1999). Temperature/emissivity separation algorithm theoretical basis document, version 2.4. In *NASA/GSFC*.

Gillespie, A., Rokugawa, S., Matsunaga, T., Steven Cothern, J., Hook, S., & Kahle, A. B. (1998). A temperature and emissivity separation algorithm for advanced spaceborne thermal emission and reflection radiometer (ASTER) images. *IEEE Transactions on Geoscience and Remote Sensing*, *36*(4). https://doi.org/10.1109/36.700995

Glen George, D. (2012). Using Airborne Remote Sensing to Study the Physical Dynamics of Lakes and the Spatial Distribution of Phytoplankton. *Freshwater Reviews*, *5*(2). https://doi.org/10.1608/frj-5.2.505

Globolakes : Data. (n.d.). Retrieved September 26, 2023, from http://www.laketemp.net/home_ARCLake/dataF/

Gomis-Cebolla, J., Jimenez, J. C., & Sobrino, J. A. (2018). LST retrieval algorithm adapted to the Amazon evergreen forests using MODIS data. *Remote Sensing of Environment*, *204*. https://doi.org/10.1016/j.rse.2017.10.015

Guillevic, P. C., Biard, J. C., Hulley, G. C., Privette, J. L., Hook, S. J., Olioso, A., Göttsche, F. M., Radocinski, R., Román, M. O., Yu, Y., & Csiszar, I. (2014). Validation of Land Surface Temperature products derived from the Visible Infrared Imaging Radiometer Suite (VIIRS) using ground-based and heritage satellite measurements. *Remote Sensing of Environment*, *154*. https://doi.org/10.1016/j.rse.2014.08.013

Guillevic, P., Göttsche, F., Nickeson, J., Hulley, G., Ghent, D., Yu, Y., Trigo, I., Hook, S., Sobrino, J. A., Remedios, J., Román, M., & Camacho, F. (2018). Land surface temperature product validation best practice protocol version 1.1. In *Best Practice for Satellite-Derived Land Product Validation: Land Product Validation Subgroup (WGCV/CEOS)* (Issue January).

Guo, L., Zheng, H., Wu, Y., Fan, L., Wen, M., Li, J., Zhang, F., Zhu, L., & Zhang, B. (2022). An integrated dataset of daily lake surface water temperature over the Tibetan Plateau. *Earth System Science Data*, *14*(7), 3411–3422. https://doi.org/10.5194/essd-14-3411-2022

Herrick, C., Steele, B. G., Brentrup, J. A., Cottingham, K. L., Ducey, M. J., Lutz, D. A., Palace, M. W., Thompson, M. C., Trout-Haney, J. V., & Weathers, K. C. (2023). lakeCoSTR: A tool to facilitate use of Landsat Collection 2 to estimate lake surface water temperatures. *Ecosphere*, *14*(1). https://doi.org/10.1002/ecs2.4357

Hodson, T. O. (2022). Root-mean-square error (RMSE) or mean absolute error (MAE): when to use them or not. In *Geoscientific Model Development* (Vol. 15, Issue 14). https://doi.org/10.5194/gmd-15-5481-2022

Hook, S. J., & Hulley, G. C. (2018). *ECOSTRESS LEVEL-2 ATBD*.

Huang, Y., Liu, H., Hinkel, K., Yu, B., Beck, R., & Wu, J. (2017). Analysis of Thermal Structure of Arctic Lakes at Local and Regional Scales Using in Situ and Multidate Landsat-8 Data. *Water Resources Research*, *53*(11). https://doi.org/10.1002/2017WR021335

Hulley, G. C., & Hook, S. J. (2018). *ECOSTRESS LEVEL-2 CLOUD ATBD*.

Hulley, G. C., Hook, S. J., & Schneider, P. (2011). Optimized split-window coefficients for deriving surface temperatures from inland water bodies. *Remote Sensing of Environment*, *115*(12). https://doi.org/10.1016/j.rse.2011.09.014

Jiménez-Muñoz, J. C. (2004). Correction to "A generalized single-channel method for retrieving land surface temperature from remote sensing data" by Juan C. Jiménez-Muñoz and José A. Sobrino. *Journal of Geophysical Research*, *109*(D8). https://doi.org/10.1029/2004jd004804

Jimenez-Munoz, J. C., Cristobal, J., Sobrino, J. A., Sòria, G., Ninyerola, M., & Pons, X. (2009). Revision of the single-channel algorithm for land surface temperature retrieval from landsat thermal-infrared data. *IEEE Transactions on Geoscience and Remote Sensing*, *47*(1). https://doi.org/10.1109/TGRS.2008.2007125

Jiménez-Munoz, J. C., & Sobrino, J. A. (2003). A generalized single-channel method for retrieving land surface temperature from remote sensing data. *Journal of Geophysical Research: Atmospheres*, *108*(22). https://doi.org/10.1029/2003jd003480

Jimenez-Munoz, J. C., Sobrino, J. A., Skokovic, D., Mattar, C., & Cristobal, J. (2014). Land surface temperature retrieval methods from landsat-8 thermal infrared sensor data. *IEEE Geoscience and Remote Sensing Letters*, *11*(10), 1840–1843. https://doi.org/10.1109/LGRS.2014.2312032

Justice, C., Belward, A., Morisette, J., Lewis, P., Privette, J., & Baret, F. (2000). Developments in the "validation" of satellite sensor products for the study of the land surface. *International Journal of Remote Sensing*, *21*(17). https://doi.org/10.1080/014311600750020000

Khalil, C. A., Khoury, E. El, & Ibrahim, E. (2017). Atmospheric correction of landsat 8 TIRS acquisitions using split window algorithms for analyzing naameh landfill, Lebanon. *2017 Sensors Networks Smart and Emerging Technologies, SENSET 2017*, *2017-January*. https://doi.org/10.1109/SENSET.2017.8125015

Klerkx, Jean., & Imanackunov, Beishen. (2002). *Lake Issyk-Kul: Its Natural Environment*. 300.

Koetz, B., Bastiaanssen, W., Berger, M., Defourney, P., Bello, U. Del, Drusch, M., Drinkwater, M., Duca, R., Fernandez, V., Ghent, D., Guzinski, R., Hoogeveen, J., Hook, S., Lagouarde, J. P., Lemoine, G., Manolis, I., Martimort, P., Masek, J., Massart, M., … Udelhoven, T. (2018). High spatio-temporal resolution land surface temperature mission - A copernicus candidate mission in support of agricultural monitoring. *International Geoscience and Remote Sensing Symposium (IGARSS)*, *2018-July*. https://doi.org/10.1109/IGARSS.2018.8517433

Lagouarde, J. P., Bhattacharya, B. K., Crébassol, P., Gamet, P., Babu, S. S., Boulet, G., Briottet, X., Buddhiraju, K. M., Cherchali, S., Dadou, I., Dedieu, G., Gouhier, M., Hagolle, O., Irvine, M., Jacob, F., Kumar, A., Kumar, K. K., Laignel, B., Mallick, K., … Ramakrishnan, R. (2018). The Indian-French Trishna mission: Earth observation in the thermal infrared with high spatio-temporal resolution. *International Geoscience and Remote Sensing Symposium (IGARSS)*, *2018-July*. https://doi.org/10.1109/IGARSS.2018.8518720

Lake surface temperatures | Copernicus. (n.d.). Retrieved September 26, 2023, from https://climate.copernicus.eu/esotc/2021/lake-surface-temperatures

Lake Surface Water Temperature | Copernicus Global Land Service. (n.d.). Retrieved September 20, 2023, from https://land.copernicus.eu/global/products/lswt

Layden, A., Merchant, C., & Maccallum, S. (2015). Global climatology of surface water temperatures of large lakes by remote sensing. *International Journal of Climatology*, *35*(15). https://doi.org/10.1002/joc.4299

Lazhu, Yang, K., Qin, J., Hou, J., Lei, Y., Wang, J., Huang, A., Chen, Y., Ding, B., & Li, X. (2022). A Strict Validation of MODIS Lake Surface Water Temperature on the Tibetan Plateau. *Remote Sensing 2022, Vol. 14, Page 5454*, *14*(21), 5454. https://doi.org/10.3390/RS14215454

Li, H., Sun, D., Yu, Y., Wang, H., Liu, Y., Liu, Q., Du, Y., Wang, H., & Cao, B. (2014). Evaluation of the VIIRS and MODIS LST products in an arid area of Northwest China. *Remote Sensing of Environment*, *142*. https://doi.org/10.1016/j.rse.2013.11.014

Li, K., Guan, K., Jiang, C., Wang, S., Peng, B., & Cai, Y. (2021). Evaluation of Four New Land Surface Temperature (LST) Products in the U.S. Corn Belt: ECOSTRESS, GOES-R, Landsat, and Sentinel-3. *IEEE Journal of Selected Topics in Applied Earth Observations and Remote Sensing*, *14*. https://doi.org/10.1109/JSTARS.2021.3114613

Li, Y., Zhang, Q., Zhang, L., Tan, Z., & Yao, J. (2017). Investigation of water temperature variations and sensitivities in a large floodplain lake system (Poyang Lake, China) using a hydrodynamic model. *Remote Sensing*, *9*(12). https://doi.org/10.3390/rs9121231

Li, Z. L., & Duan, S. B. (2017). Land surface temperature. In *Comprehensive Remote Sensing* (Vols. 1–9). https://doi.org/10.1016/B978-0-12-409548-9.10375-6

Li, Z. L., Tang, B. H., Wu, H., Ren, H., Yan, G., Wan, Z., Trigo, I. F., & Sobrino, J. A. (2013). Satellite-derived land surface temperature: Current status and perspectives. In *Remote Sensing of Environment* (Vol. 131). https://doi.org/10.1016/j.rse.2012.12.008

Li, Z. L., Wu, H., Duan, S. B., Zhao, W., Ren, H., Liu, X., Leng, P., Tang, R., Ye, X., Zhu, J., Sun, Y., Si, M., Liu, M., Li, J., Zhang, X., Shang, G., Tang, B. H., Yan, G., & Zhou, C. (2023). Satellite Remote Sensing of Global Land Surface Temperature: Definition, Methods, Products, and Applications. In *Reviews of Geophysics* (Vol. 61, Issue 1). https://doi.org/10.1029/2022RG000777

Lieberherr, G., & Wunderle, S. (2018). Lake surface water temperature derived from 35 years of AVHRR sensor data for European lakes. *Remote Sensing*, *10*(7). https://doi.org/10.3390/rs10070990

Liu, G., Ou, W., Zhang, Y., Wu, T., Zhu, G., Shi, K., & Qin, B. (2015). Validating and Mapping Surface Water Temperatures in Lake Taihu: Results from MODIS Land Surface Temperature Products. *IEEE Journal of Selected Topics in Applied Earth Observations and Remote Sensing*, *8*(3). https://doi.org/10.1109/JSTARS.2014.2386333

Liu, Y., Yu, Y., Yu, P., Göttsche, F. M., & Trigo, I. F. (2015). Quality assessment of S-NPP VIIRS land surface temperature product. *Remote Sensing*, *7*(9). https://doi.org/10.3390/rs70912215

Luo, Y., Zhang, Y., Yang, K., Yu, Z., & Zhu, Y. (2019). Spatiotemporal Variations in Dianchi Lake's Surface Water Temperature from 2001 to 2017 under the Influence of Climate Warming. *IEEE Access*, *7*, 115378–115387. https://doi.org/10.1109/ACCESS.2019.2935767

MacCallum, S., Merchant, C., Merchant, C., & Merchant, C. (2012). Surface water temperature observations of large lakes by optimal estimation. *Canadian Journal of Remote Sensing*, *389243415116116*(14), 25–45. https://doi.org/10.5589/m12-010

Mao, K. B., Shi, J. C., Li, Z. L., Qin, Z. H., Li, M. C., & Xu, B. (2007). A physics-based statistical algorithm for retrieving land surface temperature from AMSR-E passive microwave data. *Science in China, Series D: Earth Sciences*, *50*(7), 1115–1120. https://doi.org/10.1007/S11430-007-2053-X

Mccorkel, J., Goddard, N., Montanaro, M., Tveekrem, J., Stauder, J., Lunsford, A., Mentzell, E., Hair, J., & Reuter, D. (n.d.). *TIRS-2 Instrument Project Landsat 9 Thermal Infrared Sensor 2 Preliminary Stray Light Assessment*.

Measuring Lake Water Temperature From Space | Weather and Climate @ Reading. (n.d.). Retrieved September 26, 2023, from https://blogs.reading.ac.uk/weather-and-climate-at-reading/2020/measuring-lake-water-temperature-from-space/

Meng, C., & Li, H. (2019). Assimilating Satellite Land Surface States Data from Fengyun-4A. Scientific Reports, 9(1). https://doi.org/10.1038/s41598-019-55733-3

Michel, A., Granero-Belinchon, C., Cassante, C., Boitard, P., Briottet, X., Adeline, K. R. M., Poutier, L., & Sobrino, J. A. (2021). A new material-oriented tes for land surface temperature and suhi retrieval in urban areas: Case study over madrid in the framework of the future trishna mission. *Remote Sensing*, *13*(24). https://doi.org/10.3390/rs13245139

Montanaro, M., McCorkel, J., Tveekrem, J., Stauder, J., Lunsford, A., Mentzell, E., Hair, J., & Reuter, D. (2018). Landsat 9 Thermal Infrared Sensor 2 preliminary stray light assessment. *International Geoscience and Remote Sensing Symposium (IGARSS)*, *2018-July*, 8853–8856. https://doi.org/10.1109/IGARSS.2018.8519394

Nie, J., Ren, H., Zheng, Y., Ghent, D., & Tansey, K. (2021). Land Surface Temperature and Emissivity Retrieval from Nighttime Middle-Infrared and Thermal-Infrared Sentinel-3 Images. *IEEE Geoscience and Remote Sensing Letters*, *18*(5), 915–919. https://doi.org/10.1109/LGRS.2020.2986326

O'Reilly, C. M., Sharma, S., Gray, D. K., Hampton, S. E., Read, J. S., Rowley, R. J., Schneider, P., Lenters, J. D., McIntyre, P. B., Kraemer, B. M., Weyhenmeyer, G. A., Straile, D., Dong, B., Adrian, R., Allan, M. G., Anneville, O., Arvola, L., Austin, J., Bailey, J. L., … Zhang, G. (2015). Rapid and highly variable warming of lake surface waters around the globe. *Geophysical Research Letters*, *42*(24). https://doi.org/10.1002/2015GL066235

Payan, V., & Royer, A. (2004). Analysis of Temperature Emissivity Separation (TES) algorithm applicability and sensitivity. *International Journal of Remote Sensing*, *25*(1), 15–37. https://doi.org/10.1080/0143116031000115274

Peeters, F., Finger, D., Hofer, M., Brennwald, M., Livingstone, D. M., & Kipfer, R. (2003). Deep-water renewal in Lake Issyk-Kul driven by differential cooling. *Limnology and Oceanography*, *48*(4). https://doi.org/10.4319/lo.2003.48.4.1419

Peng, Z., Yang, J., Luo, Y., Yang, K., & Shang, C. (2021). Impact of climate warming on the surface water temperature of plateau lake. *Acta Geophysica*, *69*(3). https://doi.org/10.1007/s11600-021-00581-x

Pérez-Planells, L., Niclòs, R., Puchades, J., Coll, C., Göttsche, F. M., Valiente, J. A., Valor, E., & Galve, J. M. (2021). Validation of Sentinel-3 SLSTR Land Surface Temperature Retrieved by the Operational Product and Comparison with Explicitly Emissivity-Dependent Algorithms. *Remote Sensing 2021, Vol. 13, Page 2228*, *13*(11), 2228. https://doi.org/10.3390/RS13112228

Perrone, M., Scalici, M., Conti, L., Moravec, D., Kropáček, J., Sighicelli, M., Lecce, F., & Malavasi, M. (2021). Water mixing conditions influence sentinel-2 monitoring of chlorophyll content in monomictic lakes. *Remote Sensing*, *13*(14). https://doi.org/10.3390/rs13142699

Philippe Goryl, E., Buongiorno, A., Santella EUMETSAT Vincent Fournier-Sicre, C., & Santacesaria, V. (2009). *University of Leicester / NILU SENTINEL-3 OPTICAL PRODUCTS AND ALGORITHM DEFINITION SLSTR ATBD LAND SURFACE TEMPERATURE*.

Plan Grands Lacs - Communauté de Communes Gérardmer Hautes Vosges. (n.d.). Retrieved October 27, 2023, from https://ccghv.fr/environnement/plan-grands-lacs/

Plans d'eau - Fédération de Pêche du Bas-Rhin. (n.d.). Retrieved September 27, 2023, from https://www.peche67.fr/5754-plan-deau.htm

Politi, E., Cutler, M. E. J., & Rowan, J. S. (2012). Using the NOAA Advanced Very High Resolution Radiometer to characterise temporal and spatial trends in water temperature of large European lakes. *Remote Sensing of Environment*, *126*, 1–11. https://doi.org/10.1016/J.RSE.2012.08.004

Pour, H. K., Rontu, L., Duguay, C., Eerola, K., & Kourzeneva, E. (2014). Impact of satellite-based lake surface observations on the initial state of HIRLAM. Part II: Analysis of lake surface temperature and ice cover. *Tellus A: Dynamic Meteorology and Oceanography*, *66*(1). https://doi.org/10.3402/tellusa.v66.21395

Prats, J., Reynaud, N., Rebière, D., Peroux, T., Tormos, T., & Danis, P. A. (2018). LakeSST: Lake Skin Surface Temperature in French inland water bodies for 1999-2016 from Landsat archives. *Earth System Science Data*, *10*(2). https://doi.org/10.5194/essd-10-727-2018

Radiant flux - Wikipedia. (n.d.). Retrieved October 2, 2023, from https://en.wikipedia.org/wiki/Radiant_flux#units

Rahaghi, A. I., Lemmin, U., Sage, D., & Barry, D. A. (2018). *Achieving high-resolution thermal imagery in low-contrast lake surface waters by aerial remote sensing and image registration*. https://doi.org/10.1016/j.rse.2018.12.018

Reinart, A., & Reinhold, M. (2008a). Mapping surface temperature in large lakes with MODIS data. *Remote Sensing of Environment*, *112*(2). https://doi.org/10.1016/j.rse.2007.05.015

Reinart, A., & Reinhold, M. (2008b). Mapping surface temperature in large lakes with MODIS data. *Remote Sensing of Environment*, *112*(2). https://doi.org/10.1016/j.rse.2007.05.015

Ren, H., Du, C., Liu, R., Qin, Q., Yan, G., Li, Z. L., & Meng, J. (2015). Atmospheric water vapor retrieval from Landsat 8 thermal infrared images. *Journal of Geophysical Research*, *120*(5). https://doi.org/10.1002/2014JD022619

Romanovsky, V. V., Tashbaeva, S., Crétaux, J.-F., Calmant, S., & Drolon, V. (2013). The closed Lake Issyk-Kul as an indicator of global warming in Tien-Shan. *Natural Science*, *05*(05). https://doi.org/10.4236/ns.2013.55076

Rongali, G., Keshari, A. K., Gosain, A. K., & Khosa, R. (2018). Split-Window Algorithm for Retrieval of Land Surface Temperature Using Landsat 8 Thermal Infrared Data. *Journal of Geovisualization and Spatial Analysis*, *2*(2), 1–19. https://doi.org/10.1007/S41651-018-0021-Y/FIGURES/17

Ru, C., Duan, S. B., Jiang, X. G., Li, Z. L., Huang, C., & Liu, M. (2023). An extended SW-TES algorithm for land surface temperature and emissivity retrieval from ECOSTRESS thermal infrared data over urban areas. *Remote Sensing of Environment*, *290*. https://doi.org/10.1016/j.rse.2023.113544

Savvaitova, K., & Petr, T. (1992). Lake Issyk-kul, Kirgizia. *International Journal of Salt Lake Research*, *1*(2). https://doi.org/10.1007/BF02904361

Schaeffer, B. A., Iiames, J., Dwyer, J., Urquhart, E., Salls, W., Rover, J., & Seegers, B. (2018). An initial validation of Landsat 5 and 7 derived surface water temperature for U.S. lakes, reservoirs, and estuaries. *International Journal of Remote Sensing*, *39*(22). https://doi.org/10.1080/01431161.2018.1471545

Schmugge, T., French, A., Ritchie, J. C., Rango, A., & Pelgrum, H. (2002). Temperature and emissivity separation from multispectral thermal infrared observations. *Remote Sensing of Environment*, *79*(2–3). https://doi.org/10.1016/S0034-4257(01)00272-3

Schneider, P., Healey, N. C., Hulley, G. C., & Hook, S. J. (2019). 4 - Lake Surface Temperature. In G. C. Hulley & D. Ghent (Eds.), *Taking the Temperature of the Earth* (pp. 129–150). Elsevier. https://doi.org/https://doi.org/10.1016/B978-0-12-814458-9.00004-6

Schneider, P., & Hook, S. J. (2010). Space observations of inland water bodies show rapid surface warming since 1985. *Geophysical Research Letters*, *37*(22). https://doi.org/10.1029/2010GL045059

Schneider, P., Hook, S. J., Radocinski, R. G., Corlett, G. K., Hulley, G. C., Schladow, S. G., & Steissberg, T. E. (2009). Satellite observations indicate rapid warming trend for lakes in California and Nevada. *Geophysical Research Letters*, *36*(22). https://doi.org/10.1029/2009GL040846

Sharaf, N., Fadel, A., Bresciani, M., Giardino, C., Lemaire, B. J., Slim, K., Faour, G., & Vinçon-Leite, B. (2019). Lake surface temperature retrieval from Landsat-8 and retrospective analysis in Karaoun Reservoir, Lebanon. *Journal of Applied Remote Sensing*, *13*(04). https://doi.org/10.1117/1.jrs.13.044505

Sharma, S., Gray, D. K., Read, J. S., O'Reilly, C. M., Schneider, P., Qudrat, A., Gries, C., Stefanoff, S., Hampton, S. E., Hook, S., Lenters, J. D., Livingstone, D. M., McIntyre, P. B., Adrian, R., Allan, M. G., Anneville, O., Arvola, L., Austin, J., Bailey, J., … Woo, K. H. (2015). A global database of lake surface temperatures collected by in situ and satellite methods from 1985-2009. *Scientific Data*, *2*. https://doi.org/10.1038/sdata.2015.8

Shaw, J. A., & Nugent, P. W. (2013). Physics principles in radiometric infrared imaging of clouds in the atmosphere. *European Journal of Physics*, *34*(6). https://doi.org/10.1088/0143-0807/34/6/S111

Shi, J., & Hu, C. (2021). Evaluation of ecostress thermal data over south florida estuaries. *Sensors*, *21*(13). https://doi.org/10.3390/s21134341

Silvestri, M., Romaniello, V., Hook, S., Musacchio, M., Teggi, S., & Buongiorno, M. F. (2020). First comparisons of surface temperature estimations between ECOSTRESS, ASTER and landsat 8 over Italian volcanic and geothermal areas. *Remote Sensing*, *12*(1). https://doi.org/10.3390/RS12010184

Simon, R. N., Tormos, T., & Danis, P. A. (2014). Retrieving water surface temperature from archive LANDSAT thermal infrared data: Application of the mono-channel atmospheric correction algorithm over two freshwater reservoirs. *International Journal of Applied Earth Observation and Geoinformation*, *30*(1). https://doi.org/10.1016/j.jag.2014.01.005

Smyth, M., & Leprince, S. (2018). *ECOSTRESS LEVEL-1B ATBD*.

Sobrino, J. A., Caselles, V., & Coll, C. (1993). Theoretical split-window algorithms for determining the actual surface temperature. *Il Nuovo Cimento C*, *16*(3). https://doi.org/10.1007/BF02524225

Sobrino, J. A., Li, Z. L., Stoll, M. P., & Becker, F. (1994). Improvements in the Split-Window Technique for Land Surface Temperature Determination. *IEEE Transactions on Geoscience and Remote Sensing*, *32*(2). https://doi.org/10.1109/36.295038

Solheim, A. L., Austnes, K., Eriksen, E., Seifert, I., & Holen, S. (2010). *Climate change impacts on water quality and biodiversity Background Report for EEA European Environment ETC Water Technical Report 1/2010*. http://water.eionet.europa.eu

Suivi climatique national & fonctionnement des lacs : une bouée installée sur le lac de Gérardmer - Gerardmer info. (n.d.). Retrieved September 27, 2023, from https://gerardmerinfo.fr/2021/06/suivi-climatique-national-fonctionnement-lacs-bouee-installee-lac-de-gerardmer/

Tavares, M. H., Cunha, A. H. F., Motta-Marques, D., Ruhoff, A. L., Cavalcanti, J. R., Fragoso, C. R., Bravo, J. M., Munar, A. M., Fan, F. M., & Rodrigues, L. H. R. (2019). Comparison of methods to estimate lake-surface-water temperature using landsat 7 ETM+ and MODIS imagery: Case study of a large shallow subtropical lake in Southern Brazil. *Water (Switzerland)*, *11*(1). https://doi.org/10.3390/w11010168

Torgoev, I., Alioshin, Y. G., & Torgoev, A. (2013). Monitoring landslides in Kyrgyzstan. *FOG - Freiberg Online Geoscience*, *33*.

Tormos, T., Prats, J., Reynaud, N., & Danis, P.-A. (2016). *Estimation de la température de surface des plans d'eau à partir de l'imagerie Landsat : Algorithmes et Résultats*.

Tormos, T., Prats, J., Reynaud, N., & Danis, P.-A. (2017). *Estimation de la température de surface des plans d'eau à partir de l'imagerie Landsat : Algorithmes et Résultats*.

Trumpickas, J., Shuter, B. J., & Minns, C. K. (2009). Forecasting impacts of climate change on Great Lakes surface water temperatures. *Journal of Great Lakes Research*, *35*(3). https://doi.org/10.1016/j.jglr.2009.04.005

Use Excel to Calculate MAD, MSE, RMSE & MAPE - Dawn Wright, Ph.D. (n.d.). Retrieved November 4, 2023, from https://www.drdawnwright.com/use-excel-to-calculate-mad-mse-rmse-mape/

Vanhellemont, Q. (2020). Automated water surface temperature retrieval from Landsat 8/TIRS. *Remote Sensing of Environment*, *237*. https://doi.org/10.1016/j.rse.2019.111518

VITO Earth Observation - Lake Surface Water Temperature product catalogue. (n.d.). Retrieved September 26, 2023, from https://land.copernicus.vgt.vito.be/PDF/portal/Application.html#Browse;Root=1100100;Collection=1100102;Time=NORMAL,NORMAL,-1,,,-1,,

Wan, W., Li, H., Xie, H., Hong, Y., Long, D., Zhao, L., Han, Z., Cui, Y., Liu, B., Wang, C., & Yang, W. (2017). A comprehensive data set of lake surface water temperature over the Tibetan Plateau derived from MODIS LST products 2001-2015. *Scientific Data*, *4*. https://doi.org/10.1038/sdata.2017.95

Wan, Z., & Snyder, W. (1999). *MODIS Land-Surface Temperature Algorithm Theoretical Basis Document (LST ATBD)*.

Wan, Z., Zhang, Y., Li, Z. L., Wang, R., Salomonson, V. V., Yves, A., Bosseno, R., & Hanocq, J. F. (2002). Preliminary estimate of calibration of the moderate resolution imaging spectroradiometer thermal infrared data using Lake Titicaca. *Remote Sensing of Environment*, *80*(3). https://doi.org/10.1016/S0034-4257(01)00327-3

Wan, Z., Zhang, Y., Zhang, Q., & Li, Z. L. (2010). Quality assessment and validation of the MODIS global land surface temperature. *Http://Dx.Doi.Org/10.1080/0143116031000116417*, *25*(1), 261–274. https://doi.org/10.1080/0143116031000116417

Wang, F., Qin, Z., Song, C., Tu, L., Karnieli, A., & Zhao, S. (2015). An improved mono-window algorithm for land surface temperature retrieval from landsat 8 thermal infrared sensor data. *Remote Sensing*, *7*(4). https://doi.org/10.3390/rs70404268

Wang, L., Lu, Y., & Yao, Y. (2019). Comparison of three algorithms for the retrieval of land surface temperature from landsat 8 images. *Sensors (Switzerland)*, *19*(22). https://doi.org/10.3390/s19225049

Wang, M., Zhang, Z., Hu, T., & Liu, X. (2019). A Practical Single-Channel Algorithm for Land Surface Temperature Retrieval: Application to Landsat Series Data. *Journal of Geophysical Research: Atmospheres*, *124*(1). https://doi.org/10.1029/2018JD029330

Wang, S., He, L., & Hu, W. (2015). A Temperature and Emissivity Separation Algorithm for Landsat-8 Thermal Infrared Sensor Data. *Remote Sensing 2015, Vol. 7, Pages 9904-9927*, *7*(8), 9904–9927. https://doi.org/10.3390/RS70809904

Water cycle | National Oceanic and Atmospheric Administration. (n.d.). Retrieved April 5, 2023, from https://www.noaa.gov/education/resource-collections/freshwater/water-cycle

Williamson, C. E., Saros, J. E., Vincent, W. F., & Smol, J. P. (2009). Lakes and reservoirs as sentinels, integrators, and regulators of climate change. *Limnology and Oceanography*, *54*(6 PART 2). https://doi.org/10.4319/lo.2009.54.6_part_2.2273

Witze, A. (2015). Lakes warm worldwide. *Nature*. https://doi.org/10.1038/nature.2015.19034

Woolway, R. I. (2014). *Drivers, associations and consequences of the diel variability in high-resolution lake surface water temperature measurements*.

Woolway, R. I., Kraemer, B. M., Lenters, J. D., Merchant, C. J., O'Reilly, C. M., & Sharma, S. (2020). Global lake responses to climate change. In *Nature Reviews Earth and Environment* (Vol. 1, Issue 8). https://doi.org/10.1038/s43017-020-0067-5

Xiao, F., Ling, F., Du, Y., Feng, Q., Yan, Y., & Chen, H. (2013). Evaluation of spatial-temporal dynamics in surface water temperature of Qinghai Lake from 2001 to 2010 by using MODIS data. *Journal of Arid Land*, *5*(4). https://doi.org/10.1007/s40333-013-0188-5

Yang, J., Yang, K., Zhang, Y., Luo, Y., & Shang, C. (2022). Maximum lake surface water temperatures changing characteristics under climate change. *Environmental Science and Pollution Research*, *29*(2). https://doi.org/10.1007/s11356-021-15621-8

Yang, J., Zhou, J., Göttsche, F. M., Long, Z., Ma, J., & Luo, R. (2020). Investigation and validation of algorithms for estimating land surface temperature from Sentinel-3 SLSTR data. *International Journal of Applied Earth Observation and Geoinformation*, *91*. https://doi.org/10.1016/j.jag.2020.102136

Yang, K., Yu, Z., Luo, Y., Zhou, X., & Shang, C. (2019). Spatial-Temporal Variation of Lake Surface Water Temperature and Its Driving Factors in Yunnan-Guizhou Plateau. *Water Resources Research*, *55*(6), 4688–4703. https://doi.org/10.1029/2019WR025316

Yao, F., Livneh, B., Rajagopalan, B., Wang, J., Crétaux, J.-F., Wada, Y., & Berge-Nguyen, M. (2023). Satellites reveal widespread decline in global lake water storage. *Science*, *380*(6646). https://doi.org/10.1126/science.abo2812

Ye, X., Ren, H., Zhu, J., Fan, W., & Qin, Q. (2022a). Split-Window Algorithm for Land Surface Temperature Retrieval From Landsat-9 Remote Sensing Images. *IEEE Geoscience and Remote Sensing Letters*, *19*. https://doi.org/10.1109/LGRS.2022.3184980

Ye, X., Ren, H., Zhu, J., Fan, W., & Qin, Q. (2022b). Split-Window Algorithm for Land Surface Temperature Retrieval From Landsat-9 Remote Sensing Images. *IEEE Geoscience and Remote Sensing Letters*, *19*. https://doi.org/10.1109/LGRS.2022.3184980

Yu, X., Guo, X., & Wu, Z. (2014). Land Surface Temperature Retrieval from Landsat 8 TIRS—Comparison between Radiative Transfer Equation-Based Method, Split Window Algorithm and Single Channel Method. *Remote Sensing 2014, Vol. 6, Pages 9829-9852*, *6*(10), 9829–9852. https://doi.org/10.3390/RS6109829

Zarei, A., Shah-Hosseini, R., Ranjbar, S., & Hasanlou, M. (2021). Validation of non-linear split window algorithm for land surface temperature estimation using Sentinel-3 satellite imagery: Case study; Tehran Province, Iran. *Advances in Space Research*, *67*(12). https://doi.org/10.1016/j.asr.2021.02.019

Zhao, D., Aili, A., Zhai, Y., Xu, S., Tan, G., Yin, X., & Yang, R. (2019). Radiative sky cooling: Fundamental principles, materials, and applications. In *Applied Physics Reviews* (Vol. 6, Issue 2). https://doi.org/10.1063/1.5087281

Zheng, X., Li, Z. L., Nerry, F., & Zhang, X. (2019). A new thermal infrared channel configuration for accurate land surface temperature retrieval from satellite data. *Remote Sensing of Environment*, *231*. https://doi.org/10.1016/j.rse.2019.111216

List of Conferences

- **EO4Water Cycle Science**: Hernandez-Galindo Ivan, Nerry Françoise, Yésou Hervé. 16-18 November 2020 (ESA - Virtual Event). Multiscale/Multi-Temporal Study Of The Lake Surface Water Temperature (LSWT) Retrieval Using IRT Sensors.
- **4th Hydrospace-GEOGloWS**: Hernandez-Galindo Ivan, Nerry Françoise, Crétaux Jean-François, Yesou Hervé. 7-11 June 2021 (ESA-ESRIN Virtual Event). Multiscale/Multi-Temporal Study of The Lake Surface Water Temperature (LSWT) Retrieval Using IRT Sensors: Application to Issyk-Kul Lake, Kyrgyzstan.
- **TRISHNA Days**: Hernandez-Galindo Ivan, Nerry Françoise, Crétaux Jean-François, Yesou Hervé. 22-24 March 2022 (Toulouse, France). Issyk-Kul Lake Surface Water Temperature with Sentinel-3 & ECOSTRESS as TRISHNA precursors.
- **Living Planet Symposium**: Hernandez-Galindo Ivan, Nerry Françoise, Crétaux Jean-François, Yesou Hervé. 23-27 May 2022 (Bonn, Germany). Variability of the Lake Surface Water Temperature (LSWT) in Issyk-Kul Lake using Sentinel 3-SLSTR and ECOSTRESS sensors.
- **RAQRS VI**: Hernandez-Galindo Ivan, Nerry Françoise, Crétaux Jean-François, Yesou Hervé. 19-23 September 2022 (Valencia, Spain). Multiscale/multi-temporal study of the Lake Surface Water Temperature using IRT sensors: validation in the Issyk-Kul Lake, Kyrgyzstan and Grand Est Lakes, France.

Ivan HERNANDEZ-GALINDO

Etude multi-échelle/multi-temporelle de la température des eaux de surface des lacs (LSWT) à l'aide de capteurs satellitaires thermiques : application à des lacs de la région Grand-Est, France, et du Kirghizistan

Résumé

La température des eaux de surface des lacs (LSWT) a un impact significatif sur l'environnement aquatique et la chimie de l'eau, ce qui en fait un indicateur crucial de la santé des lacs. En outre, la température de l'eau de surface des lacs influence les conditions météorologiques et l'atmosphère qui entourent les grands lacs. De nombreuses applications, notamment l'étude du cycle hydrologique et du changement climatique, l'habitat des créatures aquatiques, la pêche, l'aquaculture et la gestion de la qualité de l'eau, nécessitent des données sur la température de l'eau avec des résolutions spatiales et temporelles accrues.
Cette recherche vise à acquérir et à analyser la LSWT à l'aide de capteurs satellitaires TIR tels que Landsat 8-9, ECOSTRESS, Sentinel-3 et MODIS. Ces capteurs fournissent des informations précieuses en prévision des nouvelles missions TIR telles que TRISHNA en 2025 (CNES-ISRO), LSTM (ESA Copernicus), et SBG (NASA), toutes deux en 2028. L'étude estime la LSWT du lac Issyk-Kul, au Kirghizstan, et des lacs Gerardmer, Longemer et Plobsheim, en France. Pour évaluer la 'LSWT, des multicapteurs fournissant des estimations spatiales et temporelles plus denses de la 'LSWT sont nécessaires pour comprendre les processus et la dynamique dans le domaine thermique. En outre, les estimations de la LWST provenant des satellites ont été validées par des intercomparaisons et des campagnes in situ sur les lacs mentionnés au cours de différentes périodes annuelles.

Mots-clés : Température des eaux de surface des lacs (LSWT), capteurs infrarouges thermiques (TIR), ECOSTRESS, Landsat 8-9, Sentinel-3, MODIS, CCI Lakes, campagnes de validation, lacs Issyk-Kul, Gerardmer, Longemer, Plobsheim.

Résumé en anglais

The Lake Surface Water Temperature (LSWT) significantly impacts the aquatic environment and water chemistry, making it a crucial indication of the lakes' health. Moreover, the LSWT influences the weather and atmosphere surrounding the big lakes. Many applications, including studies of the hydrological cycle and climate change, the habitat of aquatic creatures, fisheries, aquaculture, and water quality management, require data on water temperature with increased spatial and temporal resolutions.
This research aims to acquire and analyze the LSWT using TIR satellite sensors such as Landsat 8-9, ECOSTRESS, Sentinel-3, and MODIS. These sensors provide valuable information in anticipation of new TIR missions such as TRISHNA in 2025 (CNES-ISRO), LSTM (ESA Copernicus), and SBG (NASA), both in 2028. The study estimates LSWT from the Issyk-Kul Lake, Kyrgyzstan, and the Gerardmer, Longemer, and Plobsheim Lakes, France. To assess the LSWT, multisensors providing denser spatial and temporal LSWT estimates are needed to understand processes and dynamics in the thermal domain. In addition, the LSWT estimates from the satellites were validated by intercomparisons and in-situ campaigns over the mentioned lakes during different year periods.

Keywords: Lake Surface Water Temperature (LSWT), Thermal Infrared sensors (TIR), ECOSTRESS, Landsat 8-9, Sentinel-3, MODIS, CCI Lakes, Validation campaigns, Issyk-Kul, Gerardmer, Longemer, Plobsheim Lakes.